

STRATEGIES FOR IMPROVING DIAGNOSIS OF MALARIA AND SCHISTOSOMIASIS
IN LOW-RESOURCE SETTINGS

By

Christine Franzel Markwalter

Dissertation

Submitted to the Faculty of the
Graduate School of Vanderbilt University
in partial fulfillment of the requirements

for the degree of

DOCTOR OF PHILOSOPHY

in

Chemistry

May 11, 2018

Nashville, Tennessee

Approved:

David W. Wright, Ph.D.

David E. Cliffel, Ph.D.

James E. Crowe, Jr., M.D.

Janet E. Macdonald, Ph.D.

To Mom, Dad, and Katie, who shaped me into the human I am today
and to Daniel, my rock, my confidant, my encourager

No one should seek their own good,

but the good of others.

1 Corinthians 10:24

ACKNOWLEDGEMENTS

The work presented in this dissertation would not have been possible without the expertise, wisdom, support, and encouragement of a multitude of individuals, and my gratitude goes well beyond any written “thank you,” could communicate. This section is my best effort to express my appreciation.

Working under the direction of my Ph.D. advisor, Professor David Wright has unquestionably molded me as a scientist and defined my career path. Thank you, David, for teaching me to think critically, question everything, be creative, and take risks. Because of your encouragement and support, I have had an unbelievably global and exciting Ph.D. adventure (seriously—five years ago, I would never have believed you if you told me all I would experience in my graduate career). I have walked through new cities (and villages), stood in front of masterpieces and natural wonders, established a global network, and worked countless hours in labs around the world, all thanks to you. Please take Appendix F as a thank you and tribute to all you have done for me.

The insight and expertise of my committee members have also greatly enhanced this work. Thank you to Dr. Janet Macdonald for being a true role model and incredible teacher, to Dr. David Cliffel for holding me to the highest analytical standards, and to Dr. James Crowe for reminding me to always consider the “real-world” medical context of my work.

The people in the Wright lab not only made graduate school fun, but also challenged me to be a better scientist along the way. I have benefited greatly from the wisdom and experience of many former lab members (Nicholas Adams, Stephen Jackson, Alex Rutledge, Chris Gulka, Keersten Davis, Kim Fong, Jenny Nesbitt, Lauren Gibson, Anna Bitting, Alexis Wong, Lwiindi Mudenda, Joseph Conrad, and Danielle Kimmel). Thank you particularly to Keersten for being a

great mentor, friend, and travel buddy, to Chris for exemplifying scientific creativity, to Kim for demonstrating what it means to work hard, to Alexis for teaching me to stick up for myself, and to Anna for holding me to your meticulously detail-oriented standards. I am especially grateful to Lauren for always being present, listening, asking, giving advice, and watching out for me. One of the best parts of graduate school was becoming your friend. The current members of the Wright lab (Tom Scherr, Mindy Leelawong, Wes Bauer, Andrew Kantor, Carson Moore, Megan van der Horst, Kelly Richardson, Micaella Jorge, and Nate Piety) continue to shape it into a positive and uplifting environment. Wes, thank you for maintaining a down-to-earth attitude and constant stream of jokes. I am glad to be crossing the finish line with you. Andrew, your sunny demeanor was immediately evident when you rotated through our lab nearly four years ago. You've inspired us all with your perseverance and positive attitude. Tom, thanks for being a sounding board for my ideas and encouraging me to be creative. Carson, Megan, Kelly, Micaella, and Nate—you are wonderful people and scientists, and I am confident you will continue to make great contributions to the lab. Finally, I have to thank Greg, our honorary lab member, who checked in on me and encouraged me daily. Your presence and conversation always picked me up when I was down.

My most life-changing experience in graduate school was traveling to and working in Macha, Zambia. Dr. Phil Thuma graciously opened his laboratory and his home to our team. Phil, I am so grateful for your example of how a faith-driven scientist can affect positive change. Your love for people and community makes the world a better place. You are an inspiration.

I also need to thank Govert van Dam, Paul Corstjens, and Lisette van Lieshout at Leiden University, Netherlands for welcoming me to work in their departments for several months. Govert, thank you for encouraging me to stay positive, including me in discussions with schistosomiasis experts, and welcoming me into your home (and Tesla!) in the Netherlands. Paul,

your expertise was beyond helpful and ultimately led the science where it needed to go. Pytsje, thank you for showing me the ropes and helping to get me started in the lab. Additionally, I can honestly say I would not have made it through the months I spent in Leiden without the friends I made. Miriam, Chiara, and Laudine, thank you for keeping me grounded, constantly encouraging me, and reminding me that the world is bigger than the lab. I will always treasure our memories of exploring Dutch cities, sipping hot chocolate, laughing over meals of tagliatelle and pannekoeken, and enjoying stroopwafels next to the canals. See you again soon.

I also must thank those who led me to where I am today. Dr. Acio at TJHSST introduced me to the wonders and applications of chemistry in everyday life (and held my attention with exciting, exothermic demos). Dr. Kennedy taught me how to channel that enthusiasm into research projects in the Chemical Analysis Lab. What most prepared me for graduate school, however, was my experience at Agnes Scott College. There, I not only expanded my knowledge and skillset in chemistry and math, but also learned to think deeply, live honorably, and engage in ongoing social and intellectual challenges. My professors at ASC provided an empowering, nurturing, and challenging environment in which I found my voice. I am most grateful to Dr. Koch and Dr. Lewin for encouraging me to pursue math for the love of it. Dr. Venable, Dr. Harvey, Dr. Riter, Dr. Winget, and Dr. Fantz provided a foundation in chemistry that I felt confident in and have all served as role models ever since.

Every step of the way, my family has been an endless source of unconditional love and encouragement. Mom and Dad, there aren't enough words in the world to describe what you mean to me. Thank you for making me believe I can be whatever I want to be "when I grow up," for all the hard work you put into providing me with an education, and for teaching me what it means to love your neighbor. I love you. To my sister Katie, you make everything more fun just by your

presence, and you bring immense joy into my life. I am so grateful for your friendship, love, and sassy nature. I also need to thank Holly, Brian, Chet, Kelly, Kyle, Gabriela, and Teace for always being a source of love, support, and laughs. I'm so blessed to call you family.

Finally, I would like to thank my husband, Daniel Webb Markwalter. I couldn't have made it through graduate school without you and wouldn't have wanted to. Thank you for being my best friend, for loving me unconditionally, and for doing the dishes. The last five years with you have been an adventure, and I can't wait to see what the future brings.

TABLE OF CONTENTS

	Page
DEDICATION.....	ii
ACKNOWLEDGEMENTS	iv
LIST OF TABLES.....	xii
LIST OF FIGURES	xiii
Chapter	
I. INTRODUCTION	1
Diagnosis of Infectious Diseases in Low-Resource Settings	1
Malaria	4
The Malaria Parasite.....	7
Current Malaria Diagnostic Strategies	10
Schistosomiasis.....	16
Biology of <i>Schistosoma</i>	17
Current Schistosomiasis Diagnostic Strategies.....	20
Scope of This Work	23
II. EVIDENCE FOR HISTIDINE-RICH PROTEIN 2 IMMUNE COMPLEX FORMATION IN SYMPTOMATIC MALARIA PATIENTS IN SOUTHERN ZAMBIA.....	24
Introduction	24
Methods	26
Reagents and Materials	26
HRP2 Enzyme-Linked Immunosorbent Assay (ELISA)	27
Dried Blood Spot (DBS) Preparation and Extraction	27
DBS ELISA	28
HRP2 Immune Complex Pull-Down Assay	28
Study Setting, Patient Recruitment, and Ethics	29
Patient Sample DBS Preparation and Storage.....	30
DNA Extraction and PCR Amplification.....	31
Determination of Free and Immune-Complexed HRP2 in Patient Samples	31
Data Analysis.....	32
Results	32
Dissociation of Pre-Formed HRP2 Immune Complexes	32
Optimization of HRP2 Immune Complex Pull-Down Assay.....	33
Evaluation of Immune Complex Dissociation and Pull-Down in Mock Patient Samples.....	34
Patient Demographics	36
Free HRP2 Levels in Untreated and Heated Patient DBS Extracts.....	37
HRP2 Present in Immune Complexes in Patient DBS Extracts	38
Discussion.....	40
Conclusion.....	46

Acknowledgements.....	46
III. POLY(AMIDOAMINE)-COATED MAGNETIC PARTICLES FOR ENHANCED DETECTION OF <i>SCHISTOSOMA</i> CIRCULATING ANODIC ANTIGEN IN ENDEMIC URINE SAMPLES	48
Introduction	48
Methods.....	50
Materials and Reagents	50
Bead Preparation.....	50
CAA ELISA.....	51
UCP-LF CAA Assay (UCAA10).....	51
Enhancement of UCP-LF CAA Assay with PAMAM-Functionalized Magnetic Beads...	52
Analysis of Patient Samples	52
Data Analysis.....	53
Results	54
Optimization of PAMAM-Functionalized Magnetic Beads.....	54
Characterization of PAMAM Bead Robustness and Stability.....	55
Performance of Magnetic Bead-Based CAA Concentration Protocol.....	57
Patient Sample Analysis.....	57
Discussion.....	59
Conclusion.....	61
Acknowledgements.....	62
IV. BIOLAYER INTERFEROMETRY AS A TOOL FOR PREDICTING ELISA PERFORMANCE OF MONOCLONAL ANTIBODY PAIRS FOR TWO MALARIAL BIOMARKERS	63
Introduction	63
Methods.....	64
Materials and Reagents	64
Antibody Production	65
Determining Kinetic Parameters of mAbs with BLI	65
Screening Antibody Pairs by ELISA	66
rcHRP2	66
rcPvLDH.....	68
Results and Discussion.....	69
Kinetic Parameters of mAbs Measured by BLI.....	69
rcHRP2	69
rcPvLDH.....	71
Screening mAb Pairs by ELISA	72
rcHRP2	72
rcPvLDH.....	73
Predicting mAb ELISA Performance with BLI.....	74
rcHRP2	74
rcPvLDH.....	76

Conclusion.....	78
Acknowledgements.....	79
V. SIMULTANEOUS CAPTURE AND SEQUENTIAL DETECTION OF TWO MALARIAL BIOMARKERS ON MAGNETIC MICROPARTICLES	80
Introduction	80
Methods.....	83
Reagents and Materials	83
<i>p</i> LDH Antibody Pair Screen.....	83
Blood Sample Preparation.....	84
Preparation of mAb-Functionalized Magnetic Beads	84
On-Bead ELISA for <i>p</i> LDH.....	84
On-Bead ELISA for HRP2.....	85
On-Bead Simultaneous Capture and Sequential Detection (SCSD) ELISA.....	85
Validation	87
Results and Discussion.....	87
Design and Optimization of On-Bead ELISAs for <i>p</i> LDH and HRP2	87
Performance of <i>p</i> LDH On-Bead ELISA	91
Performance of HRP2 On-Bead ELISA.....	92
Design of On-Bead SCSD ELISA for <i>p</i> LDH and HRP2	93
Performance of On-Bead SCSD ELISA for <i>p</i> LDH and HRP2	94
Conclusion.....	98
Acknowledgements.....	99
VI. CHARACTERIZATION OF <i>p</i>LDH AND HRP2 CLEARANCE PATTERNS VIA RAPID ON-BEAD DETECTION FROM A SINGLE DRIED BLOOD SPOT	100
Introduction	100
Methods.....	102
Materials.....	102
Standardization of D6 <i>P. falciparum</i> Culture.....	103
DBS Preparation and Extraction.....	104
Bead Preparation.....	104
SCSD ELISA with DBS Extracts	104
Stability Study.....	105
Study Setting.....	105
Patient Recruitment and Ethics.....	105
Patient Samples.....	106
Patient DBS Sample SCSD ELISA	106
Data Analysis.....	106
Results and Discussion.....	107
DBS SCSD ELISA Optimization	107
DBS SCSD ELISA Performance.....	110
Biomarker Detectability Over Time.....	110
Patient DBS Samples from Rural Zambia.....	111

Biomarker Clearance.....	113
Conclusion.....	117
Acknowledgements.....	118
VII. CONCLUSION.....	119
Summary and Future Directions.....	119
Outlook and Perspective.....	127
Appendix	
A. SUPPORTING INFORMATION: CHAPTER II.....	129
B. SUPPORTING INFORMATION: CHAPTER IV	132
C. SUPPORTING INFORMATION: CHAPTER VI	138
D. IMMUNOMAGNETIC CAPTURE AND COLORIMETRIC DETECTION OF MALARIAL BIOMARKER <i>PLASMODIUM FALCIPARUM</i> LACTATE DEHYDROGENASE.....	146
E. TOWARD DYNAMIC PAPER-BASED DIAGNOSTICS.....	159
F. MY PH.D. EXPERIENCE	163
REFERENCES	164

LIST OF TABLES

Table	Page
1. Patients stratified by collection strategy, parasite presence, and detectable free HRP2.....	37
2. Patients stratified by parasite presence, free HRP2, and complexed HRP2.....	39
3. Optimized experimental set-up for BLI of α -HRP2 IgM.....	66
4. α -HRP2 mAbs assessed by BLI and ELISA	68
5. α -pLDH mAbs assessed by BLI and ELISA.....	69
6. Kinetic parameters for α -HRP2 antibodies measured by BLI.....	71
7. Kinetic parameters for α -pLDH antibodies against rcPvLDH measured by BLI.....	72
8. Performance of on-bead SCSD ELISA for pLDH and HRP2.....	95
9. Patient sample data for immune complex work.....	129
10. BLI binding profiles and fit residuals for anti-HRP2 IgG.....	132
11. BLI binding profiles and fit residuals for anti-HRP2 IgM.....	135
12. BLI binding profiles and fit residuals for anti-pLDH IgG against rcPvLDH	136
13. Patient biomarker concentrations over time measured by on-bead SCSD ELISA.....	141

LIST OF FIGURES

Figure	Page
1. The global burden of malaria in 2016.....	5
2. Malaria parasite life cycle.....	9
3. Life cycle of the schistosome	18
4. The effect of α -HRP2 on HRP2 detectability by ELISA	33
5. Optimization and characterization of HRP2 immune complex pull-down assay.....	34
6. Evaluation of optimized immune complex dissociation protocol and pull-down assay.....	36
7. Free HRP2 levels in patient samples.....	38
8. Dissociation and pull-down of HRP2 immune complexes in patient samples.....	40
9. Concentrations of immune-complexed and total HRP2 in HRP2-positive patient samples ...	44
10. Optimization of PAMAM-functionalized magnetic particles	55
11. Evaluation of stability and robustness of PAMAM-functionalized magnetic particles.....	56
12. Performance of magnetic bead-based CAA concentration protocol.....	57
13. PAMAM-functionalized magnetic particles concentrate CAA from patient samples.....	59
14. ELISA S/N for checkerboard screening of α -HRP2 mAb pairs.....	73
15. ELISA S/N for checkerboard screening of α -pLDH mAb pairs with rcPvLDH.....	74
16. Relationship between α -HRP2 kinetic parameters and ELISA S/N.....	76
17. Relationship between α -pLDH affinity constants and ELISA S/N	77
18. Workflow for SCSD ELISA for pLDH and HRP2.....	86
19. ELISA S/N for checkerboard screening of α -pLDH mAb pairs with D6 <i>Pf</i> culture	88
20. Pan-specific α -pLDH mAb pair screening results	89
21. Optimization of pLDH and HRP2 on-bead ELISAs.....	91
22. Standard curves for pLDH on-bead ELISA	92
23. Standard curves for HRP2 on-bead ELISA.....	92
24. Cross-reactivity study for pLDH and HRP2 on-bead ELISAs.....	93
25. Determining the order of pLDH and HRP2 detection in the SCSD ELISA	94
26. Two-user validation curves for SCSD ELISA for pLDH and HRP2	95
27. On-bead SCSD ELISA performance for W2, Benin 1, and PH1 <i>P. falciparum</i> strains.....	96
28. Recovery of pLDH and HRP2 as a function of DBS incubation time.....	107
29. Affordable 96-well plate filter for use in low-resource settings.....	108

30. Optimization of DBS on-bead SCSD ELISA.....	109
31. Standard curves for DBS on-bead SCSD ELISA	110
32. The effect of storage time on DBS SCSD ELISA signal.....	111
33. Correlations between <i>p</i> LDH and parasitemia and HRP2 and parasitemia.....	113
34. Biomarker clearance trends for three patients over 35 days.....	114
35. Normalized parasite, <i>p</i> LDH, and HRP2 clearance patterns over time.....	115
36. Individual patient sample clearance patterns for <i>p</i> LDH and HRP2.....	138
37. The Malstat assay for detection of <i>p</i> LDH	147
38. Workflow for on-bead <i>Pf</i> LDH activity assay	151
39. Michaelis-Menten curves for <i>Pf</i> LDH activity assay.....	152
40. The effect of APAD and APADH on <i>Pf</i> LDH activity assay S/N.....	152
41. Measuring the Malstat assay at 580 nm improves sensitivity	153
42. Selection of capture antibody for on-bead activity assay	154
43. <i>rcPf</i> LDH standard curve for on-bead <i>Pf</i> LDH activity assay	155
44. Parasite culture titration for on-bead <i>Pf</i> LDH activity assay.....	156
45. Workflow and performance for dynamic walls proof-of-concept	161
46. My Ph.D. experience in postcards	163

CHAPTER I

INTRODUCTION^a

Diagnosis of Infectious Diseases in Low-Resource Settings

In 2016, infectious diseases, including bacterial, viral, and parasitic infections, were estimated to claim over 8 million lives globally and greatly impact the quality of life of many others.¹ Low- and middle-income countries (LMICs) bear the greatest burden of infectious diseases, with 85% of these deaths occurring in the developing world.¹ This immense burden of disease represses economic development which, in turn, limits access to adequate healthcare, resulting in an inextricable cycle of poverty and disease.

Diagnostics are critical tools for morbidity control and elimination campaigns. On an individual level, early diagnosis and treatment of patients with infectious diseases reduces mortality, chronic symptoms, and long-term complications, thereby improving prognoses. From a population perspective, sensitive and accurate diagnosis and treatment of disease is imperative for interrupting transmission and ultimately eliminating a disease from a geographic area, regardless of strategy. Appropriate diagnostic tools are necessary for surveillance, confirmation of elimination, and evaluation of interventions, including mass drug administration, insecticide spraying, or water treatment.

One of the most important considerations when designing diagnostic assays and devices is the setting in which they will be utilized. In LMICs, a tiered system can be used to describe the three levels of healthcare infrastructure available within a health system. Tertiary facilities (Level

^a Portions of this text were reproduced in part with permission from *Chemical Reviews*, submitted for publication. Unpublished work copyright 2018 American Chemical Society.

3), including national hospitals, central hospitals, and university hospitals, provide complex care and are typically found in urban areas. These hospitals have highly technical clinical diagnostic laboratory equipment, employ specialized staff, and serve as reference laboratories.² Tertiary care is often out of reach for those living in rural areas, requiring many days of traveling. Regional and district laboratories as well as community hospitals are considered Level 2 facilities.² These hospitals and labs may have limited access to specialized equipment and personnel, and essential resources (i.e. running water and electricity) may be intermittently unavailable. Primary care (Level 1) consists of rural hospitals, local health clinics, and health outposts.² These centers are frequently the first point of contact patients have with a health system. In LMICs, Level 1 facilities often lack essential resources such as clean running water and electricity and have little to no laboratory equipment, relying instead on diagnosis via clinical symptoms or rapid diagnostic tests. Privately run pharmacies sometimes serve as primary healthcare facilities, providing rapid diagnostic tests and basic therapeutics.³

In the context of infectious disease diagnosis, Level 3 facilities frequently serve as reference laboratories, and samples from patients in the surrounding region are sent to these labs for culturing, molecular diagnostics, or complex assays. In these cases, however, time-to-result can be devastatingly long. One example of this was highlighted by Coulibaly et al. in their study of access to care for HIV-infected infants in an urban region of Burkina Faso in 2011.⁴ Early infant diagnosis of HIV-exposed children is essential for early initiation of antiretroviral treatment, which has been shown to improve infant survival by 76%.⁵ In Burkina Faso, HIV-positive mothers were advised to attend a 6-week postnatal appointment at their nearest primary healthcare facility for dried blood spot collection. Oftentimes, technicians with the expertise required to collect dried blood spots were only available once each month, so mothers would have to return to clinic on that

day for testing. Once collected, the dried blood spot samples were sent to district-level hospitals (Level 2), which then sent the samples to reference laboratory facilities (Level 3) for analysis. Test results followed the same path back to patients and were usually available within four months.⁴ The consequences of this inefficient path to answers were devastating. For HIV-infected infants, these first few months of life are associated with a peak in mortality, and 10% of the HIV-positive infants in the study died before antiretroviral therapy could even be started.^{4,6}

Early infant diagnosis of HIV is just one example of the critical need for rapid, point-of-care (POC) infectious disease diagnostics that can be performed in rural primary healthcare settings, where essential resources may be lacking. Rapid and accurate diagnosis of other infectious diseases, such as malaria, tuberculosis, neglected tropical diseases, and diarrheal diseases, in low-resource settings has the potential to greatly reduce their associated morbidities and mortalities. Disease diagnosis in these settings is particularly challenging and often requires tools that can be used by untrained personnel without significant laboratory or physical infrastructure. The World Health Organization has developed criteria (“ASSURED”) that define the ideal characteristics for POC tests in low-resource settings. According to these criteria, an ideal test should be affordable to those who are at risk of infection, result in few false-negatives (sensitive) and false-positives (specific), and be user-friendly, rapid and robust, equipment-free, and deliverable to the populations in need of the test.⁷

The development and implementation of POC diagnostics that fit the ASSURED criteria often have disease- and application-specific challenges. In the research phase, it is often advantageous to address these challenges at the individual component level. The components of a diagnostic include: (1) the biomarker, an endogenous indicator of a disease state, which is most often a pathogen or host protein, carbohydrate, or nucleic acid sequence (2) the sample matrix,

typically whole blood, urine, or saliva, (3) molecular recognition elements, which allow for specific biomarker capture and detection, (4) signal generation and amplification, and (5) instrumentation for signal readout. In this work, each component of the conventional diagnostic format is examined and optimized with the goal of improving diagnosis of two infectious diseases prevalent in LMICs: malaria and schistosomiasis. To provide background and context, the remainder of this introductory chapter will focus on parasite biology and current diagnostic strategies for these two diseases, with a strong emphasis on malaria.

Malaria

Although malaria is preventable and treatable, it remains a severe global public health problem. The World Health Organization estimates that nearly half the world's population is at risk for malaria, which caused approximately 216 million infections and 445,000 deaths worldwide in 2016 (Figure 1).⁸ Sub-Saharan Africa carries a disproportionately large share of this burden, accounting for 90% of malaria cases and 91% of deaths due to malaria.⁸ Populations most vulnerable to malaria include the immunocompromised, pregnant women, and children under 5 years of age, the latter group accounting for 70% of all malaria deaths.⁸

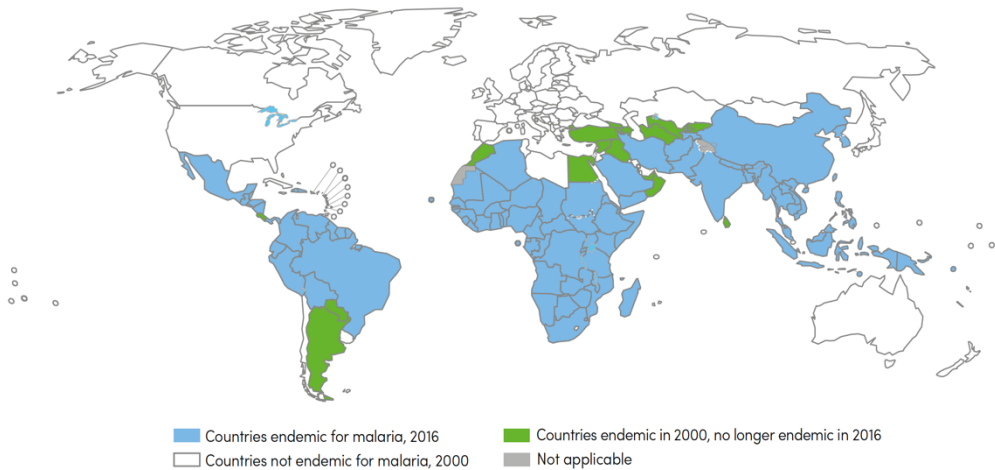


Figure 1. The global burden of malaria in 2016.⁹

The social and economic burden of malaria is immense on both the individual and population levels. For individuals and families, costs include expenses for travel and medical services, including diagnostics and therapeutics, at clinics and/or dispensaries. In 2013, Onwujekwe et al. found that these costs average US \$3.46 ± \$2.60 per case for outpatient treatment and \$10.32 ± \$5.54 for inpatient cases for families living in the rural Enugu State of Nigeria.¹⁰ In addition to these direct expenses, indirect costs such as lost days of work for both sickness and travel added up to \$9.11 ± \$6.91 and \$12.88 ± \$6.08 per case for outpatient and inpatient treatment, respectively.¹⁰ These costs represent a substantial portion of the monthly income of the largely agrarian and merchant survey respondents, more than half of whom reported a malaria case in their household within one month of the interview.¹⁰ Thus, malaria can be economically devastating to families. On a national level, governments must pay for upkeep, supply, and staffing of clinics and hospitals in addition to purchasing drugs, diagnostics, and other interventions such as insecticide spray or insecticide-treated bed nets. Globally, direct costs due to malaria have been estimated to be at least \$12 billion annually, though the cost in lost economic growth is likely much greater.¹¹

To address the immense human and socioeconomic burdens of malaria, the United Nations set a target of halting and reversing the incidence of malaria between 2000 and 2015.¹² Remarkably, these goals were achieved; millions of malaria deaths were averted, especially among young children.¹³ Between 2000 and 2015, worldwide malaria incidence fell approximately 21%, and mortality rates decreased by an estimated 29%.⁹ As a result of this progress, the World Health Organization developed a global technical strategy for the next 15 years, targeting a 90% reduction in malaria incidence and mortality and elimination of malaria from at least 35 countries by 2030.⁹ Achieving these ambitious goals will require a substantial increase in global malaria funding, from US \$2.5 billion to \$8.7 billion by 2030.⁹

Malaria elimination is defined as the disruption of local transmission of a particular parasite species in a defined geographic area (i.e. zero incidence of indigenous cases).¹⁴ Several strategies for malaria elimination have been proposed, each with their own advantages and disadvantages. Mass drug administration (MDA) involves providing antimalarial drugs to an entire population without prior testing for the presence or absence of infection. This strategy is most effective when multiple rounds of antimalarial drugs are provided to isolated populations with low malaria transmission and a high degree of participation.¹⁵ However, MDA is largely unsuccessful in high-transmission areas, and the cost of the approach is likely to be high in large geographic regions. Additionally, the widespread use of artemisinin combination therapies (ACTs) without prior malaria diagnosis in MDA may promote rapid selection for parasites resistant to first-line drugs.¹⁵ A second elimination strategy is mass screening and treatment (MSAT). In this approach, everyone in a given geographic region is tested for malaria, and individuals with positive diagnoses are provided with antimalarial treatments. MSAT relies heavily on the availability of accurate diagnostic tools capable of detecting low parasite densities in order to ensure that all individuals

carrying parasites receive treatment. The cost of MSAT for malaria elimination is likely to be similar to that of MDA, though the risk of selecting for drug resistant parasites is lower.¹⁵ Targeted MSAT has been shown to be particularly effective in low-transmission areas. In this strategy, when a case is passively detected at a local health clinic, all individuals living within a defined radius (e.g. 150 m) of the index case are tested for malaria and provided with treatment if positive. Targeted MSAT, also called reactive case detection, was applied in the catchment area of Macha Mission Hospital in the Southern Province in Zambia, and parasite prevalence was reduced by nearly 90% from 2008 to 2013.¹⁶

It is clear that successful elimination strategies in one region are not necessarily generalizable to regions with differing geography, transmission, prevalence, and parasite diversity. The strategies presented above are centered around the human host but will likely need to be coupled to vector control measures, such as insecticide spraying and insecticide-treated bed nets, to promote the highest probability of success. Regardless of elimination strategy, additional investment in research and development will be necessary to address the rising challenges facing malaria elimination campaigns, including parasite multidrug resistance, vector insecticide resistance, detectability of low-level malaria infections, and gene deletions of parasite biomarkers.

The Malaria Parasite

Malaria is caused by protozoan parasites of the *Plasmodium* genus. There are currently five species of malaria known to infect humans. *P. falciparum* is the most prevalent species in Africa and is responsible for most malaria deaths worldwide.¹⁷ The second most prevalent species, *P. vivax*, is the dominant species in Asia and the Americas, though it is also present on the African continent.¹⁸ The less common *P. ovale* is found primarily in Sub-Saharan Africa, and *P. malariae*

is found throughout the world.^{19,20} Previously considered to be rare, *P. knowlesi* is an emerging zoonotic malaria that has been found throughout Southeast Asia and is the most common form of malaria in Malaysia.²¹ Although there is little evidence of human-to-human transmission of *P. knowlesi*, it represents a major threat to malaria elimination in those regions.²²

During its life cycle, a malaria parasite infects two hosts: humans and female *Anopheles* mosquitos (Figure 2). When a malaria-infected female *Anopheles* mosquito takes a blood meal, sporozoites are injected into the human host. These sporozoites then travel through the bloodstream to the liver, where they infect hepatocytes, undergo asexual multiplication, and mature into schizonts, which rupture and release merozoites into the bloodstream. In *P. vivax* and *P. ovale* infections, liver-stage parasites can enter a dormant hypnozoite phase, persisting in the liver and causing relapses by invading the bloodstream weeks, months, or years after the initial mosquito bite.^{18,19} Once in the bloodstream, parasites begin the intraerythrocytic cycle and infect red blood cells, entering the ring stage. The parasites then develop into mature trophozoites and undergo asexual multiplication to form schizonts that rupture, releasing merozoites back into the bloodstream to reinfect red blood cells. Some merozoites develop into male and female gametocytes, which are taken up by *Anopheles* mosquitos during a blood meal. The parasites undergo sexual reproduction in the gut of the mosquito, ultimately developing into sporozoites and entering the mosquito salivary glands, from which they can be inoculated into another human host to perpetuate the transmission cycle.¹⁷

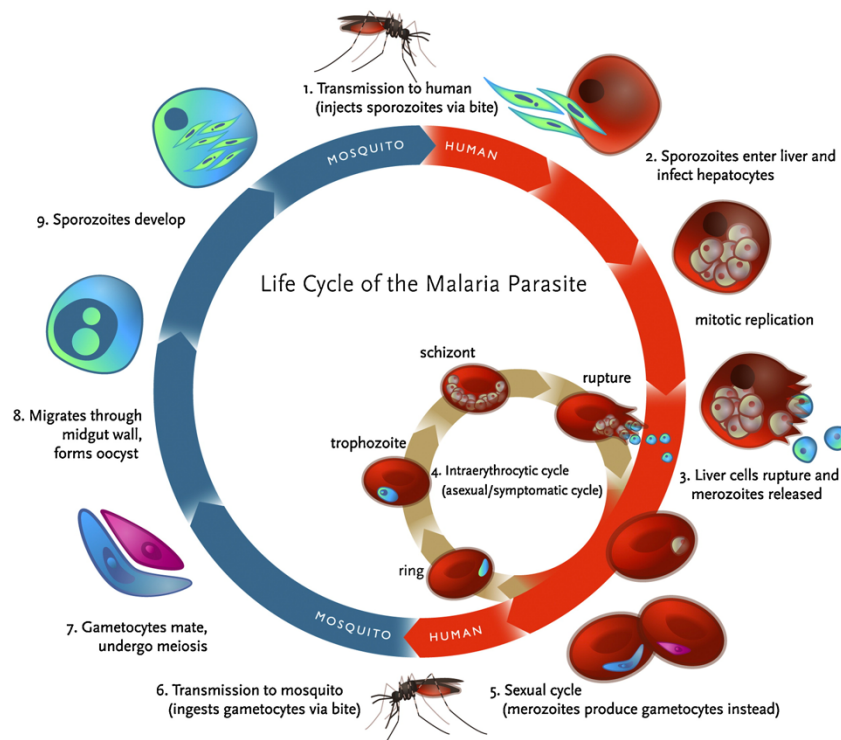


Figure 2. Malaria parasite life cycle.²³ Reproduced with permission © 2013 Elsevier B.V.

Malaria symptoms are largely caused by repeated red blood cell rupture and invasion during the intraerythrocytic cycle. Malaria-infected individuals often suffer cycles of chills, fever, muscle pain, and nausea, symptoms very similar to many other infectious diseases. In severe infections, hemolysis resulting from cell rupture can cause anemia and jaundice. In general, *P. falciparum* causes the most severe symptoms because infected red blood cells (iRBCs) can adhere to vascular endothelial cells, resulting in iRBC sequestration and obstruction of microvasculature. Cerebral and placental malaria, two severe forms of the disease, directly result from *P. falciparum* iRBC sequestration in the vasculature of the brain and placenta, respectively. Vascular obstruction in other areas of the body can cause failure of vital organs, resulting in death. Severe symptoms and mortality from other species of malaria typically result from hyperparasitemia or splenic rupture caused by phagocytic uptake of infected red blood cells by the spleen.²⁴

Current Malaria Diagnostic Strategies

Diagnostic tools are critical for accurately determining the causative pathogen in a patient presenting with nonspecific symptoms, such as fever, and providing appropriate treatment in a timely manner. If a patient is inappropriately diagnosed with malaria based on clinical symptoms alone, they will be treated with antimalarials, which will not cure the underlying cause of symptoms, delaying appropriate treatment and allowing for further disease progression. Furthermore, falsely ruling out malaria could allow the disease to progress to severe symptoms and increase the likelihood of transmission through a mosquito bite.

The utility of a diagnostic tool relies heavily on its diagnostic sensitivity and specificity. The specificity, or true negative rate, of a test is a measure of its ability to correctly identify patients who do not have a disease of interest. In contrast, the sensitivity of a diagnostic (i.e. true positive rate) represents its ability to correctly identify infections of interest in a patient population. The diagnostic sensitivity of a test is inextricably linked to its analytical parameters, particularly the limit of detection. If a diagnostic has a very low detection limit (i.e. can detect very low levels of infection), it is likely to correctly identify a greater number of patients carrying a disease of interest than tests with high detection limits.

In the context of malaria elimination, the development of highly sensitive diagnostics is imperative for detecting subpatent malaria. These asymptomatic and low-density infections contribute significantly to malaria transmission.^{25–30} Asymptomatic infections are defined by detection of a bloodstream infection in the absence of acute malaria symptoms.²⁵ In this case, an infected individual who does not experience malaria symptoms is less likely to seek treatment and thus will unintentionally continue to contribute to the infectious reservoir. An additional challenge is when extremely low parasite densities remain undetected by available diagnostics, likely

resulting in a decision not to treat a patient with antimalarials and unknowingly continuing the potential for transmission through a mosquito bite.

Several studies have investigated the prevalence of subpatent malaria infections and their contributions to the infectious reservoir. In general, asymptomatic and low-density infections make up a large portion of all infections in a low-transmission setting; in a recent pooled analysis of cross-sectional data, Wu et al. found that approximately 83% of malaria infections in low-transmission settings (prevalence < 5%) and 50% of infections in high-transmission settings (prevalence > 20%) were undetectable by available rapid diagnostic tests.²⁹ Recent advances in ultrasensitive molecular techniques have shown average asymptomatic parasite densities to be 5 parasites/ μ l, though infections as low as 0.03 parasites/ μ l have been detected.^{31,32} The contribution of these prevalent subpatent infections to malaria transmission has been investigated in a number of settings. Typically, the transmissibility of an infection is determined by the presence of gametocytes and/or the number of mosquitos infected in membrane feeding assays using venous blood samples.³³ Using these parameters, Tadesse et al. found that asymptomatic infections were responsible for 92% of the *P. vivax* and 99.2% of the *P. falciparum* infectious reservoirs in a low-endemic setting in Ethiopia.³⁰ Similarly, Slater et al. found that asymptomatic *P. falciparum* infections comprised 91% of the infectious reservoir in a high-endemic site in Burkina Faso.²⁸

The transmissibility of subpatent malaria infections highlights the need for using malaria diagnostics capable of detecting low parasite burdens in elimination campaigns. Clearly, the success of a mass or targeted screen and treat strategy hinges on the ability to detect all malaria infections, including subpatent infections, in order to interrupt transmission. In a mass drug administration campaign, highly sensitive diagnostics are important for surveillance purposes to ensure that all human infections have been cleared after treatment.

Microscopy is the current gold standard for malaria detection. In general, microscopy is robust and can be performed in rural clinics and field settings. Besides a microscope, stains, slides, and fixative agents are all that are required to perform microscopy, making it affordable in low-resource settings. In this technique, a thick or thin smear of capillary blood is stained to allow visualization of infected red blood cells under a microscope, and infection intensity is determined by counting the number of infected erythrocytes. The technical limits of detection for microscopy could be as low as 10 parasites/ μl , though in practice detection limits are dependent on the skill of individual microscopists and are typically around 100 parasites/ μl .²⁷ Thus, microscopy will miss most asymptomatic cases, resulting in many false-negative results.

Detection of parasite genetic material via polymerase chain reaction (PCR) is the most sensitive diagnostic technique for malaria and has been instrumental in defining the prevalence and parasite burden of the asymptomatic reservoir. Recently, Zainabadi et al. reported an ultrasensitive PCR method capable of detecting parasite densities as low as 0.020 parasites/ μl from dried blood spots.³⁴ While this sensitivity is highly advantageous in the context of malaria elimination, PCR is an expensive, time-consuming technique that requires technical expertise and significant laboratory infrastructure. For this reason, it is most often performed in tertiary hospitals or reference laboratories and cannot be used at the point of care. Thus, PCR is a useful laboratory tool for studying malaria epidemiology and for performing surveillance studies after interventions. However, in its current form, ultrasensitive PCR cannot be used as the primary diagnostic tool in a screen and treat strategy.

Antigen-detecting rapid diagnostic tests (RDTs) have been workhorses for detection of malaria at the point of care, accounting for 63% of diagnostic testing of suspected cases in 2016.⁸ The World Health Organization estimates that 312 million malaria RDTs were delivered globally

in 2016.⁸ These ubiquitous tests are most frequently formatted as lateral flow assays (LFAs), which rely on capillary fluid flow through microchannels in paper. In this format, sample is deposited onto a conjugate pad, where target-specific antibodies conjugated to gold nanoparticles bind to the target antigen (i.e. protein biomarker produced by malaria parasites) in the sample. Running buffer then carries these complexes down a nitrocellulose membrane until they reach a line of immobilized capture antibodies. This results in a visible line of gold nanoparticles when the target protein is present. In the absence of biomarker, no complex is formed and therefore line is visible. These tests require no electricity or expertise to perform and are generally low-cost and disposable. The readout of LFAs, visible to the naked eye, requires no instrumentation or specialized detection method. All of these qualities make LFAs the diagnostic format that most closely fits the ASSURED criteria; they are affordable, user-friendly, rapid, robust, equipment free, and deliverable to those who need them. Thus, these rapid tests fill a need and are advantageous in low-resource settings.

The primary disadvantage of malaria rapid diagnostic tests is their lack of sensitivity. Detection limits can vary depending on the manufacturer, though they are typically 100 - 200 parasites/ μ l. As such, currently available rapid diagnostic tests are only capable of detecting 41% - 55% of the infectious reservoir in certain settings.^{28,29} Highlighting the impact that high-sensitivity detection tools could have on elimination campaigns, recent models suggest that improving LFA detection limits to 20 or 2 parasites/ μ l could improve the detectability of the infectious reservoir to 83% and 95%, respectively.²⁸ In an effort to fill this need, AlereTM very recently developed an ultrasensitive RDT for malaria detection. The format and user interface of the ultrasensitive RDT are identical to other commercially available malaria LFAs. In an initial study, this test was demonstrated to detect target antigen at levels 10 times lower than a

commercially available standard LFA for malaria.³⁵ Although details of the improvements made to achieve this remarkable sensitivity have not been published, it appears that each component of the conventional lateral flow test format was optimized for enhanced performance. Inspection of the product literature suggests that standard gold nanoparticle detection elements were replaced by larger, dyed polymer particles, enabling easy signal visualization. In addition, it is likely that molecular recognition elements for target capture and detection were optimized to promote high-affinity interactions. While larger-scale studies need to be performed to fully evaluate this new ultrasensitive LFA, it represents a promising tool for malaria detection at the point of care.

Malaria rapid diagnostic tests typically detect one of two malarial protein biomarkers: *P. falciparum* histidine-rich protein 2 (HRP2) or *Plasmodium* lactate dehydrogenase (*p*LDH). In 2016, the majority of rapid malaria tests sold worldwide detected just HRP2, which is expressed only by the *P. falciparum* parasite.⁸ The function of HRP2 remains unconfirmed. However, HRP2 is a unique biomarker in that it appears to lack native tertiary structure, and its sequence is 30% histidine, consisting largely of AHHAHHAAD and AHHAAD repeat motifs.³⁶ A cleavable sequence at the N-terminus is responsible for HRP2 export from the parasite, allowing HRP2 detection in peripheral blood.^{37,38} Clinical concentrations of HRP2 can range from 100 fM to 100 nM, though expression of HRP2 varies over the erythrocytic life cycle of the parasite.^{35,39–41}

There are several drawbacks to using HRP2 as the sole diagnostic marker for malaria infections. First, HRP2 only indicates the presence of *P. falciparum* and is not produced by any of the other four malaria parasite species known to infect humans. Second, the biomarker has been shown to persist in circulation up to 35 days beyond successful treatment and parasite clearance.⁴¹ Thus, an HRP2-based test is unable to distinguish between active and recently cleared *P. falciparum* infections. Third, HRP2 is not essential to parasite survival, and clinical isolates with

pfhrp2 gene deletions have been observed with increasing frequency around the world. First reported in 2010 in Peru, *P. falciparum* strains with partial or complete *pfhrp2* deletions have since been found in Africa, Asia, Central America, and other South American countries.^{42–48} Infections lacking *pfhrp2* will result in false-negative results on HRP2-based malaria rapid diagnostics and can threaten elimination efforts. Recent models suggest that increased incidence of *pfhrp2*-deleted mutants may be a result of the introduction of HRP2-based rapid tests, particularly in low-transmission areas.⁴⁹ If this is the case, *pfhrp2* deletions may be one of the first examples of a pathogen developing resistance to a diagnostic test.⁴⁹

The use of *pLDH* as a malarial biomarker avoids many of the disadvantages of HRP2. For instance, *pLDH* is the terminal enzyme in the anaerobic glycolytic pathway, responsible for converting pyruvate to lactate using cofactor NADH. All species of malaria parasites rely on anaerobic metabolism to generate energy during the intraerythrocytic cycle. Thus, *pLDH* is an essential protein to parasite survival and is conserved across all five *Plasmodium* species known to infect humans.⁵⁰ Additionally, *pLDH* clears from host circulation within just a few days of successful parasite clearance, and as such is a good marker of active malaria infection.⁵¹ However, the measurable concentration of *pLDH* in circulation is several orders of magnitude lower than that of HRP2, making it more difficult to detect in clinical samples.⁵²

The malaria community currently faces a catch-22 with regards to the continued use of antigen-detecting rapid diagnostic tests. On the one hand, the most sensitive HRP2-based tests are the best tools we have to detect the subpatent reservoir of *P. falciparum* infections; however, these tests can only detect one out of the five human malaria species, result in false-positives in recently cleared infections, and may miss *P. falciparum* strains with *pfhrp2* deletions or potentially apply selective pressure to promote those deletions. On the other hand, switching to currently available

*p*LDH-based rapid tests would mitigate all of the aforementioned disadvantages of HRP2 but would result in a substantial sacrifice in diagnostic sensitivity and would be unable to detect a large portion of the asymptomatic and submicroscopic transmission reservoir. As a result, the World Health Organization has recommended a country-level switch to non-HRP2 rapid tests for surveillance purposes when the prevalence of *pfhrp2* deletions is confirmed to be greater than 5% in any province within that country.⁵³ Additionally, they have “loosened” the performance criteria for selection of *p*LDH-based rapid tests, since most of these tests do not fit the sensitivity requirements previously set forth by the organization.⁵³

Clearly, there is an urgent need to improve currently available malaria rapid tests and to develop laboratory tools for continued epidemiological and surveillance studies. The bulk of this dissertation aims to fill these needs by improving the sensitivity of currently-available *p*LDH and HRP2 antigen-detecting tests for malaria and also developing laboratory tools with limits of detection capable of defining the clinically relevant protein biomarker concentrations required to accurately diagnose subpatent infections.

Schistosomiasis

Schistosomiasis is one of more than 20 infectious diseases that the World Health Organization has designated as a neglected tropical disease (NTD). This diverse group of diseases is labeled “neglected” because they inordinately affect the poorest populations and receive little attention and funding compared to more prominent tropical diseases such as malaria, HIV, and tuberculosis.⁵⁴ Over 700 million people live in areas with risk of schistosomiasis transmission, and nearly 240 million people are affected by the disease. Around the world, nearly 40% of countries (78 in total) have reported schistosomiasis transmission, though over 90% of those needing

treatment live on the African continent.⁵⁵ Because of this widespread and immense burden, schistosomiasis is one of the most socioeconomically devastating parasitic diseases, second only to malaria.⁵⁶

Biology of Schistosoma

Schistosomiasis results from an infection with trematodes (i.e. parasitic blood flukes) of the genus *Schistosoma*. There are five *Schistosoma* species known to infect humans, each with differing geographic distributions. *S. haematobium* is primarily distributed across the African continent, with smaller foci in India and the Middle East. *S. mansoni* is also widespread in Africa, and it is also the only species present in the Western Hemisphere, prevalent in Brazil, Suriname, Venezuela, and some Caribbean Islands. *S. japonicum* is only found in Asia, primarily in China and the Philippines. Two additional organisms, *S. mekongi* and *S. intercalatum*, are much less prevalent than the previous three species and are found in Laos/Cambodia and Central Africa, respectively.⁵⁷

The *Schistosoma* life cycle is shown in Figure 3. Briefly, eggs are shed from the human host with feces or urine into a freshwater reservoir. Under the appropriate conditions, these eggs hatch in the water and release miracidia, which then swim and infect snails. Each *Schistosoma* species favors a particular snail species as an intermediate host. Within the snail, miracidia develop into sporocysts and progress through two generations to become cercariae. The cercariae are shed by snails and swim to infect humans by penetrating the skin, simultaneously losing their tails and becoming schistosomulae. These schistosomulae travel to the liver, where they mature into adult worms. Once mature, adult worms pair (male and female) and migrate to blood vessels associated with the intestines or the bladder, where they begin to produce eggs. The average lifespan of

schistosomes in the human host is 3 – 10 years, although infection durations up to 40 years have been observed.⁵⁸ The locations chosen by the worm pairs depend on their species. *S. japonicum* is most frequently found in veins draining the small intestine; *S. mansoni* tends to reside in veins draining the large intestine; and *S. haematobium* is primarily found in the venous plexus of the bladder.⁵⁷ Thus, some of the eggs shed by *S. japonicum* and *S. mansoni* are passed into stool, and a portion of the eggs shed by *S. haematobium* are typically passed into urine. Typically, eggs appear in stool or urine 1 to 3 months after cercariae first penetrate the skin. Some eggs remain trapped in nearby tissue or are transported to other organs within the human host.

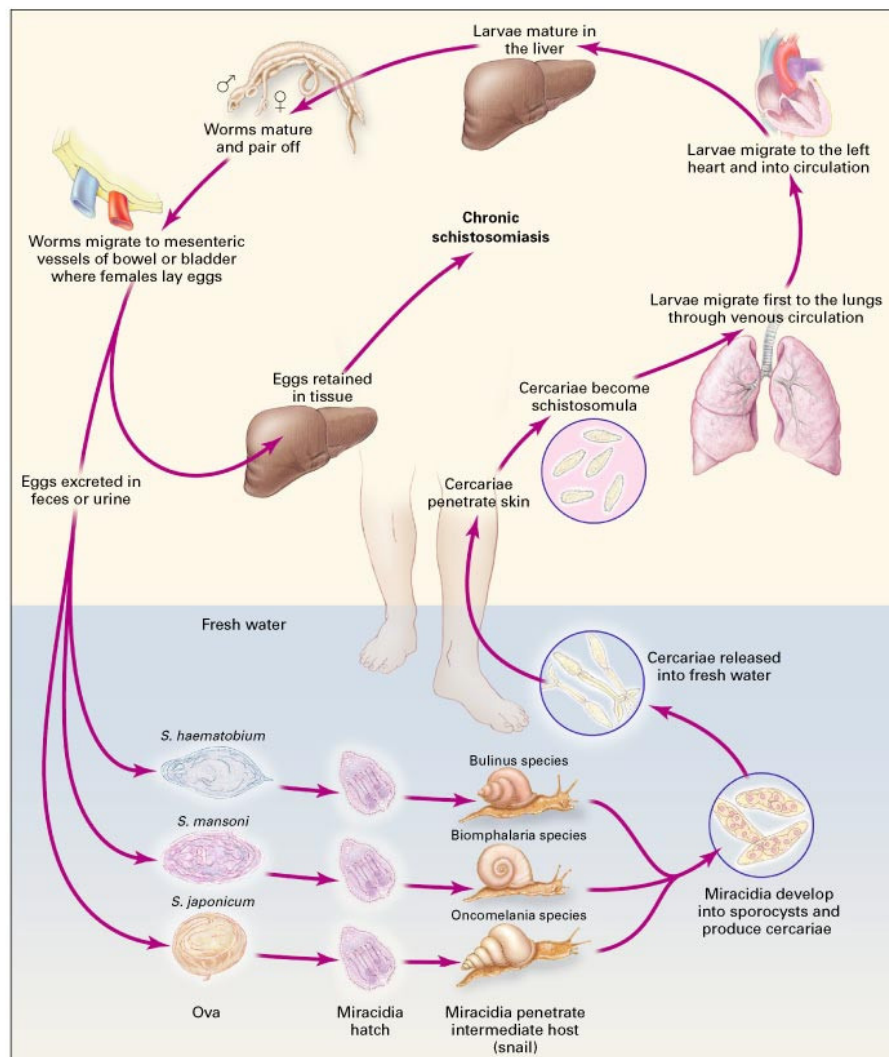


Figure 3. Life cycle of the schistosome.⁵⁹ Reproduced with permission © 2002 Massachusetts Medical Society

The clinical presentations of schistosomiasis are varied in duration and intensity. Some infected individuals remain asymptomatic, especially those with low worm burdens. Immediately after infection, a rash may appear where cercariae penetrate the skin. Acute schistosomiasis, also called Katayama fever, is most common in high-transmission areas.⁵⁹ Symptoms, including fever, chills, cough, nausea, abdominal pain, and muscle pain, are caused by the immune response to eggs deposited in host tissue.⁵⁹ If left untreated, *Schistosoma* infections can become chronic, and ulcerations in the intestines and bladder due to deposited eggs can lead to abdominal pain, diarrhea, and bloody stool and urine.⁵⁷ Eggs retained in the liver can lead to enlargement and liver failure.⁵⁹ Eggs in the urinary tract can lead to ureter obstruction, calcifications in the bladder, and renal failure. Urinary schistosomiasis is also linked to bladder cancer.⁵⁹ The effects of continued inflammatory response to egg granulomas can cause nonspecific but disabling morbidities such as anemia, malnutrition, cognitive impairment, decreased aerobic capacity, and stunted growth.⁵⁸

All human *Schistosoma* parasites can be treated with praziquantel, which causes adult worms to detach from venous walls and die.⁶⁰ Most programs targeting schistosomiasis control or elimination employ praziquantel in an MDA approach, oftentimes coupled with educational campaigns, snail control via molluscicide treatment of contaminated freshwater reservoirs, or both.⁵⁸ In 2012, the World Health Organization established the following goals: (1) to control morbidity due to schistosomiasis by 2020 (i.e. < 5% prevalence of high-intensity infections), (2) to eliminate schistosomiasis as a public health problem by 2025 (i.e. < 1% prevalence of high-intensity infections), and (3) to interrupt transmission of schistosomiasis in select regions and countries by 2025.⁶¹

Current Schistosomiasis Diagnostic Strategies

Accomplishing the goals set by the World Health Organization relies heavily on the development of accurate and field-deployable schistosomiasis diagnostics. Precise mapping of *Schistosoma* prevalence will be necessary to identify foci for targeted interventions. Strong surveillance will be needed to evaluate the success of these interventions, and as prevalence decreases, detecting low-burden asymptomatic cases will become increasingly important.⁵⁸

Microscopy is the most commonly employed tool for schistosomiasis diagnosis. For *S. mansoni* and *S. japonicum*, the Kato-Katz technique is used most often to prepare stool samples for inspection for *Schistosoma* eggs. To detect *S. haematobium*, urine filtration methods are used to concentrate eggs from large urine volumes before inspection by microscopy. Both of these methods lack the sensitivity to detect low-burden infections, which can contribute to ongoing transmission.⁶² Additionally, cut-offs have been established to distinguish between high- and low-intensity infections (100 eggs per gram feces and 50 eggs per 10 ml urine), though egg counts are highly susceptible to day-to-day variation and can be unreliable even for identifying high-intensity infections.⁶³

Beyond microscopy, several other techniques for schistosomiasis diagnosis have been developed. Detection of worm or egg genetic material in plasma, whole blood, stool, or urine via PCR is highly sensitive. However, PCR is expensive and technically demanding, requiring highly equipped laboratories and well-trained technicians to perform. Thus, although useful for research purposes, PCR is not suited for schistosomiasis detection at the point of care. Rapid tests based on serological detection of schistosomiasis have been developed.⁶² These tests rely on the detection of the human host immune response to *Schistosoma* and are advantageous because antibodies often develop before eggs are detectable in stool or urine samples.⁶² However, serology cannot

distinguish between active and previous infections, which reduces its utility, particularly in high-transmission areas.

In the past two decades, LFAs based on circulating antigens produced by *Schistosoma* worms have been developed. While in the blood vessels, schistosomes rely on glucose metabolism and digestion of host red blood cells to generate energy. The worms cannot excrete waste products but rather regurgitate them into the bloodstream.⁵⁸ In particular, two of the waste products generated by the schistosomes have proven useful for urine and blood-based diagnostic assays: the circulating cathodic antigen (CCA) and the circulating anodic antigen (CAA). These heavily glycosylated proteoglycans are named for their overall positive and negative charges, respectively, at physiological pH. Recently, van Dam et al. developed a urine-based CCA-specific LFA (POC-CCA) that is now commercially available and has been extensively evaluated in the field.⁶⁴⁻⁷¹ The POC-CCA test has demonstrated good sensitivity for the detection of *S. mansoni* infections compared to Kato-Katz.⁷² However, there are several disadvantages of the POC-CCA test. First, although CCA is a genus-specific antigen, the POC-CCA is limited to the detection of just one *Schistosoma* species (*S. mansoni*).⁷³ Second, the test can produce confounding results when hematuria, a symptom common for *S. haematobium* infections, is present.⁶⁹ Finally, recent results suggest that the POC-CCA test may be cross-reactive with non-*Schistosoma*-related markers in the urine of pregnant women.⁶⁹

CAA is present in the serum and urine of patients with *Schistosoma* infections of all known species and has been found to correspond well with *Schistosoma* worm burden, clearing soon after successful treatment.^{62,74,75} Recently, Corstjens et al. developed an ultrasensitive, upconverting phosphor-based LFA for CAA that utilizes 400 nm $Y_2O_3:Yb^{3+}, Er^{3+}$ upconverting phosphors (UCPs), which are excited at 980 nm and emit at 550 nm (green) and can detect CAA for a single

Schistosoma worm pair in serum.^{74–79} This assay has been applied to patient samples from endemic areas and has demonstrated schistosomiasis prevalence at rates much higher than those determined by microscopy, serology, and nucleic acid-based gold standards.^{75,78–80}

The workflow of the CAA assay in its current form, however, differs from a typical field-ready test. First, a trichloroacetic acid (TCA) extraction is performed on a urine or serum sample, requiring a centrifugation step. The extract supernatant is then combined with running buffer and anti-CAA-functionalized UCP particles and incubated for 1 hr at 37°C before the lateral flow strip is added to the solution. The test is allowed to develop and must dry completely (at least 3 hrs) before scanning and analyzing the strip.

To increase the analytical sensitivity of the assay, Corstjens et al. added a spin-filter concentration step to the sample preparation method.⁷⁵ This allowed for CAA in urine sample volumes of 0.5 - 7.5 ml to be concentrated into 20 µl before addition to the lateral flow strip. The resulting detection limits improved at a rate that scaled with increasing sample volumes, reaching as low as 0.03 pg/ml for the 7.5 ml assay. To demonstrate clinical applicability, the concentration step was performed on 2-ml patient urine samples from Kenya (high-endemic, *S. mansoni*) and China (low-endemic, *S. japonicum*). In both cases, the high-volume UCP assay for CAA detected more schistosomiasis cases compared to Kato-Katz, with a 2-fold increase in measured prevalence in the high-endemic area and a 6-fold increase in the low-endemic area.^{75,79} Though this sample concentration step improves the sensitivity of the assay, it requires significant laboratory infrastructure; all patient samples in these studies were processed in well-equipped tertiary laboratories. Further, the additional concentration step increases the cost of this ultrasensitive CAA assay, though sample pooling could make this test more cost-effective and allow for monitoring of worm burdens at the sub-population level for large-scale surveillance.⁸¹ However, it is clear that

for this UCP-based ultrasensitive assay to be utilized in a field setting, a more robust, field-ready sample preparation method is needed. The present work aims to fill this need by developing a sample preparation method that requires less laboratory infrastructure.

Scope of this Work

In this work, each of the components of the conventional diagnostic format is examined and optimized with the goal of improving diagnosis of malaria and schistosomiasis in endemic settings. In **Chapter II**, the effects of sample matrix effects on malaria diagnostics are evaluated and mitigated. More specifically, the extent to which the host immune response affects detection of malarial biomarker HRP2 in a low-transmission setting is determined, and strategies for reducing this potential matrix effect are evaluated. **Chapter III** explores a novel, equipment-free sample preparation method in which dendrimer-coated magnetic particles are used to capture, purify, and concentrate the CAA biomarker from its variable urine sample matrix before application to the ultrasensitive UCP lateral flow assay. In **Chapter IV**, the affinities of molecular recognition elements for two malarial biomarkers, HRP2 and *pLDH*, are screened using biolayer interferometry. **Chapter V** employs these data to inform the development of highly sensitive magnetic bead-based assays for both biomarkers, ultimately resulting in a rapid multiplexed assay in which detection of both *pLDH* and HRP2 can be completed in less than 1 hour with detection limits 10 times better than commercially available ELISA kits. In **Chapter VI**, the developed assay is applied to the characterization of *pLDH* and HRP2 clearance patterns in patients living in a highly endemic region of Zambia, demonstrating the sensitivity and clinical utility of the multiplexed assay.

CHAPTER II

EVIDENCE FOR HISTIDINE-RICH PROTEIN 2 IMMUNE COMPLEX FORMATION IN SYMPTOMATIC MALARIA PATIENTS IN SOUTHERN ZAMBIA

Introduction

Approximately 75% of malaria RDTs delivered in 2016 detected only *Plasmodium falciparum*, which is the most prevalent species of human malaria and is responsible for the majority of severe malaria cases and mortality worldwide.⁸ Most RDTs specific for this species rely on the detection of HRP2, which was the first antigen targeted in commercial tests.⁸² As discussed in Chapter I, there are several disadvantages to using HRP2 as a singular malarial biomarker, including persistence after parasite clearance, which can result in false-positives, and the rising incidence of *pfhrp2* deletions, leading to false-negatives.

Added to these challenges are potential matrix effects that can result from biomolecules present in finger-prick whole blood samples applied to RDTs. Endogenous host antibodies are one class of biomolecules known to interfere with antibody-based detection methods such as enzyme linked immunoassays (ELISAs) and LFAs. For example, rheumatoid factor (RF) and human-anti-mouse antibodies (HAMA) have been shown to crosslink capture and detection antibodies in immunoassays, leading to false-positive results.⁸³ Endogenous host anti-HRP2 (α -HRP2) antibodies represent another possible source of interference, as they may bind the antigen before a sample is applied to a detection assay. Because HRP2 consists of a series of tandem repeat motifs, and therefore repeated epitopes, any endogenous α -HRP2 bound to the antigen could potentially block binding sites for assay capture and detection antibodies, resulting in decreased signal or even

false negative results. Although there is significant precedent for endogenous antibody interference with immunochromatographic detection of other infectious diseases, including HIV,^{84,85} dengue,^{86,87} and tuberculosis,^{88,89} only a handful of studies have been published on the potential effects of endogenous α -HRP2 antibodies on biomarker detectability.⁹⁰⁻⁹³ In the first of these studies, Biswas et al. measured HRP2 and α -HRP2 in the serum of patients in India with acute *P. falciparum* infections before treatment and over 28 days after treatment.⁹⁰ HRP2 decreased gradually over time, with HRP2-specific IgM following the same pattern. Anti-HRP2 IgG titres increased gradually over the 28 days. Importantly, 3 patients who were RDT-negative and microscopy-positive upon enrollment had significantly higher α -HRP2 IgM and IgG titres compared to the 42 RDT-positive individuals, indicating that the presence of these circulating antibodies could interfere with HRP2-specific RDTs.⁹⁰ More recently, Ho et al. found endogenous α -HRP2 antibodies were present in the plasma of 25% of symptomatic malaria patients from Cambodia, Nigeria, and the Philippines and 11% of asymptomatic individuals in the Solomon Islands.⁹² The group also found that incubating serum from high α -HRP2 titre individuals with in vitro parasite culture resulted in a marked decrease in RDT signal for several RDT brands.⁹² Both of these studies suggest that the humoral immune response against HRP2 could decrease the detectability of HRP2, resulting in false-negative RDT readings.

In direct contrast to the aforementioned reports, two investigations have found an absence of endogenous α -HRP2 antibodies in patients from malaria-endemic regions. In a study aimed to determine the immunomodulatory properties of the biomarker, Das et al. found that PBMCs isolated from *P. falciparum*-exposed patients in India did not produce a detectable HRP2-specific antibody response when stimulated with the antigen.⁹¹ Most recently, Taylor et al. evaluated plasma samples from Cameroonian individuals living in a region with high *P. falciparum*

transmission with the goal of determining the prevalence, class, subclass, and avidity of circulating α -HRP2 antibodies.⁹³ Although these patients had robust levels of antibodies specific for other *P. falciparum* antigens, including three malaria merozoite surface proteins (MSP1, MSP2, and MSP3), the levels of detectable circulating α -HRP2 antibodies were no different from those of malaria-naïve control patients from the United States.

These discordant results in the literature led us to investigate whether individuals living in a low-transmission region in Southern Zambia produce HRP2-specific antibodies that could interfere with HRP2 detection. However, unlike the four published studies, all of which detected freely available circulating α -HRP2 using a direct immunoassay format, this work specifically sought to determine whether patient samples contain HRP2 immune complexes. To do this, magnetic particles were used to isolate IgG and IgM (free and complexed) from patient sample dried blood spot (DBS) extracts. The captured antibodies were then exposed to denaturing immunoprecipitation conditions in order to release any complexed HRP2, which was subsequently measured by ELISA. Additionally, free HRP2 in untreated and heated DBS extracts was measured to determine whether signal could be enhanced by dissociating any immune complexes present.

Methods

Reagents and materials

Human Whole Blood (CPD) was purchased from Bioreclamation IVT (catalog no. HMWBCPD). Recombinant HRP2 protein (rcHRP2) was generously provided by PATH (Seattle, WA). *P. falciparum* D6 strain was cultured in-house. Dynabeads® Protein A, Dynabeads® Protein G, and Pierce Protein L Magnetic Particles were purchased from Fisher Scientific (10-002-D, 10-004-D, PI88850). Anti-HRP2 antibodies were purchased from Abcam (ab9203, ab9206, ab30384).

TMB One was purchased from Promega (G7431). 903 Protein Saver Cards were purchased from GE Healthcare Life Sciences (10534612). A Fisher Scientific Analog Vortex Mixer (02-215-365) was used for all vortexed incubations. A VWR Digital Dry Heat block (12621-086) with an external thermocouple (11301-112) was used for sample heating. Absorbance was measured on a Biotek Synergy H4 microplate reader (Vanderbilt University) or Biotek ELx808 microplate reader (Macha Research Trust). All other reagents and materials were purchased from either Fisher Scientific or Sigma Aldrich.

HRP2 enzyme-linked immunosorbent assay (ELISA)

A previously reported HRP2 ELISA protocol was employed.^{41,94} Briefly, 100 μ l of 1 μ g/ml α -HRP2 IgM (ab9206, clone PTL3) was added to the wells of an Immulon 2HB 96-well plate for 1 hr. After 3 washes with 1x phosphate buffered saline with 0.1% Tween-20 (PBST), the plate was blocked with 300 μ l of 5% BSA in PBST for 2 hrs. Standards and samples (100 μ l) in PBST with 0.1% BSA were then added to the plate for 2 hrs. Next, 100 μ l of 0.5 μ g/ml α -HRP2 conjugated to horseradish peroxidase (HRPx) (ab30384, clone MPFG55P) in PBST with 0.5% BSA was added for 1 hr while protected from light. Signal was generated using TMB One solution, and the reaction was stopped with 2M H₂SO₄ after 10 minutes. Absorbance was measured at 450 nm. For all ELISAs performed in this study, the average LOD was 0.012 pM \pm 0.004 pM rCHRP2. The average intra-assay variability was 3.4% and the inter-assay variability was 22%.

Dried blood spot (DBS) preparation and extraction

To prepare control mock DBS patient samples, in-house *P. falciparum* D6 culture (stock: 43,600 parasites/ μ l) and a high affinity α -HRP2 mouse monoclonal antibody (C1-13) were spiked

into whole blood to desired concentrations and spotted (10 μ l) onto Protein Saver 903 cards. The DBS were air-dried for a minimum of 4 hrs and a maximum of overnight. A modified 6.35 mm office hole-punch (Office Depot® #825232 with punch tray removed) was used to remove DBS from the cards. Five punches of clean DBS cards were performed between each sample punch to reduce cross-contamination. Each DBS was placed in a 2-ml microcentrifuge tube, and 300 μ l of PBST was added to each tube. The tubes were placed on a vortexer at maximum speed (3200 rpm) for 10 minutes and then a mini-centrifuge for 1 minute to remove bubbles. The supernatant was removed and reserved for analysis. For each sample, half of the DBS extract supernatant was added to a separate 2-ml microcentrifuge tube and placed on an 80°C heat block for 10 minutes. These heated samples were then allowed to cool to room temperature before ELISA analysis.

DBS ELISA

ELISA plates were prepared as described above. Heated and untreated DBS extracts were diluted 10-fold in PBST with 0.1% BSA, and 100 μ l of each diluted sample was placed on the plate in duplicate. Each plate also contained an rHRP2 standard curve (0 – 10 pM) in sample buffer. Incubation times, washes, and addition of detection antibody, HRPx substrate, and quenching solution were identical to the HRP2 ELISA protocol above. Signal was measured at 450 nm.

HRP2 immune complex pull-down assay

In order to determine the amount of HRP2 complexed with antibodies in each sample, 10 μ l of untreated DBS extract was added to 40 μ l of PBST in a 1.5-ml microcentrifuge tube. Next, 30 μ l of a 1:1:1 mixture (10 mg/ml) of Dynabeads® Protein G, Dynabeads® Protein A, and

Pierce™ Protein L magnetic beads was added to the diluted DBS extract, and samples were incubated on a vortexer (3200 rpm) for 10 minutes. Using a magnetic tube holder (Invitrogen MagnaRack CS15000), the supernatant was removed. Next, the magnetic beads were washed by vortexing with 50 µl of PBST, and the wash supernatant was removed using the magnetic tube holder. To elute any HRP2 complexed to antibodies captured by the beads, a classic denaturing immunoprecipitation protocol was followed: 40 µl of 0.5 M glycine buffer (pH 3) was added to the beads, which were vortexed and then placed on an 80°C heat block for 10 minutes. Using the magnetic rack, the supernatant was removed from the beads and placed in a 1.5-ml microcentrifuge tube before the addition of 15 µl 1M TRIS pH 8. After neutralization, 50 µl of ELISA sample buffer was added to each tube. This process was performed in duplicate for each sample. Thus two 100-µl neutralized and diluted samples were placed on an ELISA plate to measure HRP2 concentrations for each DBS sample. ELISAs were carried out as described above.

Study setting, patient recruitment, and ethics

Clinical DBS samples were collected in the catchment area of Macha Mission Hospital in Choma District, Southern Province, Zambia, a rural 1200 km² area where roughly 30,000 individuals live.¹⁶ In this region, there is a single rainy season from November through April in which malaria transmission peaks, though the prevalence of malaria has declined steadily over the last decade to less than 1%.^{95,96} Patients were enrolled into the present study from both passive and active surveillance settings. For the former, patients presenting to Macha Mission Hospital with fever (> 37.5°C) were prescribed a malaria RDT (SD Bioline Pf) according to Hospital protocol. After provision of written informed consent and completion of a questionnaire, capillary whole blood was collected by finger prick once the prescribed RDT was performed. In the case of minors

under 18 years of age, consent and survey responses were requested from a parent or guardian. As fever was a requirement for recruitment in the clinic, all patients providing samples in this setting were classified as symptomatic. 70 patients were enrolled in the Hospital setting in March and April 2017. In addition to the clinic setting, patients already enrolled in Step D of the reactive screen-and-treat efforts implemented in this area of Southern Province, Zambia were recruited for this study.⁹⁷ These patients were either known index malaria cases, living in the same household as an index case, or living in a household located within 140 m of an index case. Patients were recruited for this study only if they or a parent/guardian provided written informed consent. Finger prick capillary blood was collected after the prescribed RDT (SD Bioline Pf) for Step D surveillance was performed. In this reactive surveillance setting, 56 patients were enrolled in March – April 2017. A total of 126 samples were analyzed in this study. This study and all sample collection were performed under IRB approval (MRT IRB # E.2014.01v 4.0) and after approval for the study was granted by the Zambian National Health Research Authority (MH/101/23/10/1).

Patient sample DBS preparation and storage

Finger-prick whole blood samples were collected in 300 µl SAFE-T-FILL Capillary Blood Collection Tubes containing sodium citrate (Ram Scientific). Several 10 µl spots were placed on Protein Saver 903 cards and dried at room temperature overnight. Samples were either punched and analyzed the next morning or placed in a zip-lock bag with desiccant and stored at -80°C. All samples were analyzed in April and May 2017.

DNA extraction and PCR amplification

DNA was extracted from dried blood spots using the Chelex method as previously described,⁹⁸ with minor modifications. The spots were punched with a 6.35 mm hole punch directly into 1 ml of a 0.1% saponin solution and incubated at room temperature for 10 minutes. After discarding the supernatant, PBS was used to rinse the spot and 150 μ l of 2% Chelex-100 and 50 μ l of water were added. Samples were incubated at 100°C for 8 minutes. The tubes were centrifuged and the supernatant was collected. Samples were stored at -20°C. Real-time PCR to detect the *Plasmodium falciparum* 18S gene was performed with the previously described Fal-F⁹⁹ and Plasmo2-R primers and the Falc 6-carboxyfluorescein (FAM)-labeled probe.¹⁰⁰ The primers were used at a concentration of 200 nM each and the probe at 50 nM in QuantiFast Probe PCR Master Mix (Qiagen). Samples and controls were run in triplicate. A standard curve was included with each 96-well plate. Reactions were amplified and analyzed with the Roche Lightcycler 480 II using the following cycling conditions: initial denaturation at 95°C for 5 minutes and 45 cycles of 95°C for 10 seconds and 60°C for 30 seconds.

Determination of free and immune-complexed HRP2 in patient samples

When available, two DBS per patient sample were extracted. Half of the DBS supernatant was reserved (“untreated”), and the remainder was heated on an 80°C heat block for 10 minutes. 20 μ l of untreated DBS extract was used to determine the amount of HRP2 complexed with antibodies using the protein A/G/L extraction protocol described above in duplicate. Additionally, untreated and heated DBS extracts were diluted 10-fold in ELISA sample buffer, and a DBS ELISA was performed in duplicate as detailed above. Samples for which signal did not fall in the linear range were re-run at the appropriate dilutions. Note that in this manuscript, “free” HRP2

refers to HRP2 not bound in immune complexes regardless of whether it was solubilized in the plasma or originated from within infected erythrocytes.

Data analysis

HRP2 concentrations were interpolated from rcHRP2 standard curves run on each plate. Limits of detection were calculated as the concentration at which the absorbance was equal to $S_{blank} + 3SD_{blank}$. Intra- and inter-assay variability (%CV) were determined as the average relative standard deviation of duplicate measurements on a single plate and the average relative standard deviations of all measurements at each concentration on the standard curve across all assays performed over the duration of the study, respectively. All error bars represent the standard error of measurement. A paired t-test was used to determine whether the measurable [HRP2] was significantly different in untreated and heated samples ($\alpha = 0.05$). An individual sample was defined as “enhanced” if the concentration of HRP2 in the heated sample was greater than that in the untreated sample (One-sided t-test, $\alpha = 0.05$). A sample was determined to contain HRP2 complexed to IgG or IgM if the concentration measured in the protein A/G/L extraction protocol was different from the limit of detection of the HRP2 ELISA (Student’s t-test, $\alpha = 0.05$).

Results

Dissociation of pre-formed HRP2 immune complexes

A series of laboratory controls were performed before analysis of patient samples. First, rcHRP2 was incubated with varying equivalents of a mouse monoclonal antibody (clone C1-13), which was previously shown to have excellent affinity for rcHRP2.¹⁰¹ A portion of these HRP2-antibody mixtures was then placed on an 80°C heat block for 20 minutes, and the detectable HRP2

concentrations in both untreated and heated samples were measured by ELISA. The C1-13 clone was not employed in the ELISA protocol. As shown in Figure 4, α -HRP2 antibodies interfere with ELISA detection of HRP2 by forming immune complexes. Heating samples at 80°C dissociates these complexes and completely restores ELISA signal, regardless of α -HRP2 excess. This dissociation was found to be irreversible. Fully restored HRP2 ELISA signal was maintained even after allowing dissociated samples to cool for several hours. This is consistent with the literature; Leow et al. reported the melting temperature of C1-13 as 72°C, and the rapid rate of heating in this experiment (i.e. placing samples directly on an 80°C heat block) likely resulted in irreversible precipitation of the denatured IgG.^{102,103} Additional optimization found that 5 minutes heating time was sufficient to fully dissociate complexes, so a final heating time of 10 minutes was chosen for further experiments.

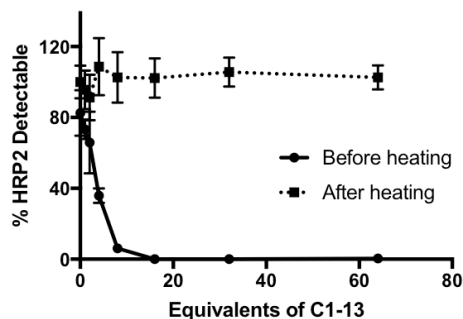


Figure 4. Increasing equivalents of α -HRP2 antibodies reduced free HRP2 detectable by ELISA by forming immune complexes. Heating samples at 80°C for 20 minutes dissociated these complexes, completely restoring ELISA signal, regardless of α -HRP2 excess.

Optimization of HRP2 immune complex pull-down assay

A pull-down assay was developed to determine the quantity of HRP2 complexed with antibodies in a given sample. Magnetic particles functionalized with proteins A, G, and L were incubated with diluted DBS extracts in order to capture all IgG and IgM from a sample. These

beads were washed with buffer before they were subjected to denaturing immunoprecipitation conditions (0.5 M glycine, 80°C for 10 minutes) in order to release any complexed HRP2. The supernatant was removed and neutralized with TRIS buffer, and HRP2 was quantified by ELISA. To optimize this process, rcHRP2 (500 pM) and 20 equivalents of C1-13 (10 nM) were spiked into whole blood, incubated for 10 minutes to allow immune complex formation, and spotted onto DBS cards. It was found that DBS extracts required a minimum 5-fold dilution in order to maximize HRP2 capture, and multiple bead mixing techniques (vortexer, orbital microplate shaker, and rotisserie) were found to perform similarly to one another (Figure 5A and 5B). The final optimized system successfully captured 90% of HRP2 in the sample, and the immunoprecipitation protocol released about 70% of the eluted biomarker. Thus, the pull-down assay successfully detected approximately 60% of HRP2 when all antigen was bound in immune complexes (Figure 5C).

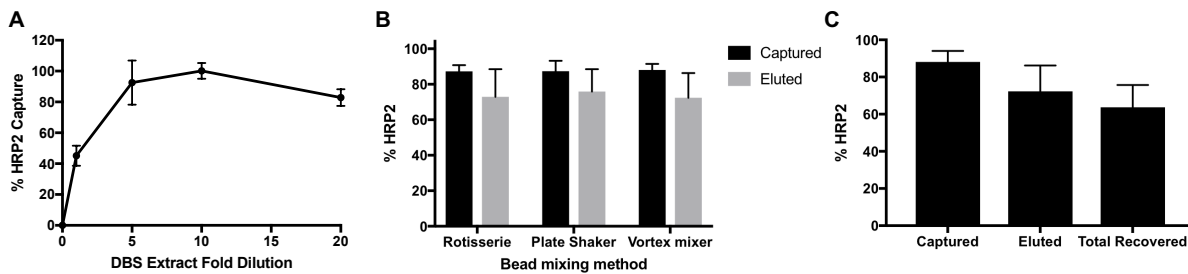


Figure 5. Optimization and characterization of HRP2 immune complex pull-down assay. (A) A minimum DBS extract dilution of 5x was required in order to ensure efficient immune complex capture. (B) Several bead-mixing methods were equivalent in performance. (C) Using the optimized conditions for the immune complex pull-down assay, 90% of complexed HRP2 was captured and 70% of the captured biomarker was eluted, resulting in an overall recovery of about 60%. In these samples, all detectable HRP2 was initially complexed to C1-13.

Evaluation of immune complex dissociation and pull-down assay in mock patient samples

In order to evaluate the optimized immune complex dissociation and pull-down protocols, a panel of mock patient samples was prepared by spiking in-house D6 *P. falciparum* culture and C1-13 antibodies into human whole blood. The panel of mock samples was designed to test the

limits of the optimized systems and included the following whole blood controls: (1) no parasites and no C1-13, (2) no parasites with C1-13 (50 nM) (2) varied parasite concentration (up to 6400 parasites/ μ l) and no C1-13, (3) constant parasite concentration (2000 parasites/ μ l) with varied C1-13 (up to 100 nM), and (4) varied parasite concentration with constant C1-13 (50 nM). These whole blood samples were incubated for 10 minutes to allow any HRP2 immune complexes to form before spotting onto DBS cards. After drying, DBS samples were punched and analyzed according to the optimized dissociation and pull-down protocols. Untreated and heated samples were diluted 10-fold before HRP2 quantitation by ELISA.

As shown in Figure 6A, in the absence of C1-13 α -HRP2, no HRP2 was detected in the immune complex pull-down assay, even at high parasite densities. Importantly, this demonstrates that only HRP2 complexed to α -HRP2 antibodies and *not* free HRP2 is pulled down in the bead-based assay, regardless of the magnitude of HRP2 concentration present. The data in Figure 6A also demonstrate that no signal is lost when samples containing only free HRP2 are subjected to heating. Additionally, the immune complex pull-down assay worked well over a broad range of α -HRP2 C1-13 concentrations and that dissociating complexed samples by heating completely restored positive signal (Figure 6B). The pull-down assay also demonstrated the expected 60% HRP2 recovery over a broad range of parasite concentrations in the presence of excess C1-13 (Figure 6C). Taken together, these data show that the optimized protocols behaved as expected for all controls in samples that closely mimicked patient dried blood spot samples.

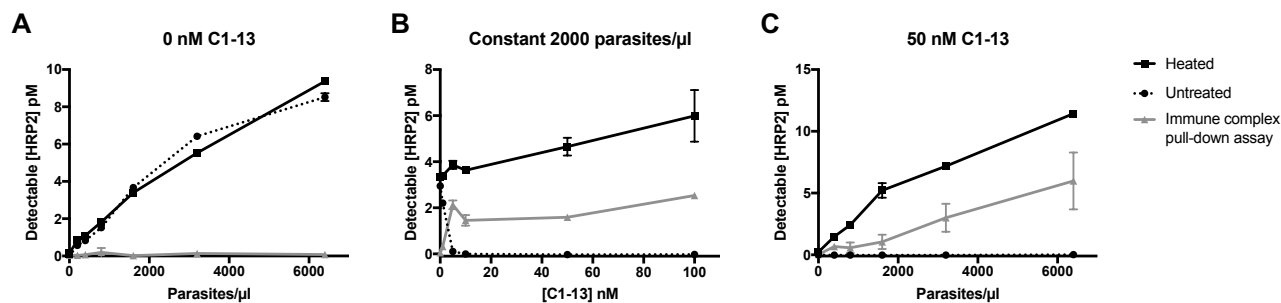


Figure 6. Evaluation of optimized immune complex dissociation protocol and pull-down assay in mock patient samples. (A) In the absence of α -HRP2 antibodies, no HRP2 was detectable in the immune complex pull-down assay. Additionally, heating free HRP2 did not diminish ELISA signal. (B) Increasing equivalents of α -HRP2 C1-13 decreased ELISA signal, but heating fully restored that signal. (C) Immune complex pull-down recovered 60% of complexed HRP2 over a wide range of parasite concentrations.

Patient demographics

A total of 126 patient samples were collected for this study. The patients recruited at the hospital were significantly younger than those recruited through active case detection ($P = 0.010$). All patients who presented to the hospital (passive case detection) were symptomatic at the time of sample collection. Only two patients recruited through active case detection had active *P. falciparum* infections (determined by PCR) and one of these patients reported no symptoms at the time of sample collection. Of the parasite-positive individuals, samples collected from the hospital generally had higher parasite densities (median: 6072, range: 59 – 161764 parasites/ μ l) than those of individuals recruited through active case detection (median: 255, range 84 – 426 parasites/ μ l), though no statistical significance was determined due to the low number of parasitemic patients recruited through active case detection.

Table 1. Patient samples stratified by collection strategy, parasite presence, and detectable free HRP2

Sample collection strategy	n	Age (Years)		No active <i>P. falciparum</i> infection - PCR (-), n (%)		Active <i>P. falciparum</i> infection - PCR (+), n (%)	
		Median	Range	HRP2 (-)	HRP2 (+)	HRP2 (-)	HRP2 (+)
Passive case detection	70	4	0 - 67	50 (71)	4 (6)	0 (0)	16 (23)
Active case detection	56	12.5	0 - 74	46 (82)	8 (14)	0 (0)	2 (4)
Total	126	8.5	0 - 74	96 (76)	12 (10)	0 (0)	18 (14)

Free HRP2 levels in untreated and heated patient DBS extracts

Free HRP2 was quantified for all available patient samples. As shown in Table 1, 96 (76%) recruited patients had no active *P. falciparum* malaria and no detectable free HRP2. The remaining 30 samples (24%) were HRP2-positive, 12 of which were parasitemic according to PCR. All individuals with an active *P. falciparum* infection had detectable HRP2 levels. Overall, a positive association between parasitemia and detectable free HRP2 was found (Spearman coefficient: 0.7563, $P < 0.0001$) (Figure 7A). There were no significant differences in parasitemias nor [HRP2] by one-way ANOVA ($P = 0.3069$, $P = 0.4235$, respectively) when the data were classified by the following age groups: < 5 years old, 5 – 15 years old, and > 15 years old. (Figure 7B and 7C). The results of heating DBS extracts are shown in Figure 8A. Heating DBS extracts did not result in an overall higher concentration of detectable HRP2 compared to untreated samples (Paired t-test, $P = 0.1333$). On an individual level, a significant increase in detectable HRP2 was observed in 7 patient samples ($P < 0.05$). These patients with enhanced HRP2 signal fell into a wide age range from 1 – 52 years old, though the median age was 6 years old. All patients for which HRP2 detectability in DBS extracts was significantly enhanced by heating were parasitemic, and the initial free [HRP2] in the corresponding DBS extracts was greater than 600 pM. Among these 7 samples, the average

signal enhancement factor was 1.2 ± 0.2 . In other words, in these samples, 20% more HRP2 was detectable in the heated samples compared to the untreated samples.

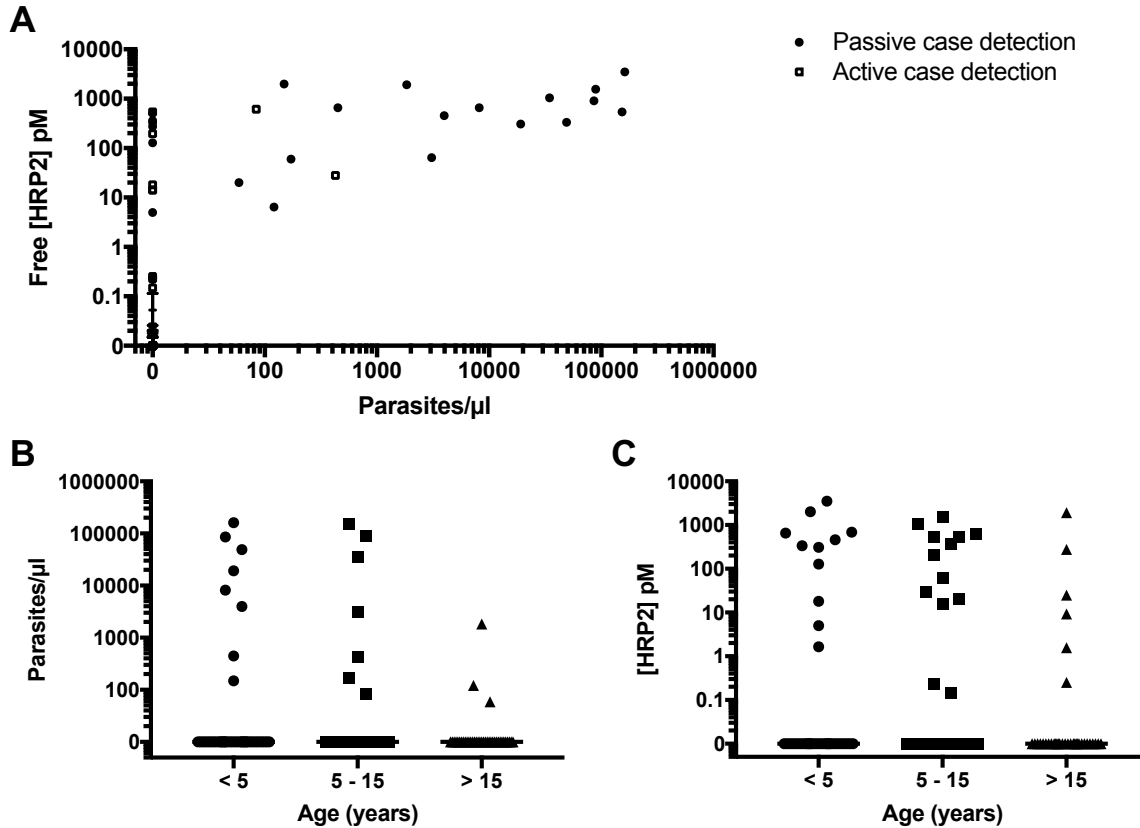


Figure 7. Free HRP2 levels in patient samples. (A) A significant positive association between free [HRP2] and parasitemia at the time of sample collection was found. (B) Parasitemia and (C) [HRP2] binned by age group. No significant differences were found between age groups.

HRP2 present in immune complexes in patient sample DBS extracts

Due to inadequate sample volume, the immune complex pull-down assay was performed on 111/126 DBS samples. Immune-complexed HRP2 was detected in the DBS extracts of 20 patient samples, which represents 18% of all samples evaluated and 69% of samples with detectable free HRP2. As shown in Table 2, a majority of the samples containing immune-complexed HRP2 were also positive for free HRP2 (90%) and had detectable parasitemia (60%). Only 6 (30%) of the samples found to contain immune-complexed HRP2 were collected in the

active case detection setting. The DBS sample for the sole individual in this study with an asymptomatic active *P. falciparum* infection contained immune-complexed HRP2. Notably, 2 samples for which no free HRP2 and no active *P. falciparum* infection were detected contained complexed HRP2, albeit at very low, but detectable, levels (1.6 ± 0.05 pM). Among the samples containing complexed HRP2, there was a significant and strong negative association between the total [HRP2] (free [HRP2] + complexed [HRP2]) and the percent of total [HRP2] present in immune complexes (Spearman coefficient: -0.8281 , $P < 0.0001$) (Figure 8B). The median percent of total [HRP2] present in immune complexes was 1.7% (range: 0.2% - 100%). As visualized in Figure 8B, the percent of total HRP2 present in immune complexes was less than 10% for most patient samples containing HRP2 immune complexes. However, for 5 patient samples, more than 20% of total HRP2 was present in immune-complexed form. No significant differences in the percent total [HRP2] present in immune complexes was found when the data were binned by age group ($P = 0.2035$) (Figure 8C and 8D). All patient sample data is presented in Appendix A.

Table 2. Samples stratified by parasite presence, detectable free HRP2, and detectable complexed HRP2.

	n	No active <i>P. falciparum</i> infection - PCR (-), n (%)		Active <i>P. falciparum</i> infection - PCR (+), n (%)	
		HRP2 (-)	HRP2 (+)	HRP2 (-)	HRP2 (+)
Immune-complexed HRP2 detected	20	2 (10)	6 (30)	0 (0)	12 (60)
No immune-complexed HRP2 detected	91	83 (91)	6 (7)	0 (0)	2 (2)
Total	111	85 (76)	12 (11)	0 (0)	14 (13)

Immune-complexed HRP2 was not found in 8/26 samples with detectable HRP2 in untreated DBS extracts. Most (75%) of these were from patients who did not have detectable parasitemia at the time of sample collection, though the average free [HRP2] in this group was not significantly different from samples in which complexed HRP2 was detected ($P = 0.3709$). In the

context of the heat dissociation results, free HRP2 signal was significantly enhanced after heating for only 5 (25%) of the samples with detectable immune-complexed HRP2. This discrepancy could arise from the fact that, for many samples with immune-complexed HRP2, the percent of total [HRP2] in complexed form was so low that differences in [HRP2] after dissociation could not be distinguished by duplicate ELISA measurements.

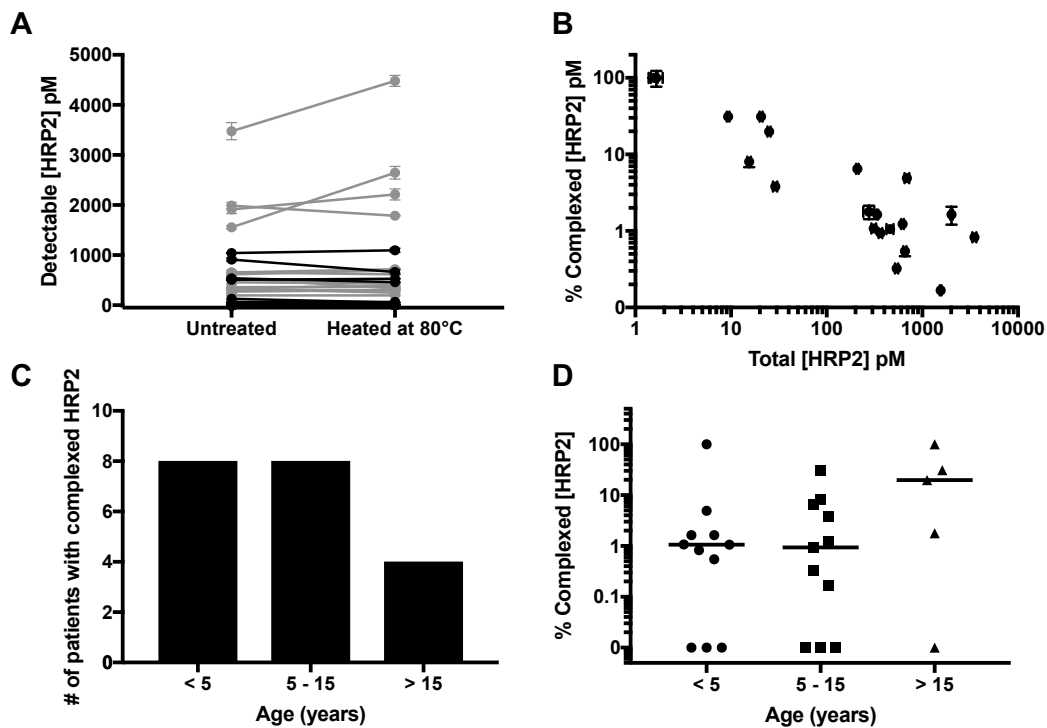


Figure 8. Dissociation and pull-down of HRP2 immune complexes in patient samples from rural Southern Zambia. (A) Heat dissociation of HRP2 immune complexes did not result in a statistically significant overall enhancement effect. Grey color indicates samples in which immune complexed HRP2 was detected using the pull-down assay. (B) Samples with lower total [HRP2] had a greater percentage of HRP2 present in immune complexes. (C) Number of patients with immune-complexed HRP2, binned by age group. (D) Percent of total HRP2 present in immune complexes, binned by age. Horizontal bars are median values.

Discussion

Because HRP2 is so frequently used as a biomarker for *P. falciparum* malaria, it is imperative to thoroughly investigate potential matrix interferants that could result in false-positive

or false-negative results in a diagnostic format. Recent conflicting reports call into question whether circulating α -HRP2 antibodies are present in human host circulation and if they could interfere with HRP2 detection on malaria RDTs. Biswas et al. and Ho et al. found circulating α -HRP2 antibodies in patient samples from a variety of endemic areas.^{90,92} In contrast, Taylor et al. found no circulating α -HRP2 in patients from a high-transmission region in Cameroon, and Das et al. found that HRP2 did not stimulate production of α -HRP2 in PBMCs isolated from *P. falciparum*-positive patients from India.^{91,93} Shared among all of these reports is that the presence or absence of freely circulating α -HRP2 was measured in a direct immunoassay format, in which recombinant HRP2 was employed as a capture reagent, and enzyme-conjugated α -human detection antibodies were used to generate signal. There are a couple disadvantages to this approach. First, while the presence of circulating α -HRP2 antibodies suggests the antigen may be present in immune complexed form, it does not guarantee that this is the case. Immune-complexed antigens could be only transiently present and rapidly cleared by phagocytes. Second, the absence of detectable, freely circulating α -HRP2 does not exclude the possibility that immune-complexed antigen may be present, especially in the case when the antigen concentration is very high. Indeed, Ho et al. found that samples with low HRP2 concentrations generally had greater free circulating α -HRP2 than those with high levels of HRP2.⁹²

For these reasons, we approached the question of endogenous α -HRP2 interference from a new angle and sought to directly interrogate the presence or absence of HRP2-containing immune complexes, rather than freely circulating α -HRP2 antibodies, in patient samples. To this end, two assays were developed and optimized in this work. First, an immune complex dissociation strategy was developed based on the observation that rapidly heating DBS extracts to 80°C permanently dissociated HRP2 immune complexes. In this assay, the concentration of free HRP2 in DBS

extracts was measured before and after heating. For mock samples consisting of DBS spotted with parasitized whole blood, HRP2 ELISA signal was completely diminished when α -HRP2 antibodies were present in excess greater than 10-fold; however, heat-based dissociation fully recovered HRP2 ELISA signal. Additionally, heating did not diminish HRP2 signal in the absence of α -HRP2. When this protocol was applied to patient DBS and paired samples were evaluated individually, HRP2 ELISA signal was found to be enhanced after heating for 7 patients, with an average enhancement factor of 1.2 ± 0.2 . However, no overall significant difference was found between untreated and heated samples, even for the subset of samples in which immune-complexed HRP2 was found. This could be due to the fact that, in many samples containing complexes, only a small percentage of the total HRP2 was in complexed form, a difference that may not be discernable by duplicate ELISA measurements. Additionally, it is possible that other known interferants, such as rheumatoid factor (RF) and human α -mouse antibodies (HAMA), which can falsely elevate ELISA signal, were denatured as a result of heating, resulting in no net enhancement. Thus, simply heating samples did not prove to be effective for enhancing overall HRP2 detectability for all samples containing immune complexed biomarker, and further investigation into effective dissociation methods should be considered.

The second developed assay employed protein A, protein G, and protein L-functionalized magnetic particles to isolate IgG and IgM from patient DBS sample extracts. After washing the particles to remove any nonspecifically bound material, a denaturing immunoprecipitation protocol was applied to release any HRP2 from immune complexes that bound to the particles. The resulting HRP2 signal was measured by ELISA. In mock patient samples, this protocol was found to recover 60% of immune-complexed HRP2. Importantly, in parasitized whole blood DBS samples, HRP2 was detectable by this method if and only if α -HRP2 antibodies were present.

When this pull-down assay was applied to patient DBS, 20 samples were found to have detectable immune-complexed HRP2, representing 18% of all samples and 69% of samples containing free HRP2. Eight samples containing free HRP2 did not have detectable complexed HRP2, most of which (75%) were not parasitemic. A majority (60%) of samples with immune-complexed HRP2 had parasitemias detectable by PCR, and nearly all of them (90%) also contained free HRP2. Although most patients without immune-complexed HRP2 did not have active *P. falciparum* infections and a majority of patients with immune-complexed HRP2 did have active infections, larger sample sizes are needed to determine if these trends are significant. For three quarters of patients with immune-complexed HRP2, less than 10% of the total HRP2 present was in complexed form (Figure 9). There are three potential explanations for this. First is the possibility that HRP2 concentrations in these samples were vastly greater than the concentration of α -HRP2. Although this seems unlikely, since freely circulating α -HRP2 has been detected in previous studies, it could explain why Taylor et al. did not find detectable levels of α -HRP2 in their study population. Second, HRP2 tagged with endogenous α -HRP2 may be rapidly cleared by phagocytes, thus reducing the relative amount of complexed HRP2 in a sample. The high number of repeated epitopes on HRP2 suggests that this antigen could result in large immune complexes, which rapidly trigger phagocytic clearance.¹⁰⁴ Third, freely circulating α -HRP2 antibodies can only access and bind soluble HRP2, which has been found to represent just a portion of total HRP2 with in vitro studies.³⁸

Importantly, some samples (5) had a large proportion ($\geq 20\%$) of total HRP2 present in immune complexes (Figure 9). Two samples (VZH130 and VZH133) with detectable immune-complexed HRP2 had no detectable free HRP2, which suggests all HRP2 present in these samples was complexed by α -HRP2. Two of the patients with a high proportion of complexed HRP2 had

active *P. falciparum* infections (VZH125 and VZH128). In the context of HRP2-based detection by malaria RDT, such a high proportion of complexed HRP2 is worrisome. For example, Scherr et al. found that the visual limit of detection for one brand of malaria RDT was 12.5 - 100 parasites/ μ l of in vitro parasite culture, depending on the experience of the reader.¹⁰⁵ This corresponds to 6 - 50 pM of rcHRP2 used in this study. In this regime, a decrease in detectable HRP2 of 20% or more could be the difference between a reader categorizing a test as positive or negative. It is important to note, however, that many of the samples (40%) that contained immune complexed HRP2 were from patients without detectable *P. falciparum* infections. Thus, although integrating an immune complex dissociation step into the diagnostic workflow would likely improve sensitivity, specificity may suffer due to an increase in detectable, persistent HRP2 in patients with resolved infections.

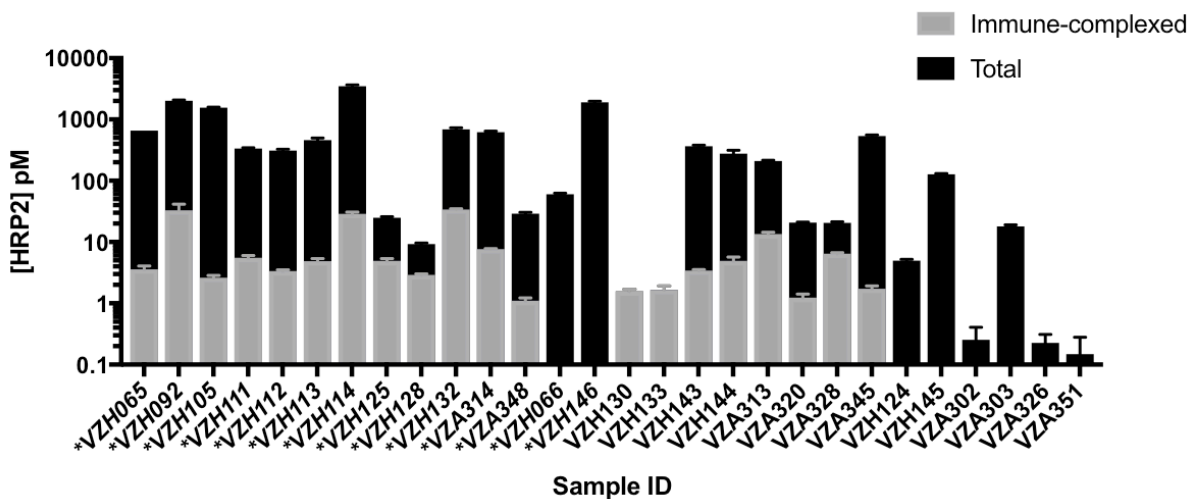


Figure 9. Concentrations of immune-complexed and total HRP2 in all HRP2-positive samples evaluated using the immune-complex pull-down assay. Note that the y-axis is on a logarithmic scale. Sample IDs preceded by asterisks represent patients infected with *P. falciparum* parasites detected by PCR.

One limitation of this study is that the recovery of the immune complex pull-down assay was found to be 60% in mock patient samples. Thus, the complexed [HRP2] reported herein could

underestimate of the true complexed HRP2 concentrations, and potential implications on HRP2 malaria RDTs could be even greater than what is reported here.

The techniques used in this work to evaluate whether HRP2-containing immune complexes are present represent unique and valuable tools for further studies. Ideally, future investigations of α -HRP2 interference with malaria detection would couple detection of free and immune-complexed HRP2, as reported herein, with detection and characterization of freely circulating α -HRP2 antibodies as performed in previous studies. This would provide a full picture of the conditions that could potentially lead to significant interference with malaria detection. In fact, we attempted to develop direct immunoassays for α -HRP2 antibody detection. However, even with assay conditions similar to those of Biswas et al. and Ho et al., we found high and variable background when DBS extracts from non-endemic US control samples were tested. Because of this, we felt it unlikely that circulating α -HRP2 antibodies could be reliably quantified in endemic patient DBS samples using the conditions tested. The bead-based α -HRP2 assays presented by Taylor et al. also show high and variable background signal in non-endemic US control samples, confounding the results for endemic patient samples.⁹³ Thus, future work on developing a reliable assay for α -HRP2 detection and characterization will be important for gaining a full understanding of the human host immune response to HRP2.

Future studies should also investigate the implications of HRP2 immune complexes in the asymptomatic malaria-infected population. In this study, all but one patient with active *P. falciparum* infection were symptomatic. Thus, this study effectively excludes the asymptomatic malaria-infected population, which is thought to contribute significantly to transmission in some settings.²⁷ In the asymptomatic population, false-negative results caused by immune-complexed

HRP2 on malaria RDTs could be a serious threat to elimination campaigns and, thus, should be investigated further in future studies.

Conclusion

Overall, we have developed unique methodology for the detection of immune complexed HRP2 and demonstrated its utility in patient DBS samples. The data presented here provide evidence that endogenous α -HRP2 antibodies form immune complexes with HRP2 in the symptomatic patient population of a low-transmission area in rural Southern Zambia. In many patients with immune-complexed HRP2, the proportion of complexed HRP2 was low compared to the total HRP2 present. However, for several patients, more than 20% of the total HRP2 present in the sample was in immune-complexed form and therefore, likely not detectable on malaria RDTs. For these patients, the presence of α -HRP2 could have profound effects on whether false-negative malaria RDT results occur, and thus serious implications in surveillance and elimination settings. Future studies investigating the prevalence and proportion of immune-complexed HRP2 in asymptomatic individuals will be required to assess whether α -HRP2 affects RDT performance for this portion of the transmission reservoir.

Acknowledgements

First and foremost, I would like to thank the patients who participated in this study. This work would not have been possible without the Step D team and staff at Macha Mission Hospital, who aided with sample collection. Additionally, Macha Research Trust generously welcomed us to use their on-site laboratories. Thank you to Dr. Lwiindi Mudenda, Dr. Mindy Leelawong, Dr. Danielle Kimmel, Armin Nouroni, Saidon Mbambara, and Dr. Philip Thuma for contributing to

this work. The chapter is based on work supported by the Bill and Melinda Gates Foundation (OP1135840), PATH: Diagnostics for malaria elimination toward eradication (1758-00-06-00), the National Institute of Health/Fogarty International Center [D43 TW009348], Vanderbilt University through Laboratories for Innovation in Global Health Technologies, and the National Science Foundation Graduate Research Fellowship (C.F.M.) [DGE-1445197].

CHAPTER III

POLY(AMIDOAMINE)-COATED MAGNETIC PARTICLES FOR ENHANCED DETECTION OF *SCHISTOSOMA* CIRCULATING ANODIC ANTIGEN IN ENDEMIC URINE SAMPLES

Introduction

One of the simplest ways to improve the sensitivity of a diagnostic is to deliver more biomarker to the test. This principle is demonstrated in the work of Corstjens et al., discussed in Chapter I, which leveraged spin filter devices to concentrate CAA prior to performing the ultrasensitive UCP-based lateral flow assay (UCP-LF CAA). Theoretically, the easiest way to deliver more biomarkers to a lateral flow test would be to simply add a larger volume of sample. However, in their current structures, LFAs and other low-resource diagnostic formats cannot accommodate large sample volumes for several reasons.¹⁰⁶ First, limited bed volumes in porous paper substrates physically limits the amount of liquid a test can hold. Second, the increase in the number of interfering molecules that results from an increase in sample volume could result in nonspecific cross-reaction with molecular recognition elements on the test. Additionally, colored biological matrices, such as whole blood, can increase the background signal of the test and decrease the user's ability to distinguish between positive and negative results. Sample preparation techniques that enable biomarker enrichment not only allow for concentration of a target from a large-volume sample, delivering an increased amount of biomarker to the test, but also remove the target from its original, complex biological matrix. Thus, the development of low-cost, field-

friendly sample preparation methods could have a drastic impact on the overall performance of diagnostic tests in low-resource settings.

In the shift from morbidity control to elimination, detection of low-burden *Schistosoma* infections at the point of care will become increasingly important. As such, there is a pressing need for highly sensitive schistosomiasis detection tools to be applicable in low-resource settings. As discussed in Chapter I, the ultrasensitive UCP-LF CAA test requires significant laboratory infrastructure to carry out the assay, particularly sample concentration. Several centrifugation steps are needed in order to perform the TCA extraction and concentrate large-volume samples. For samples 2 ml and greater, temperature-controlled centrifugation is needed. This limits the use of the ultrasensitive UCP-LF CAA assay in its current format to well-equipped reference laboratories or tertiary facilities. Thus, the utility of the ultrasensitive assay at the point of care depends on the development of alternative methods for concentration of CAA from urine samples.

To address this need, we developed an alternative large-volume urine sample preparation method for the UCP-LF CAA assay that requires little-to-no laboratory equipment. The new method relies on electrostatic interactions between magnetic particles functionalized with positively-charged poly(amidoamine) (PAMAM) dendrimers and negatively-charged CAA in urine. Once CAA was captured on the surface of the PAMAM-functionalized magnetic beads, which could be manipulated with an external magnet, the supernatant was removed, and CAA concentrated into a small volume with a high-salt elution buffer. This concentrated, CAA-containing eluate was subsequently applied to the UCP-LF CAA assay. The PAMAM bead-based sample concentration method achieved full theoretical enhancement compared to the unenhanced UCP-LF CAA protocol. Additionally, the method was successfully applied to a panel of 15 patient

samples and demonstrated equal performance compared to the laboratory-based spin column method.

Methods

Materials and reagents

Dynabeads® MyOne™ Carboxylic Acid magnetic particles were purchased from ThermoFisher Scientific (65012). All poly(amidoamine) dendrimers were purchased from Sigma-Aldrich. Proprietary mouse monoclonal anti-CAA antibodies (α -CAA; clone 147-3G4-A) were available from the Department of Parasitology, Leiden University Medical Center. Horseradish peroxidase (HRPx) was conjugated to α -CAA (α -CAA:HRPx) using EZ-Link™ Plus Activated Peroxidase Kit (ThermoFisher Scientific 31489). CAA standards were derived from the TCA-soluble fraction of *Schistosoma* adult worm antigen (AWA-TCA), which contains 3% w/w CAA.⁷⁷ TMB One was purchased from Promega (G7431). A Cole-Palmer vortex mixer (UX-04726-01) with a modified ThermoFisher 15mm tube-holder (88880122) was used for all vortexed incubations. Absorbance was measured on a Biotek Synergy H4 microplate reader (Vanderbilt University) or a MultiSkán™ FC Microplate Photometer (Leiden University Medical Center). All other reagents and materials were purchased from either Fisher Scientific or Sigma Aldrich.

Bead preparation

Dynabeads® MyOne™ Carboxylic Acid magnetic particles (1 ml, 10 mg/ml) were washed three times with 0.1M 2-(N-morpholino)ethanesulfonic acid (MES) pH 5. On the final wash, the supernatant was removed, and a 1 ml solution of 78 mM NHS, 31 mM EDC, and 78 μ M PAMAM generation 4.0 in 0.1M MES pH 5 was added to the beads, which were then vortexed and incubated

on a rotisserie for 2 hours at room temperature. Next, the beads were washed 3 times with 1 ml of MES pH 5 before a 15-minute incubation with 10 mM hydroxyl amine in MES pH 5. Finally, the beads were washed 3 times and re-suspended in MES pH5 with 0.1% Tween-20.

CAA enzyme-linked immunosorbent assay (ELISA)

The ELISA protocol for CAA detection was based on previous reports.^{107,108} Briefly, MaxiSorp plates (Thermo Scientific 430341) were coated with 75 μ l of 2 μ g/ml α -CAA in 1x phosphate buffered saline (PBS). The plate was then washed with 4 times with 150 μ l 20x diluted PBS before blocking with 100 μ l 0.33 mg/ml BSA in 1x PBS. After washing 4 times, 50- μ l samples were added to the plate. Next, the plate was washed 4 times, and incubated with 50 μ l of 1 μ g/ml α -CAA:HRPx. After washing, 100 μ l of TMB One Solution was added to the plate, and the reaction was quenched with 100 μ l 2M H₂SO₄ after 10 minutes. Absorbance was measured at 450 nm. Unless noted otherwise, all reagents were diluted in PBS with 0.3% Tween-20 and 0.1% bovine serum albumin (PBST with 0.1% BSA). All incubation steps were carried out on a heated plate shaker for 15 minutes. Standard curves consisting of serial dilutions of AWA-TCA were included on each plate to enable CAA quantitation.

UCP-LF CAA assay (UCAA10)

The UCP-based lateral flow assay for CAA was performed as previously described.⁷⁴ Briefly, 50 μ l 4% TCA was added to an equal volume of urine in a 1.5 ml microcentrifuge tube, vortexed, incubated for 5 minutes, and subsequently centrifuged for 5 min at 13000 rpm. The α -CAA-functionalized 400 nm Y₂O₂S:Yb³⁺,Er³⁺ UCP particles were sonicated and diluted to 1 μ g/ml in UCP-LF CAA running buffer (200 mM Tris pH 8, 270 mM NaCl, 0.5% Tween-20, 1% BSA).

Next, 20 μl of the TCA extraction supernatant was combined with 100 μl of the prepared UCP particles in a 96-well plate and incubated on an orbital shaker at 37°C for 1 hr. Lateral flow strips with α -CAA test lines and α -mouse IgG control lines were added to the wells. The strips were allowed to develop and dry before scanning on a Packard FluoroCount microplate reader adapted with an IR laser (980 nm) modified to scan lateral flow strips. Emission was measured at 550 nm.

Enhancement of UCP-LF CAA assay with PAMAM-functionalized magnetic beads

To perform the bead-based enhancement protocol, 400 μl of 12% w/v trichloroacetic acid (TCA) was added to a 2-ml urine sample in a 5-ml microcentrifuge tube. The sample was then filtered through a 0.45 μm cellulose acetate syringe filter (VWR 28145-479) and neutralized with 200 μl 0.5 M Na_3PO_4 . Next, 50 μl of prepared PAMAM-functionalized magnetic beads (10 mg/ml) was added to the sample and vortexed for 5 minutes. Using a custom 3D-printed adaptor, a MagnaRack™ (Invitrogen) was used to separate magnetic particles and remove the supernatant. Next, 70 μl of UCP-LF CAA running buffer was added to the beads, which were then vortexed for 5 minutes for CAA elution. The resulting supernatant was then run according to the UCP-LF CAA protocol as described above, with the exception that 50 μl of 2 $\mu\text{g}/\text{ml}$ UCP particles was combined with the 70- μl magnetic bead eluate before subsequent incubation and addition of the lateral flow strips.

Analysis of patient samples

The patient urine samples analyzed in this study were collected in 1989 - 1990 for a previous study¹⁰⁸ and have since been stored at -20°C. Informed consent was obtained from all individuals who provided samples. In total, 15 patient samples were evaluated for the present

study. All patients were Egyptian males and fell within the age range of 10 - 49 years of age. All patient samples were processed using the bead enhancement protocol described above with the exception that samples were diluted 10-fold after neutralization. Thus, PAMAM-functionalized beads were added to 2 ml of 10x diluted samples. In addition to the bead enhancement protocol, all samples were processed using the standard UCAA10 protocol as well as a spin filter-based concentration protocol for comparison purposes. For the latter, 200 μ l of 4% TCA was added to an equal volume of urine, and the supernatant resulting from the TCA extraction was placed in a 0.5-ml spin filter with a 10 kDa molecular weight cut-off (Amicon Ultra, Millipore Sigma UFC5010BK). After concentration (15 min at 14000 x g), 20 μ l of concentrate was combined with 100 μ l of 1 μ g/ml UCP particles, and the UCP-LF CAA protocol was performed as usual. For all three protocols applied to patient samples, standard curves of AWA-TCA spiked in non-endemic control urine were processed simultaneously to calculate CAA concentrations. Additionally, urine reagent strips (LW Scientific URS-10) were used to determine the specific gravity of all patient samples.

Data analysis

For optimization experiments (signal measured by ELISA), CAA concentrations were interpolated from the line of best fit based on standard curves run on each plate. For the UCP-LF CAA, the areas of emission peaks on line scans were measured, and the test signal was defined as the ratio of the test line peak area to the control line peak area. All standard curves run on the UCP-LF CAA assay were fit with 4-parameter logistic curves, regardless of sample preparation method employed. Limits of detection were calculated as the concentration at which the assay signal was $S_{blank} + 3SD_{blank}$. All error bars represent the standard error of measurement.

Results

Optimization of PAMAM-functionalized magnetic beads

Several parameters of the PAMAM-functionalized beads were optimized to maximize CAA capture and recovery. For all optimization experiments, the CAA ELISA was used to measure biomarker capture and recovery. Capture efficiency was determined by measuring the difference in CAA concentration between the original AWA-TCA-spiked sample and the supernatant after incubation with PAMAM-functionalized particles. Percent recovery was calculated based on the ratio of CAA eluted from the beads in UCP-LF CAA running buffer and the original sample. Each ELISA plate also contained standard curves in the appropriate sample matrices, and CAA-negative controls were run for each condition tested during optimization.

The first parameter optimized was the size of PAMAM conjugated to the magnetic particles. The size of these iteratively synthesized and radially symmetric polymers is defined by generation (G), which is related to the number of terminal functionalities (n) such that $n = 2^{G+2}$. Thus, optimization of dendrimer size was performed by evaluating CAA capture efficiency of a panel of magnetic particles with PAMAM of varying generations, the concentrations of which were normalized to the number of terminal functionalities during bead functionalization. A constant bead volume (20 μ l) was incubated with 1 ml of 4 ng/ml CAA in PBST with 0.1% BSA for 5 minutes. As shown in Figure 10A, the smallest PAMAM size required for maximal CAA capture was G 4.0.

Next, the concentration of PAMAM G 4.0 in the bead conjugation reaction, and therefore the degree of bead surface functionalization, was optimized. Both CAA capture and elution were evaluated. As shown in Figure 10B, PAMAM G 4.0 maintained optimum capture efficiency at nearly all concentrations of dendrimer. However, recovery of CAA in the elution step was

optimum at low PAMAM 4.0 concentrations. Thus, the lowest PAMAM concentration tested, 78 μM , was chosen as the optimal dendrimer concentration for particle functionalization.

Finally, the total volume of beads required to fully capture and recover CAA from 2 ml of spiked, non-endemic control urine was determined. For this experiment, beads were functionalized with PAMAM G 4.0 at the optimum conditions determined above. Results confirmed that 50 μl of PAMAM-functionalized magnetic beads achieved full capture and recovery in 2-ml urine samples containing 1 ng/ml CAA (Figure 10C).

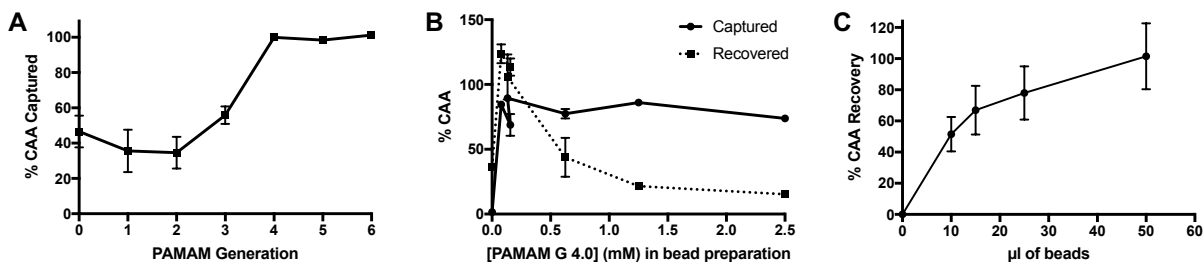


Figure 10. Optimization of PAMAM-functionalized magnetic particles. (A) Optimal dendrimer size was determined to be PAMAM G 4.0 for full CAA capture. (B) Extent of particle functionalization was found to significantly impact CAA elution, with lower surface densities more readily releasing CAA. (C) In 2-ml spiked urine samples, 50 μl of magnetic beads was required to fully recover CAA from solution.

Characterization of PAMAM bead robustness and stability

The stability and robustness of the PAMAM-functionalized magnetic beads were investigated in order to evaluate their applicability to point-of-care settings and tolerance of sample matrix variation. First, the stability of the PAMAM-functionalized beads in solution (MES pH 5 0.1% Tween-20) was studied over time for room temperature and 4 $^{\circ}\text{C}$ storage conditions. The functionalized particles effectively captured all CAA spiked into buffered solutions for the duration of time study (46 days) at both storage temperatures, demonstrating remarkable solution stability, even in ambient conditions (Figure 11A).

Next, the particle performance in variable matrices was determined, since urine is known to have variable pH values between 5 and 7, as well as a wide osmolality range of 38 - 1400 mOsm/kg H₂O. These variables, in particular, would be expected to influence the electrostatic interactions between positively-charged PAMAM and negatively-charged CAA. To determine the tolerance of the PAMAM-functionalized magnetic particles to changes in pH, AWA-TCA was spiked into phosphate buffers (10 mM) with pH values ranging from 4 to 10. As shown in Figure 11B, capture was maintained across all pH values tested. The good performance in basic solutions can be attributed, in part, to the high pK_a of 9.32 on the terminal amines on PAMAM G 4.0.¹⁰⁹ Additionally, while the pI of CAA has not been measured, the predicted pK_a of the β-D-glucopyranuronic acid portion of the disaccharide repeating unit on the proteoglycan biomarker is 2.78, which would account for the good performance observed in acidic solutions (ACD/Labs Software V11.02). Finally, the effect of increasing salt concentration on CAA capture was evaluated by adding NaCl into non-endemic control urine spiked with AWA-TCA. As shown in Figure 11C, when the salt concentration of urine was increased by 0.5 M or more, the capture efficiency of the PAMAM-functionalized magnetic particles was markedly decreased. This was likely due to the formation of a more diffuse double layer on the surface of the PAMAM-functionalized particles as a result of the increased electrolyte concentration. However, it should be noted that an increase of 0.5 M NaCl corresponds to an increase in osmolality of 1000 mOsm/kg

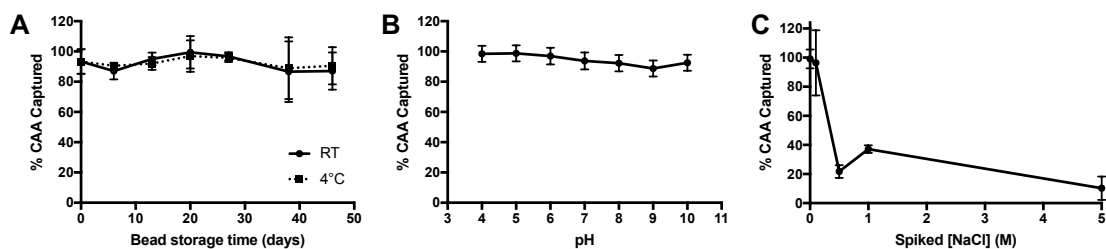


Figure 11. Evaluation of the stability and robustness of PAMAM-functionalized magnetic particles. (A) After 46 days of storage in solution at RT and 4°C, the beads maintained full CAA capture efficiency. (B) The PAMAM-based CAA capture was robust to variable pH. (C) High salt concentrations decrease CAA capture efficiency.

H₂O. Although the osmolality of the original urine sample is unknown, salt concentrations above the 0.5 M spiked sample would likely be considered abnormal.

Performance of magnetic bead-based CAA concentration protocol

After optimization and characterization, the PAMAM-functionalized magnetic particles were integrated with the UCP-LF CAA. This workflow required minimal laboratory equipment and could be completed with just 10 minutes of total incubation time. The performance of the bead-based CAA concentration was evaluated against the UCAA10 method in AWA-TCA-spiked non-endemic control urine samples. Similar to Corstjens et al., we found the limit of detection of the UCAA10 protocol to be 10 pg/ml.⁷⁵ Integration of the optimized PAMAM bead-based CAA concentration protocol resulted in a limit of detection of 0.050 pg/ml, achieving the full theoretical 200-fold enhancement expected (Figure 12).

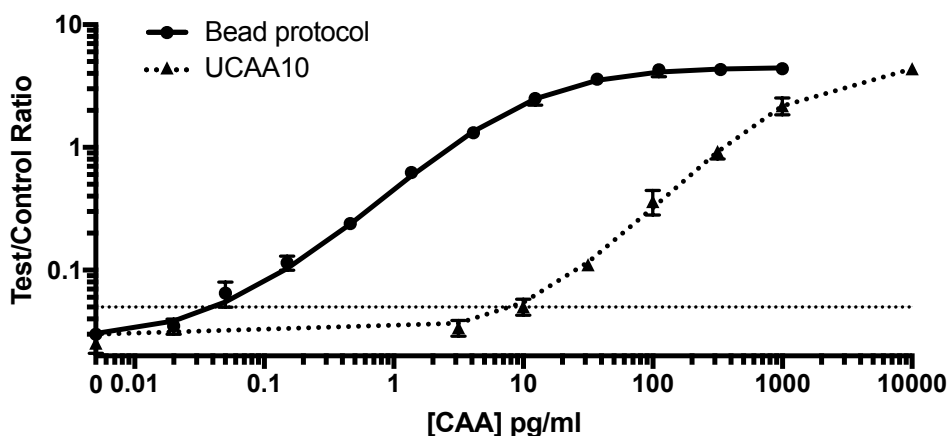


Figure 12. Performance of magnetic bead-based CAA concentration protocol. Standard curves for the UCAA10 and the PAMAM magnetic bead enhancement method, which successfully concentrated CAA from spiked 2-ml urine samples, achieving full theoretical improvement in LOD of 200x.

Patient sample analysis

Fifteen patient samples from Egypt were analyzed using three sample preparation methods: (1) the original UCAA10 protocol, (2) spin filter-based concentration (UCAA200), and (3)

PAMAM magnetic bead-based concentration protocol. Because the average specific gravity, which is known to correlate well with urine osmolality, of the patient samples (1.020 ± 0.007) was significantly greater than the non-endemic control urines (1.005) ($P < 0.0001$), patient samples were diluted 10-fold before the magnetic bead-based concentration protocol was performed.^{110,111} Because of this dilution, the theoretical enhancement possible for the bead-based protocol was 20-fold. As shown in Figure 13A, the full theoretical improvement of the LOD was achieved. Additionally, the standard curves for both the bead-based and spin-filter concentration methods aligned as expected, indicating that the two methods are equal in performance despite the large difference in laboratory infrastructure required.

Using the PAMAM magnetic bead protocol, UCP-LF CAA signal was enhanced compared to the UCAA10 for all but three patient samples tested (Figure 13B). The average signal enhancement factor was 22x across all samples, confirming the theoretical concentration limits of the system were reached. The 3 samples that were not enhanced were negative by UCAA10 and remained below the LOD after PAMAM-based concentration. Two UCAA10-negative samples were found to be positive after CAA concentration using the magnetic beads. Additionally, 4 patient samples with CAA concentrations at or near the UCAA10 LOD were found to be definitively positive after employing the magnetic bead concentration protocol. All PAMAM bead-based concentration results were confirmed using spin filters in a manner similar to previous reports,⁷⁵ and good agreement was found between the two methods (paired t-test, $P = 0.3008$) (Figure 13C).

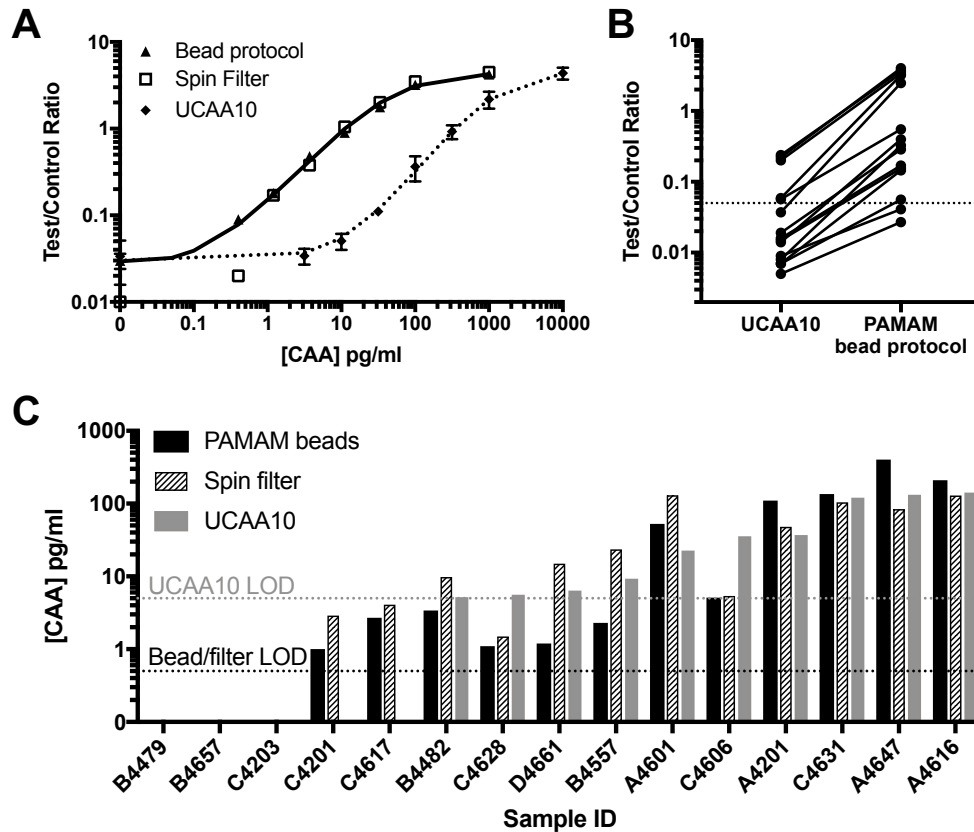


Figure 13. PAMAM-functionalized magnetic particles successfully concentrated CAA from patient samples. (A) The bead-based protocol performed similarly to spin filter methods in 10x diluted samples. (B) UCP-LF CAA signal was enhanced for all patient samples analyzed with an average enhancement factor of 22x. (C) Results from the bead-based CAA concentration method agreed with the spin filter method developed by Corstjens et al.

Discussion

Schistosomiasis diagnostic tests capable of detecting low-intensity infections are critical for accurate surveillance and precision mapping of infection prevalence. The UCP-LF CAA is a promising schistosomiasis diagnostic tool that derives its extremely high analytical sensitivity from three components: (1) high-affinity CAA-specific monoclonal antibodies, (2) upconverting phosphor particle labels that effectively eliminate background signal, and (3) a sample preparation step that concentrates CAA from a large volume sample into a smaller volume that can be applied to the test. However, the current protocol for CAA concentration employs spin filters, requiring laboratory infrastructure that prevents use of the UCP-LF CAA assay at the point of care.

To address this challenge, we have developed a more field-friendly method for CAA concentration from large-volume urine samples. The protocol relies on electrostatic interactions between the negatively-charged CAA biomarker and positively-charged PAMAM dendrimers functionalized to the surface of magnetic particles. These charge-based interactions occur in less than 5 minutes, after which an external magnet is used to remove the CAA-PAMAM-magnetic particle complexes from the large-volume (2-ml) sample and into a small-volume elution buffer. High salt concentration in the elution buffer disrupts the charge-based interactions between CAA and PAMAM, releasing CAA into solution. This concentrated CAA solution is then applied to the UCP-LF CAA test. The PAMAM-functionalized magnetic beads were found to be extremely stable in solution in varied storage conditions, and the protocol tolerated variation in sample pH. When applied to 2-ml CAA-spiked urine samples, the bead-based concentration protocol improved the detection limit of the UCP-LF CAA assay from 10 pg/ml to 0.05 pg/ml, achieving the full theoretical 200-fold enhancement factor and performing just as well as the more resource-intensive spin filter method.

The developed magnetic bead-based assay was then applied to 15 patient samples from Egypt. In order to achieve UCP-LF CAA signal enhancement, we found that the patient samples had to be diluted 10-fold. We hypothesize that high salt concentrations in undiluted endemic patient samples relative to non-endemic control urine disrupted the electrostatic interactions between PAMAM and CAA. Indeed, the average specific gravity, which correlates with urine osmolality,^{110,111} of the endemic patient samples was significantly higher than that of non-endemic control urine. Nonetheless, in 10x-diluted patient samples, the PAMAM-functionalized magnetic particles successfully concentrated CAA, resulting in an average UCP-LF CAA signal enhancement factor of 22x, indicating that this equipment-free protocol reached its full theoretical

potential. Additionally, the bead-based concentration method identified 2 positive samples that were otherwise negative according to the unenhanced UCAA10 protocol and provided definitively positive results for 4 samples which had CAA concentrations at or below the detection limits of the UCAA10. These data demonstrate that electrostatic interactions between positively-charged PAMAM dendrimers and the negatively-charged *Schistosoma* CAA biomarker can be leveraged for biomarker enrichment prior to detection on the UCP-LF CAA assay. This robust, magnetic-bead based strategy eliminates the need for laboratory infrastructure for urine sample preparation, bringing the ultrasensitive schistosomiasis detection one step closer to application at the point of care.

One limitation of this study was the relatively small patient sample population tested. Thus, the developed protocol must be validated on a larger set of samples in order to fully assess its diagnostic sensitivity and specificity. Additionally, while the use of magnetic beads eliminates the need for laboratory equipment for CAA concentration, the protocol requires many user steps. A device that fully integrates sample preparation step the lateral flow assay, similar to those developed by Davis et al. and Bauer et al., could fill the need to further simplify CAA concentration at the point of care.^{106,112} Additionally, PAMAM-functionalization of paper membranes (i.e. cellulose) could open the door to paper fluidic devices that combine the advantages of sample preparation and sensitive detection into a single integrated device applicable in a field setting.

Conclusion

We have developed a robust and equipment-free sample preparation method for concentration of the CAA biomarker for schistosomiasis that leverages electrostatic interactions between positively-charged PAMAM dendrimers and the negatively-charged proteoglycan

biomarker. When coupled with the highly sensitive UCP-LF CAA assay, this sample preparation method resulted in a 200-fold improvement in CAA, performing just as well as infrastructure-intensive spin filter methods. The developed method demonstrated full theoretical enhancement in patient samples, identifying 2 samples as positive that otherwise would have been considered negative on an unenhanced test. Thus, the PAMAM-functionalized magnetic bead-based CAA concentration method represents a promising step toward ultrasensitive schistosomiasis detection at the point of care.

Acknowledgements

This work would not have been possible without Dr. Govert van Dam and Dr. Paul Corstjens, who provided guidance, laboratory facilities, and patient samples (collected by Dr. Lisette van Lieshout). I would also like to acknowledge Claire Mommoser and Garrett Camps for their contributions to this work. Claudia J. de Dood (LUMC) prepared all UCP-LF CAA reagents and strip materials. Tom Scherr and Nick Adams designed and printed the custom magnetic rack adaptor. This work was supported by the Bill and Melinda Gates Foundation (OP1160703), Vanderbilt University through the Laboratories for Innovation in Global Health Technologies, Leiden University Medical Center, the National Science Foundation (NSF) Graduate Research Fellowship (DGE-1445197), and an international travel allowance through the NSF Graduate Research Opportunities Worldwide (GROW).

CHAPTER IV

BIOLAYER INTERFEROMETRY AS A TOOL FOR PREDICTING ELISA PERFORMANCE OF MONOCLONAL ANTIBODY PAIRS FOR TWO MALARIAL BIOMARKERS^b

Introduction

The performance of protein-based diagnostics depends heavily on the strength of the interactions between the target antigen and molecular recognition elements incorporated into the test, making optimization of this diagnostic component critical for development of high-sensitivity tests. Biolayer interferometry (BLI) is a label-free bioanalytical technique that can be used to quantify the strength of antibody-antigen interactions, enabling measurement of kinetic parameters such as the dissociation constant (K_D), on-rate constant (k_{on}), and off-rate constant (k_{off}).^{113,114} This optical technique allows for real-time monitoring of the interference pattern of white light reflected from two surfaces within fiber optic sensors that are immersed in biomolecule solutions. This experimental set-up is advantageous over evanescent (e.g. surface plasmon resonance) or acoustic label-free systems for characterization of biomolecular interactions, which typically require microfluidics to deliver the sample to the sensing surface. These systems are prone to clogging when complex sample matrices are used. Further, evanescent and acoustic measurements are prone to bulk signal shifts when the solution above the surface changes. Since BLI detection occurs at the biosensor tip surface, matrix effects, such as those from unbound proteins in solution, are minimized.¹¹⁴

^b Portions of this chapter have been previously published in Markwalter, C.F. et al., *Analytical Biochemistry*, 2017. 534: 10 - 13. © 2017 The Authors. Published by Elsevier Inc.

The crucial need for improved malaria diagnostics and laboratory assays and the reliance of these tools on the strength of antibody-antigen interactions highlight the importance of building these tests from the bottom up by selecting the very best molecular recognition elements for capture and detection. In this chapter, we assess the utility of biolayer interferometry as a tool for predicting antibody pair performance in an enzyme-linked immunosorbent assay (ELISA) for both HRP2 and recombinant *P. vivax* lactate dehydrogenase (rcPvLDH), the two most common protein targets for malaria diagnostics. To do this, novel monoclonal antibodies specific for HRP2 were developed, and their kinetic parameters were determined using BLI alongside commercially available clones. These kinetic parameters were compared to antibody pair performance in a sandwich ELISA format. A similar analysis of commercial monoclonal antibodies against rcPvLDH was performed and trends observed for each biomarker was compared.

Methods

Materials and reagents

Recombinant ITG histidine-rich protein 2 (rcHRP2) and HRU20 were kindly provided by D. Sullivan (Johns Hopkins University, Baltimore, MD). Protein concentrations were determined in triplicate by amino acid analysis (University of Nebraska, Protein Structure Core Facility, Omaha, NE). In vitro *P. falciparum* culture supernatant was used as source of native HRP2 protein for monoclonal antibody (mAb) screening. Sources for commercial α -HRP2 and α -pLDH antibodies are listed in Tables 4 and 5, respectively. Recombinant *P. vivax* lactate dehydrogenase (rcPvLDH) was purchased from CTK Biotech (A3004).

Antibody production

Custom anti-HRP2 monoclonal antibodies (mAbs) were developed under contract with Precision antibody, Inc (Columbia, MD). For mouse immunization, three BALB/c mice were inoculated with recombinant HRP2 mixed with a proprietary adjuvant. Tail bleeds were analyzed for α -HRP2 titers by direct ELISA. When a desirable antibody titer ($A_{450} > 2.0$ at 1:100,000 dilution) was achieved, a mouse was euthanized and its spleen removed under aseptic conditions. A single-cell suspension of splenocytes was prepared, and cells were subjected to electrofusion with myeloma cells. Cells were distributed into 96-well plates, and incubated at 37°C. The hybridoma culture supernatants were then screened for the presence of anti-HRP2 mAbs by direct ELISA. The direct ELISA was performed on microtiter plates, and all reagents were diluted in 1x PBS containing 5% non-fat dried milk (PBSM). Plates were coated with HRP2 ITG or HRU20 at two protein concentrations, 100 ng/well or 1 ng/well, in PBSM and washed with PBS containing 0.05% Tween 20. Hybridoma growth media diluted (1:2) in PBSM was used as negative control.

The mAbs were purified from hybridoma culture supernatant by affinity chromatography using protein G followed by acid elution and neutralization. The Abs were buffer-exchanged into PBS and tested for purity with SDS-PAGE. The concentration of purified mAbs was determined by absorbance at 280 nm.

Determining kinetic parameters of mAbs with BLI

All IgG antibodies were biotinylated in PBS with EZ-Link NHS-PEG4-Biotin (ThermoFisher #21329) at 20x molar excess according to the commercial protocol. Unreacted biotin was removed using Thermo Zeba Spin Columns (ThermoFisher # 89882). Kinetics experiments were performed using an OctetRed96 system equipped with streptavidin biosensors

(ForteBio LLC, Fremont, CA). All solutions were made in octet kinetics buffer (1x PBS with 0.1% BSA and 0.02% Tween-20). Each kinetic experiment consisted of 5 steps: (1) streptavidin biosensors were equilibrated in kinetics buffer for 3 to 5 minutes, (2) a biotinylated mAb (0.5 $\mu\text{g/ml}$) was loaded onto the streptavidin biosensors for 400 seconds (3) a baseline was established in kinetics buffer for 1 minute, (4) rcHRP2 antigen (0 - 14 nM) or rcPvLDH antigen (0 – 200 nM) in kinetics buffer was associated to the functionalized sensors for 400 seconds, and (5) sensors were placed in kinetics buffer, and the antigen was allowed to dissociate for 15 minutes. The assay was performed at 26°C with 1000 rpm plate rotation. Software provided with the Octet system (version 7.1) was used to fit the data to a one-to-one model and obtain k_{on} , k_{off} , and K_D values.

To determine the kinetic parameters of anti-HRP2 IgM, rcPvHRP2 was biotinylated at 20x molar excess as noted above. Kinetics experiments were performed with streptavidin biosensors. In these experiments, 10 nM rcHRP2 was loaded onto the tips, and the IgM antibodies were allowed to associate and dissociate from the rcHRP2-functionalized sensors. Loading, association, and dissociation times were optimized for each IgM antibody, and are shown below in Table 3.

Table 3. Optimized experimental set-up for measuring kinetic parameters of α -HRP2 IgM.

Step/IgM	MPFM-55A	PTL3
Loading	500 s	150 s
Association	400 s	700 s
Dissociation	900 s	900 s

Screening antibody pairs by ELISA.

rcHRP2. Antibodies were conjugated to horseradish peroxidase using EZ-Link Plus Activated Peroxidase kit (Thermo Scientific #31489). Briefly, 0.2 mg mAb in 100 μl of carbonate bicarbonate buffer was incubated with 0.2 mg of horseradish peroxidase in 200 μl of ultrapure

water for 1 hour at room temperature. Next, 4 μl of sodium cyanoborohydride was added and incubated for 15 minutes at room temperature. The reaction was stopped by adding 4 μl of quenching buffer and incubating for 15 minutes. The reaction was then subjected to desalting using Vivaspin 500 (Sartorius # VS0101).

A checkerboard-formatted sandwich ELISA was performed with all possible combinations of 9 custom and 6 commercial HRP2-specific antibodies (Table 4) to determine the best antibody pairs for HRP2 detection according to a modified previous method.¹¹⁵ Briefly, a 96-well plate (Costar, #3361) was coated with 100 μl /well of each antibody solution at 1 $\mu\text{g}/\text{ml}$ in PBS. The plates were sealed and incubated overnight at 4°C. The antibody solutions were discarded, and the plate was blocked for 2 hours with 200 μl /well of 2 % bovine serum albumin (BSA) in PBS. The plates were washed five times with 200 μl /well PBS, pH 7.4, with 0.05% (PBST). Next, 100 μl of rHRP2 (1 ng/ml; 34.1 pM) in PBST was placed in the wells, and the plates were incubated in a humidified chamber for 1 hour at room temperature. Next, the plate was washed five times before 100 μl of 0.5 $\mu\text{g}/\text{ml}$ of the detection antibody-HRP conjugate in 2% bovine serum albumin and 0.1 % Tween 20 in PBS was added to each well. The plate was incubated for one hour at room temperature and washed five times with PBST. The enzymatic reaction was visualized using TMB substrate with hydrogen peroxide (Sigma, T0440) and stopped with 50 μl of 1 M H_2SO_4 . Spectrophotometric analysis was performed at 450 nm using SpectraMAX 340 Microplate spectrophotometer (Molecular Devices, Sunnyvale, CA).

Table 4. HRP2 monoclonal antibodies assessed by BLI and ELISA.

Source	Clone	Isotype
ICL	MPFG-55A	IgG
	MPFM-55A	IgM
NBI	C1-13	IgG
	PTL-3	IgM
Vista Diagnostics	2g6	IgG
	0445	IgG
Precision Antibody	4D6	IgG
	6C8	IgG
	8D3	IgG
	10C1	IgG
	10F5	IgG
	11E10	IgG
	11H7	IgG
	12D4	IgG
	12F12	IgG

rcPvLDH. A total of 8 α -*pLDH* antibodies (Table 5) were conjugated to alkaline phosphatase (AP) for detection (Abcam, ab102850). Thus, 64 antibody pairs were tested (8 x 8 matrix) in a checkerboard 96-well plate ELISA format. 100- μ l solutions of 1 μ g/ml unmodified α -*pLDH* IgG were incubated for one hour in Immulon 2 HB 96-well plates (Thermo Scientific #3455). The plates were then washed 3 times with 1x phosphate buffered saline (PBS) containing 0.1% Tween-20 (PBST). Next, 250 μ l of 5% w/v bovine serum albumin (Fisher BP1600) in PBST was incubated for 2 hours in each well. The plates were then washed 3 times with PBST. Samples consisting of 0 and 500 pM *rcPvLDH* were added to the plates in triplicate in PBST containing 0.1% BSA and incubated for 2 hours. The plate was then washed 5 times with 1x TRIS buffered saline (TBS) containing 0.1% Tween-20 (TBST). Next, 100 μ l of 0.5 μ g/ml detection antibodies in TBST with 0.5% BSA was added to each well, and the plates were incubated for 1 hour while protected from light. The plates were then washed 5 times with TBST, and 100 μ L of BluePhos® Microwell Phosphatase Substrate was added to each well and incubated for 20 minutes while

protected from light. The absorbance was measured at 620 nm using a Synergy H4 microplate reader. Signal-to-noise ratios were determined for each pair.

Table 5. *p*LDH monoclonal antibodies assessed by BLI and ELISA.

Source	Clone	Isotype
AccessBio	14c2	IgG
	6c9	IgG
Vista Diagnostics	12g1	IgG
	19g7	IgG
	1201	IgG
	1246	IgG
Fitzgerald	10-P09CS	IgG
	10-P09I	IgG

Results and Discussion

Kinetic parameters of mAbs measured by BLI

rcHRP2. The strength of mAb-rcHRP2 interactions was measured using biolayer interferometry. For each α -HRP2 IgG mAb, the antibody was biotinylated, loaded onto streptavidin biosensors, and rcHRP2 (0 – 14 nM) was allowed to associate and dissociate. The binding profiles, pseudo-first order fit curves, and the corresponding residuals are plotted for each IgG in Table 10 (Appendix B). For α -HRP2 IgM, the orientation of the experiment was flipped; rcHRP2 was biotinylated, loaded onto streptavidin biosensors, and anti-HRP2 IgM was allowed to associate and dissociate. Reversing the orientation was necessary because very little binding was observed when the IgM antibodies were biotinylated and loaded onto the tips. This lack of signal was likely attributable to poor IgM orientation on the tip upon loading. Similar to the α -HRP2 IgG experiments, the experimental conditions for α -HRP2 IgM were optimized such that

the resulting binding profiles resembled pseudo-first order reactions. The binding profiles, fit curves, and residual plots for these IgM are displayed in Table 11 (Appendix B).

The kinetic parameters for all α -HRP2 mAbs are listed in Table 6. Notably, 11 out of the 15 anti-HRP2 antibodies that were assessed by BLI had off-rate constants that were below the limit of detection of the OctetRed96 instrument ($< 1 \times 10^{-7}$ 1/s). Although the experimental parameters were optimized such that one-to-one fits could provide accurate estimations of the mAb-HRP2 affinities, it is likely that the unique structure of HRP2—repeated motifs throughout the protein—allowed for re-binding of HRP2 to the mAb-functionalized sensors during the dissociation phase. In other words, when an HRP2 molecule dissociated from the sensor, the high number of potential epitopes on a single HRP2 in close proximity to the mAb-functionalized tip allowed for quick rebinding to the sensor, resulting in no net dissociation.

While the off-rate constants make distinguishing the anti-HRP2 mAbs by k_{off} or K_D difficult, the measured association rate constants varied over three orders of magnitude. The 3 mAbs with the highest on-rate constants were all IgG from Precision Antibody (10F5, 10C1, 6C8). Three commercial antibodies had the lowest k_{on} values, two of which were IgM (MPFM-55A and PTL3). This was not surprising, since the experiments were optimized for one-to-one interactions, and IgM generally have low-affinity, high-avidity interactions with their respective targets.¹¹⁶

Table 6. Kinetic parameters for α -HRP2 antibodies measured by BLI.

Source	Clone	Class	Kinetic parameter		
			K_D (M x 10^{-12})	k_{on} (1/Ms x 10^5)	k_{off} (1/s x 10^{-7})
ICL	MPFG-55A	IgG	7 ± 1	58.8 ± 0.3	410 ± 10
	MPFM-55A	IgM	< 1.0	4.22 ± 0.01	< 1.0
NBI	C1-13	IgG	< 1.0	47.7 ± 0.5	< 1.0
	PTL-3	IgM	< 1.0	6.70 ± 0.01	< 1.0
Vista Diagnostics	2g6	IgG	1.6 ± 0.1	93.4 ± 0.6	150 ± 15
	0445	IgG	< 1.0	3.52 ± 0.02	< 1.0
Precision Antibody	4D6	IgG	< 1.0	96.9 ± 0.5	< 1.0
	6C8	IgG	< 1.0	107.0 ± 0.7	< 1.0
	8D3	IgG	53.5 ± 0.1	14.30 ± 0.06	766 ± 12
	10C1	IgG	< 1.0	137.0 ± 0.4	< 1.0
	10F5	IgG	< 1.0	164.0 ± 0.7	< 1.0
	11E10	IgG	< 1.0	87.4 ± 0.5	< 1.0
	11H7	IgG	4.9 ± 0.1	80.5 ± 0.4	400 ± 20
	12D4	IgG	< 1.0	93.0 ± 0.8	< 1.0
	12F12	IgG	< 1.0	47.8 ± 0.2	< 1.0

rcPvLDH. The kinetic parameters of 8 anti-*p*LDH IgG antibodies against *rcPvLDH* were determined as described above. The binding profiles, calculated fits, and residual plots are displayed in Table 12 (Appendix B), and the corresponding kinetic parameters are listed in Table 7. Compared to HRP2, the anti-*p*LDH-*rcPvLDH* interactions were generally lower-affinity interactions; on-rate constants were several orders of magnitude lower, and more off-rate constants could be measured. This difference is attributable to the fact that *rcPvLDH* contains no repeat motifs, so the number of epitopes available match the *rcPvLDH* solution concentration, whereas there are multiple HRP2 epitopes available per biomolecule. Interestingly, although 14c2 previously has been shown to bind to *p*LDH from D6 *P. falciparum* culture, we found that it did not bind to the recombinant *PvLDH* used in this experiment.¹¹⁷ There are two possible explanations for this lack of binding. First, despite being a pan-specific anti-*p*LDH antibody, 14c2 may not bind

to *P. vivax* LDH. Second, the recombinant protein used in this experiment is fused to a glutathione transferase (GST) tag, which may be blocking or nearby the *p*LDH epitope that 14c2 targets. We believe that the latter is most likely, since 14c2 also showed no activity toward GST-tagged recombinant *P. falciparum* LDH, though it was active against the native *P. falciparum* protein in our in-house culture.

Table 7. Kinetic parameters for α -*p*LDH antibodies against rc*Pv*LDH measured by BLI.

Source	Clone	Class	Kinetic parameter		
			K_D (M x 10 ⁻¹²)	k_{on} (1/Ms x 10 ⁵)	k_{off} (1/s x 10 ⁻⁷)
AccessBio	14c2	IgG	No binding	0	--
	6c9	IgG	140 ± 90	0.1360 ± 0.0014	20 ± 13
Vista Diagnostics	12g1	IgG	52 ± 11	1.180 ± 0.005	60 ± 13
	19g7	IgG	235 ± 3	2.790 ± 0.007	657 ± 9
	1201	IgG	1110 ± 30	0.2080 ± 0.0006	231 ± 6
	1246	IgG	< 1.0	0.2460 ± 0.0009	< 1.0
	10-P09CS	IgG	< 1.0	0.348 ± 0.0012	< 1.0
Fitzgerald	10-P09I	IgG	1240 ± 11	1.110 ± 0.004	1370 ± 11

Screening antibody pairs by ELISA

rcHRP2. To identify the best performing antibody pairs for an HRP2 sandwich immunoassay, all 225 possible pairs of the anti-HRP2 mAbs discussed herein (15 x 15 matrix) were screened in a checkerboard format. The average signal-to-noise ratio (S/N) for each pair was determined by dividing the average A₄₅₀ at 34.1 pM of rcHRP2 by the average absorbance of the blank (Figure 14). Several mAbs, such as MPFG, C1-13, 4D6, 8D3, 11H7, and 12F12 performed poorly as capture, while MPFM, PTL3, 2g6 and 0445 generally performed well as capture elements. Additionally, numerous custom mAb as were successful as detection components, including 4D6, 6C8, 10C1, 10F5, 11E10, 12D4 and 12F12.

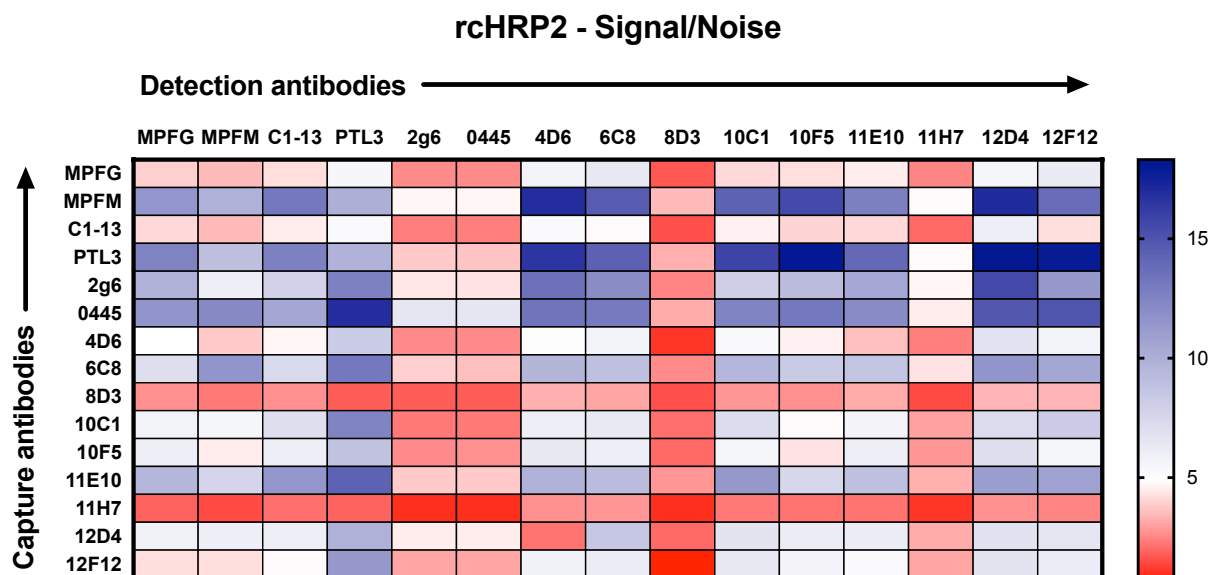


Figure 14. ELISA signal-to-noise ratios for checkerboard screening of anti-HRP2 mAb pairs

rcPvLDH. To identify the best performing antibody pairs for a *PvLDH* ELISA, all 64 possible pairs of the α -*pLDH* mAbs discussed herein (8 x 8 matrix) were screened in a checkerboard format. The average signal-to-noise ratio (S/N) for each pair was determined by dividing the average A_{450} at 500 pM *rcPvLDH* by the average absorbance of the blank (Figure 15). Two mAbs, 14c2 and 6c9, performed poorly as both capture and detection elements. This behavior was expected for 14c2, as it demonstrated no binding in the BLI study. The performance of 6c9, on the other hand, was more surprising; one important note is that the commercial lots of 6c9 used in the BLI experiment and the ELISA checkerboard were different. Interestingly, clone 1246 performed reasonably well as a detection antibody, though it produced extremely high background signal as a capture antibody (regardless of detection mAb). Overall, 19g7, 1201, and 12g1 performed best as both capture and detection antibodies, though performance varied significantly depending on the corresponding paired mAb.

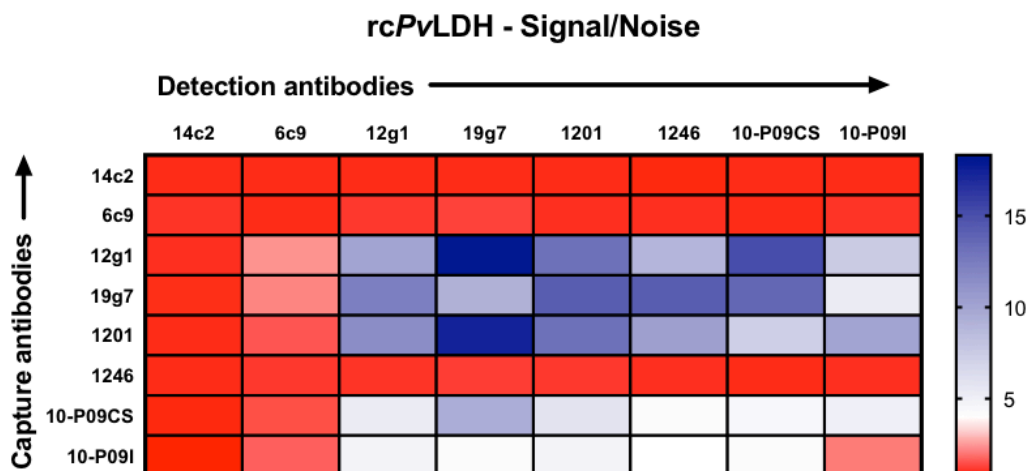


Figure 15. ELISA signal-to-noise ratios for checkerboard screening of α -pLDH mAb pairs against rcPvLDH (0 and 500 pM).

Predicting mAb ELISA performance with BLI

rcHRP2. With the quantification of individual mAb-HRP2 interactions by BLI and the relative ranking of anti-HRP2 mAb pairs in a checkerboard ELISA screening comes the question: can BLI be used to predict antibody pair performance in a traditional plate ELISA format?

Figure 16 relates the measured kinetic parameters of the α -HRP2 capture and detection antibodies to the S/N measured for each pair in the checkerboard ELISA. In these plots, a kinetic parameter for the capture antibody is plotted on the abscissa, and a kinetic parameter for the detection antibody is plotted on the ordinate. The size of the circle at the ordinate pair (capture, detection) represents the relative S/N for that pair measured by ELISA. The best-performing mAb pairs in the ELISA format included capture and detection antibodies with low K_D values, since the largest circles are concentrated in the lower left-hand corner of the plot Figure 16A. This result is anticipated, as one would expect stronger interactions to lead to better ELISA performance. However, when the ELISA data is compared to the on-rate constants and off-rate constants of the capture and detection antibodies, some interesting trends emerge. Figure 16B plots the k_{on} values

for capture and detection mAbs versus the ELISA S/N. In this visualization, it becomes clear that there was no trend relating ELISA S/N to the k_{on} of the capture antibodies along the x-axis. However, there was a clear dependence of the ELISA S/N on the k_{on} of the detection antibody along the y-axis; greater on-rate constants for detection antibodies resulted in better ELISA antibody pair performance for α -HRP2 mAbs. For off-rate constants (Figure 16C), the trends were less clear since there were fewer discrete k_{off} values for the anti-HRP2 mAbs compared to k_{on} values. However, Figure 16D shows that the highest concentration of high-performing anti-HRP2 ELISA antibody pairs occurred when the capture antibody k_{off} was low and the detection antibody k_{on} was high and consequently the overall K_D was low.

Using these BLI parameters, it would be predicted that pairs with 10F5, 10C1, and 6C8 in the detection position paired with capture mAbs with low off-rate constants, such as the two IgM mAbs (MPFM-55A, PTL-3) or an IgG such as 0445, would perform well in an ELISA format. In fact, these pairs are some of the top performers in the ELISA checkerboard screening, despite the low k_{on} values for the capture mAbs (Figure 14). Capture antibodies with low off-rate constants may be favored due to the high number of washes and additional incubation steps the capture mAb-HRP2 complex is subjected to during the ELISA protocol. In contrast, on-rate constants may be most important for detection antibodies since the time scale of this interaction in the ELISA is lower. In summary, these results demonstrate that BLI can be used as a predictive tool for development of an HRP2 ELISA.

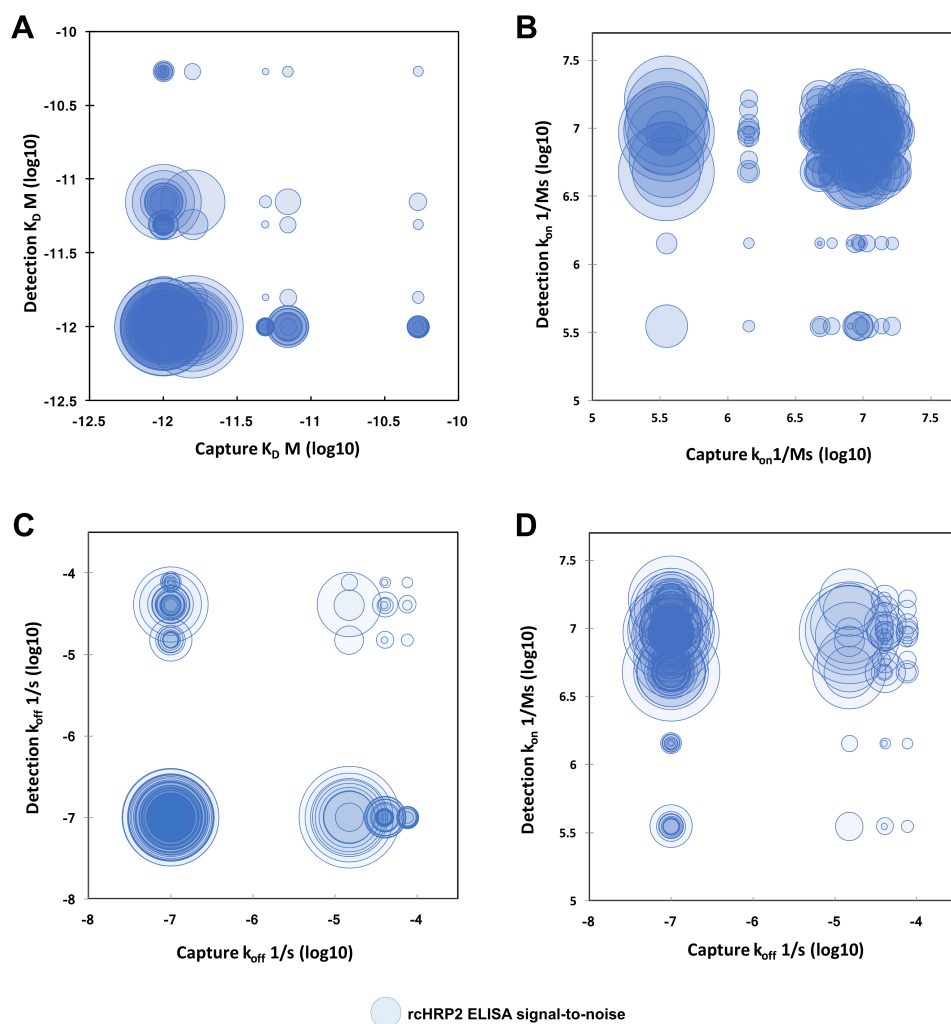


Figure 16. Relationship between anti-HRP2 (A) K_D , (B) k_{on} , and (C) k_{off} in the capture (x-axis) and detection (y-axis) positions as measured by BLI and ELISA signal-to-noise ratios (size of circles). (D) Plot of capture k_{off} (x-axis) vs. detection k_{on} (y-axis) vs. ELISA signal-to-noise (circles). Note: only anti-HRP2 IgG pairs are plotted.

rcPvLDH. Because HRP2 is a unique biomarker that lacks structure and contains a series of repeated epitopes for mAb binding, it is important to ask whether the trends observed for HRP2 are generalizable to typical protein biomarkers with defined tertiary structure and no or few repeat motifs in the primary sequence. To answer this question, a similar analysis was performed for *P. vivax* lactate dehydrogenase, comparing the kinetic parameters of α -*pLDH* antibodies to the ELISA performance against *rcPvLDH* of those antibody pairs. As shown in Figure 17, there was

no trend in the rcPvLDH data relating ELISA S/N from the checkerboard screening to the dissociation constants of the capture and detection antibodies. Although these results differ from the trends observed for HRP2, they are not surprising. For HRP2, if a capture and detection antibody target the same epitope, both may be able to bind to the protein due to the repeat motifs in the amino acid sequence. Therefore, ELISA performance for α -HRP2 pairs is largely dependent on the strength of the mAb-HRP2 interaction. However, for targets lacking repeated epitopes, such as rcPvLDH, the compatibility of the capture and detection antibodies heavily influences their performance as an ELISA pair. For example, if two anti-pLDH antibodies have very strong interactions with rcPvLDH but both target the same epitope, no ELISA signal will be observed.

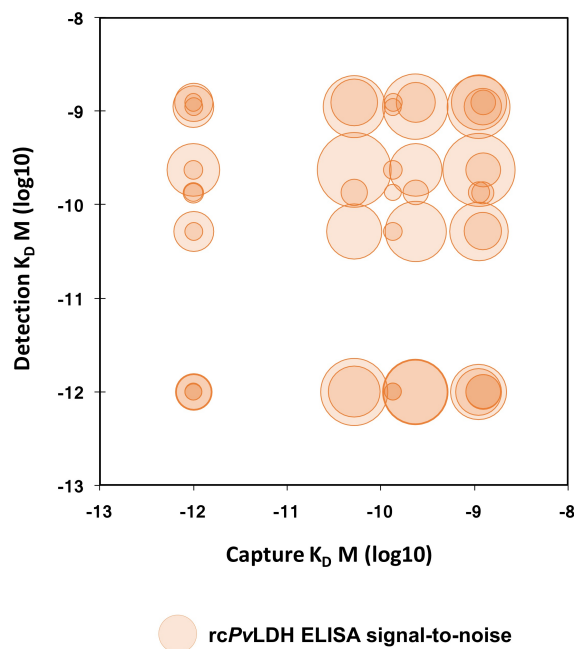


Figure 17. Relationship between anti-pLDH K_D in the capture (x-axis) and detection (y-axis) positions as measured by BLI and ELISA signal-to-noise ratios (size of circles). Note: 14c2 is excluded, since no binding was observed on BLI.

Comparing and contrasting the results for rcHRP2 and rcPvLDH highlights the limitations and advantages of using BLI as a tool for ELISA development and generates a general workflow

for selecting optimal molecular recognition elements for immunoassays. If the antigen does not contain a series of repeat motifs, then the optimal mAb pair is best determined empirically. However, if the antigen—like HRP2—does have multiple repeated epitopes, then the antibody with the lowest off-rate constant should be chosen as a capture antibody, and the antibody with the highest on-rate constant should be chosen as the detection antibody.

The utility of BLI for quantifying the strength of antibody-antigen interactions is clear; however, performing BLI on individual mAbs is only useful for predicting the ELISA performance of antibody *pairs* when the antigen contains multiple repeats in its sequence. While this limitation is significant, there are many targets of interest that could benefit from building a sensitive ELISA from the bottom-up using BLI as a predictive tool. For example, the circulating anodic antigen biomarker for *Schistosoma* infections is decorated with repeating polysaccharide motifs.^{118,119} Further, BLI may be useful for developing ELISAs for viral capsids containing many oligomeric subunits or multimeric proteins with identical subunits. Future investigations probing the number of repeat-motifs required for the trends observed for HRP2 to hold could provide a cut-off threshold for when BLI can be used to predict ELISA performance. Further, additional studies into the applicability to these results to the LFA format are needed. While LFAs and ELISAs have similar sandwich format, LFAs lack extensive washes and occur on a faster time-scale, potentially favoring antibodies with higher on-rates.

Conclusion

The ability to predict antibody pair performance in a sandwich format would streamline development of critically important antibody-based diagnostics and laboratory research tools. We have evaluated panels of monoclonal antibodies for two malarial biomarkers with biolayer

interferometry and screened antibody pairs in a checkerboard ELISA format. BLI proved to be a useful, predictive tool for determining antibody pair ELISA performance for HRP2, the primary biomarker used in malaria diagnostics. Specifically, pairs that included capture antibodies with low off-rate constants and detection antibodies with high on-rate constants performed best in an ELISA format. These trends were likely due to the series of repeat-motifs within the HRP2 sequence as well as the protein's lack of tertiary structure. While these results were not generalizable to *rcPvLDH*, which is highly structured and lacks repeat-motifs, they may be applicable to other infectious disease biomarkers, such as viral capsids and multimeric proteins with identical subunits.

Acknowledgements

I would like to thank Dr. Ihn Kyung Jang and Dr. Robert Burton for their contributions to this work. The material in this chapter was supported by the Bill and Melinda Gates Foundation (Grant OPP1135840), PATH: Diagnostics for malaria elimination toward eradication (1758-00-06-00), and the National Science Foundation Graduate Research Fellowship Program under Grant #1445197.

CHAPTER V

SIMULTANEOUS CAPTURE AND SEQUENTIAL DETECTION OF TWO MALARIAL BIOMARKERS ON MAGNETIC MICROPARTICLES^c

Introduction

Thus far, we have explored the impact of sample matrix interferants on biomarker detectability (Chapter II), the improvements afforded when a target is removed from its biological matrix and concentrated before detection (Chapter III), and the utility of quantifying the strength of interactions between molecular recognition elements and their targets for building an immunoassay from the bottom-up. In this chapter, we integrate these concepts to build a highly sensitive ELISA for *p*LDH and HRP2.

ELISAs are the gold standard laboratory technique for quantitative and qualitative protein detection, which serve both as powerful research tools and clinical diagnostics. These highly sensitive assays are typically performed in a microtiter plate, utilizing surface-bound antigen or antibody to bind a protein analyte and enzyme-conjugated, target-specific antibodies for detection. Although traditional singleplex ELISAs are laboratory “workhorses” for sensitive and specific protein detection, they require 5 – 8 hours for completion and several incubation steps to ultimately develop signal. Further, conventional ELISAs are limited to detecting just one analyte from a single sample.

^c Portions of this chapter have been previously published in Markwalter, C.F. et al., *Talanta*, 2016. 161: 443 - 449.
© 2016 The Authors. Published by Elsevier B. V.

While traditional ELISAs are useful for diagnoses arising from one biomarker, diseases requiring multi-analyte detection to identify or inform treatment have led to the development of multiplexed immunoassays. A multiplexed immunoassay utilizes the same “sandwich” format (capture antibody, sample, detection antibody) as a conventional singleplex ELISA, except the former usually adopts fluorescent or chemiluminescent reporter systems rather than amplification of a colorimetric substrate by enzymes.¹²⁰ Two common formats for multiplexed immunoassays include planar arrays and bead-based suspension assays.¹²¹ In typical, commercially available planar arrays (Quansys, MSD®), microliter volumes of capture antibodies for multiple protein biomarkers are printed discretely onto two-dimensional supports, such as slides or microtiter plates, using a high-resolution printer. The functionalized supports are then treated with sample followed by reporter-labeled antibody. Signal is detected using a high-resolution scanner or fluorescence microscope.¹²⁰ In addition to multiplexing capabilities, planar micro-array immunoassays benefit from ambient analyte theory. According to this theory, reducing the concentration of capture antibodies results in increased antibody binding site occupancy and thus higher assay sensitivity.^{122,123} However, these benefits are often off-set by mass transport limitations.¹²⁰

In contrast to planar arrays, bead-based suspension immunoassays are advantageous because they overcome mass transport limitations via active mixing throughout the liquid sample.¹²⁴ In a typical bead-based immunoassay (Luminex™, Bio-PlexPro™, Cytometric Bead Arrays), fluorescent microbeads are functionalized with capture antibodies, mixed with a sample, and subsequently mixed with fluorescently-tagged detection antibodies, which allow for analyte detection via flow cytometric methods. Multiplexing capabilities arise when target-specific

antibodies are functionalized to microbeads with varying fluorescent signatures distinguishable by flow cytometry.¹²⁵

There are several disadvantages to current multiplexed immunoassays. Both planar and bead-based immunoassays require laboratory infrastructure beyond that needed to perform singleplex conventional ELISAs; planar micro-array assays require high-resolution fluorescence scanners, and bead-based immunoassays require flow cytometric instrumentation for detection.¹²⁰ Further, planar micro-arrays require several addition, wash, and incubation steps totaling up to 3 hours.¹²⁶ Commercially available bead-based suspension assays often require 3 – 4 hours for completion, up to 1 hour dedicated to the detection step.¹²⁷ To address these pitfalls, we have developed a magnetic bead-based ELISA in which two biomarkers are simultaneously captured and sequentially detected in less than 1 hour with no laboratory infrastructure beyond what is required to perform a conventional singleplex well-plate ELISA.

We applied the developed magnetic bead-based ELISA to the detection of the two primary malarial biomarkers: *p*LDH and HRP2. An assay that detects both *p*LDH and HRP2 is beneficial for several reasons. As discussed in Chapter I, *p*LDH is a parasite metabolic enzyme, so it is present for infections resulting from any of the five species of malaria known to infect humans, whereas HRP2 is only present in *P. falciparum* infections.^{50,128} Thus, an assay that detects both biomarkers can differentiate between *P. falciparum* and non-*falciparum* infections, a distinction that determines proper treatment.¹²⁹ Second, HRP2 remains in host circulation for up to one month, whereas *p*LDH is known to clear within 24 hours post parasite clearance, so a dual assay can distinguish resolved and active *P. falciparum* infections.⁵¹ The magnetic bead-based simultaneous capture and sequential detection (SCSD) ELISA for *p*LDH and HRP2 would not only inform patient management, but also allow for more efficient and sensitive *P. falciparum* and non-

falciparum epidemiology and transmission studies. The presented assay design is modular and can be applied to any set of two biomarkers provided validated antibody pairs are available.

Methods

Reagents and materials

Dynabeads® MyOne™ Streptavidin T1 beads were purchased from Life Technologies (Cat #65601). Recombinant *P. falciparum* lactate dehydrogenase (rcPfLDH) and recombinant *P. vivax* lactate dehydrogenase (rcPvLDH) were purchased from CTK Biotech (Cat #A3005, #A3004). *P. falciparum* D6 strain was cultured in the lab. *P. falciparum* W2, Benin 1, and PH1 reference strains were obtained from the Foundation for Innovative New Diagnostics (FIND). Anti-HRP2 capture and detection antibodies were purchased from Abcam (ab9203 and ab30384). Pan-specific α -pLDH antibodies were purchased from AccessBio, Fitzgerald, and Vista Diagnostics (Table 5 [Chapter IV]). BluePhos® Microwell Phosphatase substrate was purchased from KPK (#50-88-02), and TMB One was purchased from Promega (G7431). The ELISA kit for pLDH was purchased from SD Bioline, S. Korea (05EK40), and the ELISA kit for HRP2 was purchased from Cellabs, Australia (KM2).

pLDH antibody pair screen

Capture and detection antibodies were screened for use in the pLDH on-bead ELISA in a manner identical to the rcPvLDH ELISA screening in Chapter IV, with the exception that samples consisted of 0 and 100 parasites/ μ l *P. falciparum* D6 culture.

Blood sample preparation

Pooled human whole blood (Bioreclamation IVT, HMWBCPD) was spiked with D6 *P. falciparum* culture (stock: 18,450 parasites/ μ l) to the desired parasitemia. An equal volume of 2x lysis buffer (100 mM potassium phosphate pH = 8.0, 600 mM NaCl, 250 mM imidazole, 2% Triton-X-100) was then added, and the lysed blood was filtered through glass wool in a plastic syringe.

Preparation of mAb-functionalized magnetic beads

Target-specific antibody-functionalized beads were prepared as reported previously.¹³⁰ Briefly, α -pLDH (Vista, 19g7) or α -HRP2 (Abcam, ab9203: clone C1-13) antibodies were biotinylated with EZ-Link NHS-PEG4-Biotin, No-Weigh Format (Thermo Pierce #21329) in PBS with a 20x excess of NHS-PEG4 Biotin. Remaining NHS-PEG4 biotin was removed using Zebra Spin Desalting Columns with a 7K molecular weight cut-off (Thermo Pierce #89882). Next, 5 mg of Dynabeads® MyOne™ Streptavidin T1 was washed 3 times with PBS before incubating for 30 minutes with 500 μ L of 0.4 mg/mL of biotinylated antibody in PBS. The beads were then washed 3 times with PBS and blocked with excess D-biotin in PBS for 30 minutes. Finally, the beads were washed 3 times and re-suspended in 500 μ L of PBS with 0.01% Tween-20.

On-bead ELISA for pLDH

Solutions (200 μ L) of parasitized lysed whole blood were placed in a Fisherbrand Flat-bottom PS 96-well plate (#12565501). Four μ l HAMA blocker (Fitzgerald 85R-1001), 10 μ L of α -pLDH (19g7) magnetic beads, and 1.57 μ l of 1201:AP (1.27 mg/ml) were added to each well and incubated on an orbital shaker for 15 minutes. Using a MagWell™ Magnetic Separator

(EdgeBio #57624), the beads were separated from the supernatant and washed with 200 μ l 1x PBS with 0.1% Tween-20 (PBST). As a second wash, 100 μ l PBST was added to the beads, which were then moved to new wells. Next, 100 μ l BluePhos® Microwell Phosphatase Substrate was added to each well containing beads, and the plate was incubated for 15 minutes while protected from light. The supernatant was removed, and signal was measured by absorbance (620 nm) on a plate reader.

On-bead ELISA for HRP2

Solutions (200 μ L) of parasitized lysed whole blood were placed in a Fisherbrand Flat-bottom PS 96-well plate. Four μ l HAMA blocker, 5 μ l of α -HRP2 (C1-13) magnetic beads, and 2 μ l of MPFG-55P (0.1 mg/ml) were added to each well and incubated on an orbital shaker for 15 minutes. Using a MagWell™ Magnetic Separator, the beads were separated from the supernatant and washed with 200 μ l PBST. As a second wash, 100 μ l PBST were added to the beads, which were then moved to new wells. Next, 100 μ l TMB One was added to each well containing beads, and the plate was incubated for 5 minutes while protected from light. The supernatant was removed, and the reaction was stopped with 100 μ l of 2M H₂SO₄. Signal was measured by absorbance (450 nm) on a plate reader.

On-bead simultaneous capture and sequential detection (SCSD) ELISA for pLDH and HRP2

Solutions (200 μ l) of parasitized lysed whole blood were placed in a Fisherbrand Flat-bottom PS 96-well plate. Four μ L of HAMA blocking reagent, 10 μ L of 19g7-conjugated magnetic beads, 5 μ L of C1-13-conjugated magnetic beads, 1.57 μ L of 1201:AP (1.27 mg/ml), and 2 μ l of ab30384 (0.1 mg/ml) were added to each well and incubated on an orbital shaker for 15 minutes.

The beads were pulled to the sides of the wells using a MagWell™ Magnetic Separator, and the supernatant was removed. The beads were washed with 200 µl PBST. As a second wash, 100 µl PBST were added to the beads, which were then moved to new wells. Next, 100 µl of BluePhos® Microwell Phosphatase Substrate was added to each well and incubated for 15 minutes while protected from light. The supernatant was removed and absorbance was measured at 620 nm (*p*LDH detection). The beads were then washed three times with PBST and moved to new wells on the third wash. Next, the beads were re-suspended in 100 µl of TMB One Solution and incubated for 5 minutes while protected from light. Finally, the supernatant was removed, and the reaction was quenched with 100 µl 2M H₂SO₄ before absorbance was measured at 450 nm for detection of HRP2. For both biomarkers, absorbance vs. concentration was plotted, and limits of detections (LODs) were calculated as the concentration at the minimum detectable signal ($3SD_{blank} + S_{blank}$). See Figure 18 for on-bead SCSD ELISA workflow.

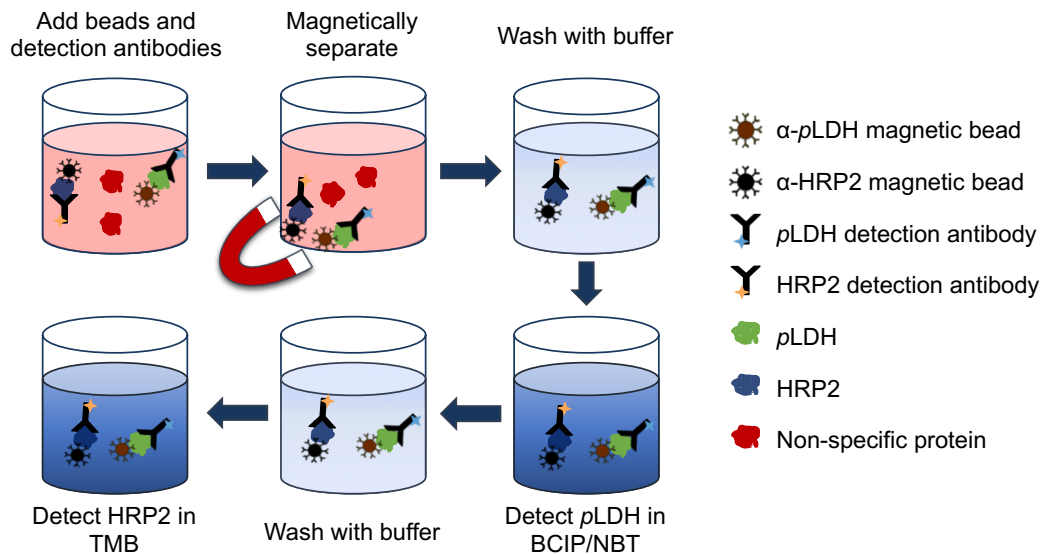


Figure 18. Workflow for simultaneous capture and sequential detection (SCSD) ELISA for *p*LDH and HRP2.

Validation

Intra-assay variation for the developed assays was determined by repeating standard curve measurements in triplicate (singleplex assays) or sextuplicate (SCSD assay) on the same plate (one user). The intra-assay variation (%CV) was found by taking the average relative standard deviation (RSD) of each repeated measurement. Inter-assay variation was determined by measuring standard curves in triplicate (singleplex assays) or sextuplicate (SCSD assay) over 5 days (one user). The inter-assay variation (%CV) was calculated by dividing the standard deviation of all absorbance measurements at a given concentration over 5 days by the mean absorbance value at that concentration over the 5 days. For establishing inter-user variation, two users performed standard curves in sextuplicate over 5 days. The inter-user variation (%CV) was calculated as the average percent difference between the mean values for both users across all replicates for all days. Finally, the simplicity of the SCSD assay was evaluated by providing 5 blinded samples (including a blank) to a novice user. The user was allowed two practice rounds before measuring the unknown samples via the on-bead SCSD ELISA for *p*LDH and HRP2. Using a paired Student's T Test, novice absorbance values for these samples were compared to the expected values from standard curves generated by the inter-assay variation measurements.

Results and Discussion

Design and optimization of on-bead ELISAs for pLDH and HRP2

Selection of the best capture and detection antibody pairs is crucial for developing sensitive and specific immunoassays. For HRP2 assays, C1-13 capture and MPFG-55P, a detection antibody conjugated to horseradish peroxidase (HRP_x), have been previously validated as an appropriate pair for ELISA formats.¹³¹ Piper et al. performed extensive screening of *p*LDH antibody pairs for

immuno chromatographic assays on nitrocellulose membranes.¹³² However, binding kinetics in a lateral flow assay format do not represent the same equilibrium kinetics found in ELISAs.¹³³ Thus, a comprehensive screening of antibody pairs was conducted to evaluate performance in an ELISA format.

In total, 64 antibody pairs were screened (8 x 8 matrix) in a checkerboard format. Each monoclonal antibody (Table 5 [Chapter IV]) was conjugated to alkaline phosphatase for detection. All antibodies were immobilized in a polystyrene plate and allowed to bind to *Pf*LDH from *P. falciparum* D6 culture at 0 or 100 parasites/ μ l. Detection antibodies were then added to the plate, and signal was generated using a BCIP/NBT substrate. The resulting signal-to-noise ratio for each pair is shown in Figure 19.

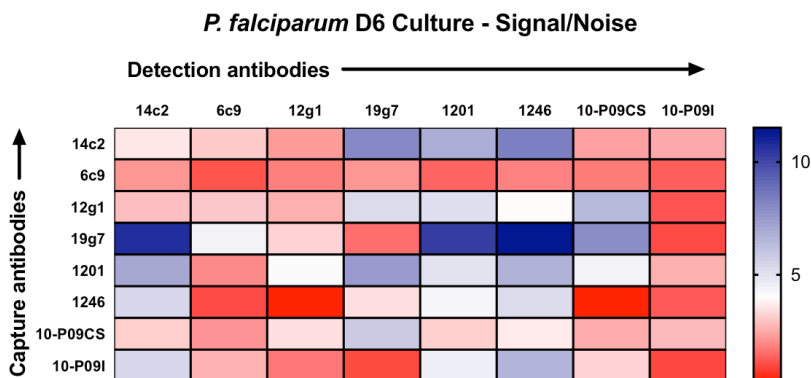


Figure 19. ELISA signal-to-noise ratios for checkerboard screening of α -*p*LDH mAb pairs against D6 *P. falciparum* culture (0 and 100 parasites/ μ l).

Next, the signal-to-noise values in this experiment as well as the rcPvLDH checkerboard experiment in Chapter IV were normalized and plotted in Figure 20. In this plot, each point represents one antibody pair, where the abscissa is the normalized signal-to-noise ratio for *Pf*LDH, and the ordinate is the normalized signal-to-noise ratio for rcPvLDH. An ideal antibody pair would reside along the line $y = x$ in the upper right-hand quadrant, indicating that it worked well for

*p*LDH antigens from both species. Based on these criteria, two candidate pairs were identified and tested in an on-bead format (highlighted in red). Both highlighted pairs included 19g7 as a capture antibody and differed in detection antibodies (10-P09CS and 1201). Neither of these pairs were tested by Piper et al., nor were they sold as matched pairs from their respective manufacturer(s). However, Piper et al. did show that 19g7 worked well for several pairs as a capture antibody in a paper immunochromatographic assay format.¹³² The pair with 19g7 capture and 1201:AP detection was chosen for the on-bead format, because it displayed lower background signal in the on-bead ELISA format.

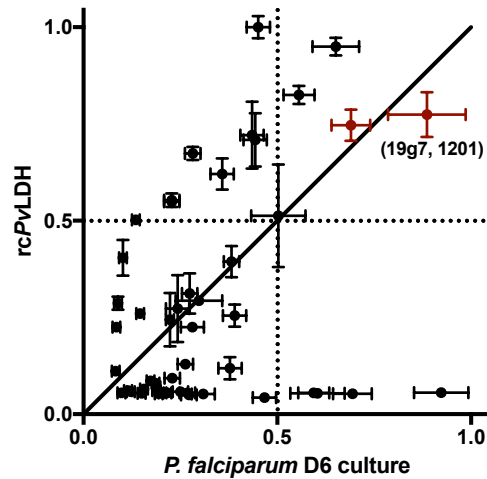


Figure 20. Pan-specific α -*p*LDH antibody pair screening results. Two candidate pairs are highlighted in red. 19g7 capture and 1201 detection antibodies were chosen for the *p*LDH on-bead ELISA.

With antibody pairs selected for *p*LDH and HRP2, a one-step, on-bead ELISA was developed and optimized for each individual biomarker. These individual assays were carried out by incubating magnetic beads functionalized with capture antibodies as well as enzyme-conjugated detection antibodies in samples consisting of 100 μ l parasitized whole blood and 100 μ l lysis buffer, allowing the sandwich complexes to form on the surface of the particles. The beads were then washed and re-suspended in the appropriate detection antibody substrate, and colorimetric

signal was measured by absorbance. In order to maximize signal-to-noise ratios, several variables were optimized by varying the parameter of interest while holding all other assay parameters constant (Figure 21). First, the amount of magnetic beads for biomarker capture was optimized to ensure there were enough binding sites to capture all the biomarker available, while minimizing nonspecific binding. Interestingly, for HRP2, as the amount of C1-13-conjugated beads increased beyond 50 μg , we observed a reduction in signal-to-noise ratio, likely due to the unique protein structure of HRP2 (Figure 21A - bottom). Because its secondary structure is simply a series of repeat-motifs, several capture antibodies may bind one HRP2 antigen, causing aggregation of the magnetic particles and preventing detection antibody from binding and producing signal.¹³⁴ In contrast, we did not see a significant decrease in signal-to-noise ratio for detection of *p*LDH when 19g7-conjugated beads were increased above saturation, since *p*LDH does not display repeated epitopes. Next, detection antibody concentration, sample incubation time, and substrate incubation time were optimized for each biomarker. Ideal conditions for the *p*LDH assay were found to be 100 μg 19g7-conjugated magnetic beads, 10 $\mu\text{g}/\text{ml}$ 1201:AP detection antibody, 15-minute sample incubation, and 15-minute incubation in BCIP/NBT. For the HRP2 assay, 50 μg of C1-13-functionalized magnetic beads, 1 $\mu\text{g}/\text{ml}$ MPFG-55P detection antibody, 15-minute sample incubation, and 5-minute incubation in TMB were chosen.

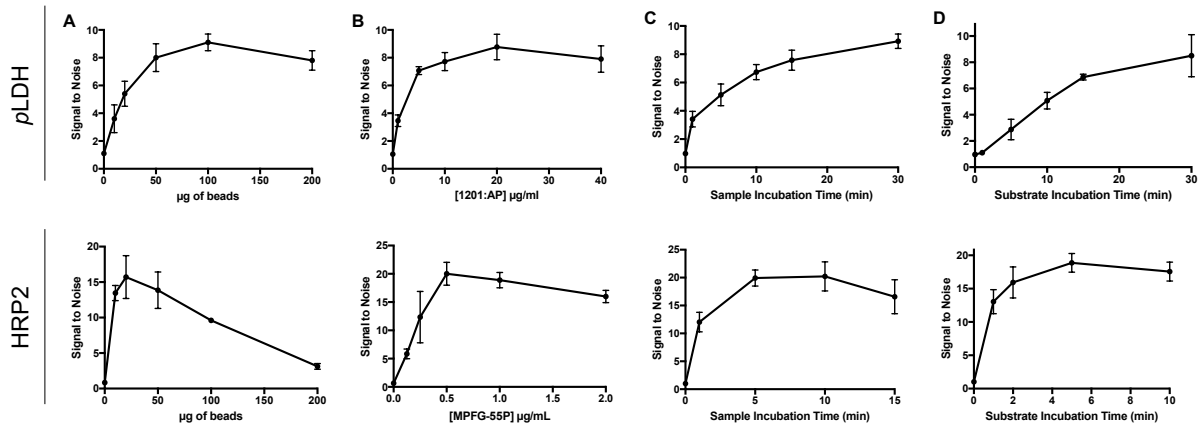


Figure 21. Optimization of (A) bead mass, (B) detection antibody concentration, (C) sample incubation time, and (D) substrate incubation time for the *pLDH* (top) and *HRP2* (bottom) on-bead ELISAs.

Performance of pLDH on-bead ELISA

The *pLDH* on-bead ELISA was performed in lysed whole blood in triplicate, once per day over five days (Figure 22). The linear range of the assay was 7.0 – 520 pM *pLDH*. The intra-assay variation was 7.5%, and the inter-assay variation was 11%, below the acceptable biomedical assay variation values of 15%.¹³⁵ The limit of detection (LOD), defined by the concentration at which the signal is $s_{blank} + 3SD_{blank}$, was 6.7 ± 3.4 pM, corresponding to about 5.2 parasites/ μ l of our in-house D6 *P. falciparum* culture, well within the asymptomatic regime. This LOD is three times lower than a commercially available well-plate ELISA kit for *pLDH* (Malaria Ag ELISA, SD Bioline, LOD = 19.3 ± 0.7 pM). Further, while the commercially available ELISA kit provides a pre-coated and blocked microtiter plate, it still required over 2 hours of incubation time before results were generated. In contrast, our on-bead ELISA for *pLDH*, which is an order of magnitude more sensitive, is completed with a mere 30 minutes' total incubation time.

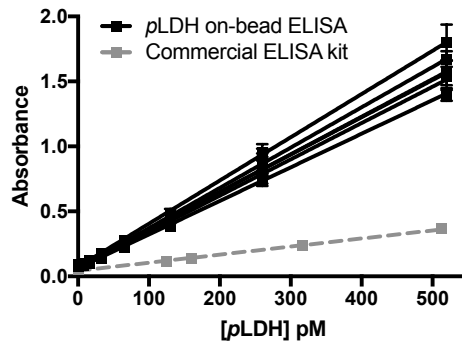


Figure 22. Standard curves for *pLDH* on-bead ELISA, measured at 620 nm, repeated in triplicate over 5 days (black) and SD Bioline Malaria Ag ELISA, measured at 450 nm (grey).

Performance of HRP2 on-bead ELISA

The HRP2 on-bead ELISA was evaluated in lysed whole blood in the same manner as the *pLDH* assay (Figure 23). The linear range of the assay was found to be 1.0 – 85 pM HRP2. The intra-assay variation was 4%, and the inter-assay variation was 7%, well below the acceptable value of 15%.¹³⁵ The LOD was 0.4 ± 0.2 pM, corresponding to about 0.2 parasites/ μ l of our in-house D6 *P. falciparum* culture. This LOD for our 20-minute HRP2 on-bead ELISA is over one order of magnitude lower than a 2.5-hour, commercially available well-plate ELISA kit for HRP2 (Malaria Antigen (HRP2) CELISA, Cellabs, LOD = 8.2 ± 0.2 pM).

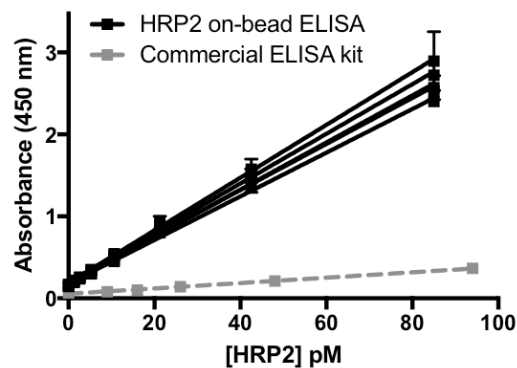


Figure 23. Standard curves for HRP2 on-bead ELISA repeated in triplicate over 5 days (black) and Cellabs Malaria Antigen (HRP2) CELISA (grey).

Design of on-bead SCSD ELISA for pLDH and HRP2

Figure 18 shows the workflow for the on-bead SCSD ELISA. Before combining the two independent assays into the dual format, it was demonstrated that there was no cross-reactivity between *p*LDH and the HRP2 assay and vice versa (Figure 24).

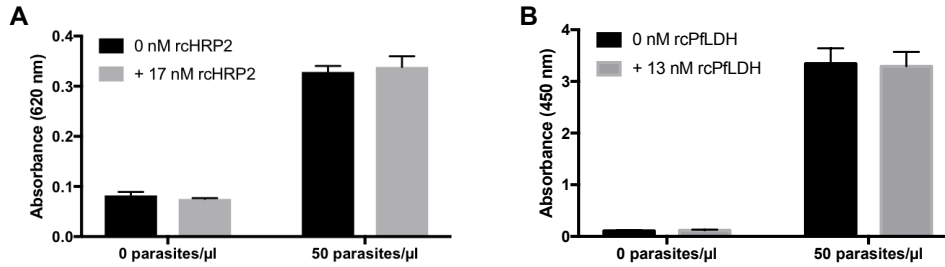


Figure 24. The (A) *p*LDH on-bead ELISA was not cross-reactive with recombinant HRP2 ($p = 0.8304$), and the (B) HRP2 on-bead ELISA did not react with recombinant *Pf*LDH ($p = 0.7179$) by two-way ANOVAs. The spiked concentrations (17 nM and 13 nM, respectively), represent a 20x excess of the biomarker concentration expected at 50 parasites/μl.

To perform the SCSD assay, magnetic particles functionalized with capture antibodies for *p*LDH and HRP2 were incubated in lysed whole blood samples along with the detection antibodies for each biomarker. Throughout the assay, the beads for both biomarkers were processed and washed simultaneously. The optimized bead masses and detection antibody concentrations determined in the development of the individual assays were also used in the SCSD format. A sample incubation time of 15 minutes was chosen, since this time was found to be sufficient for sandwich complex formation in both the *p*LDH and HRP2 assays. The beads were then washed and re-suspended in BCIP/NBT for 15 minutes for the detection of *p*LDH via the AP-conjugated detection antibody. Absorbance of the supernatant was measured at 620 nm. It was found that AP detection must precede HRPx detection, due to the pH sensitivity of AP and the acidic nature of the HRPx substrate (Figure 25). After *p*LDH detection, the beads were washed and re-suspended in TMB One solution for detection of HRP2. The reaction was stopped and HRP2 signal was

measured by absorbance at 450 nm. In this work, the capture beads for the SCSD assay were prepared separately for each biomarker; however, to facilitate large-scale SCSD detection, a single batch of capture beads could be prepared using the proper 2:1 ratio of *p*LDH to HRP2 capture antibodies.

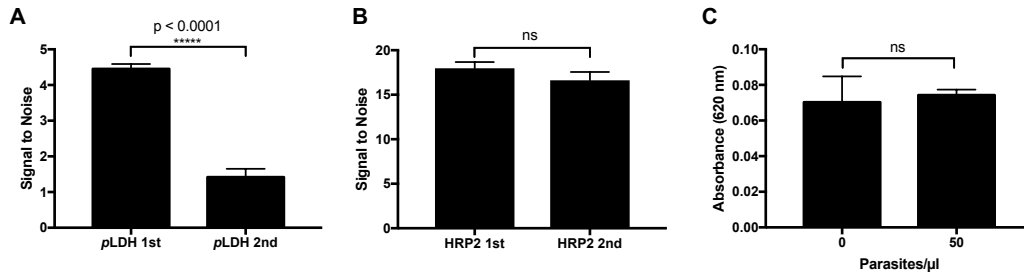


Figure 25. Signal to noise ratios for (A) *p*LDH and (B) HRP2 portions of the on-bead SCSD ELISA when the order of alkaline phosphatase (*p*LDH) and horseradish peroxidase (HRP2) detection was switched. A significant decrease in signal-to-noise ratio for *p*LDH was observed when HRP2 was detected first. However, there was no significant difference for HRP2 detection in either order of detection. Thus, alkaline phosphatase must be detected first. (C) The hypothesis that the acidic nature of the TMB substrate deactivates alkaline phosphatase was tested by performing a *p*LDH on-bead ELISA in which the beads were incubated in citrate buffer pH 3.5 (same as Promega TMB One Solution) before detection. Signal for a 50 parasites/μl sample was not significantly different from the blank.

Performance of on-bead SCSD ELISA for pLDH and HRP2

The on-bead SCSD ELISA for *p*LDH and HRP2 was evaluated by two users measuring standard curves ($n = 6$) once per day over five days. A summary of the SCSD assay parameters for each biomarker is shown in Table 8. Linear ranges for each biomarker in the SCSD format were unchanged compared to the individual assays. The intra- and inter- assay variabilities for *p*LDH and HRP2 detection remained below the accepted value of 15%. The assay was reproducible between users for both biomarkers, with a 7.5% coefficient of variation for *p*LDH and a 20% coefficient of variation for HRP2 (Figure 26). The simplicity of the assay was determined by providing a novice user blinded samples and comparing the signal obtained to that of an expert user. The novice measurements are highlighted in red in Figure 26 and were not found to be

significantly different from the expected absorbance values predicted by standard curves from expert measurements by paired T-tests ($P = 0.1699$ and $P = 0.495$ for *p*LDH and HRP2, respectively). The LODs for *p*LDH and HRP2 were 2.6 ± 1.5 pM and 1.6 ± 1.0 pM, corresponding to 2.0 and 0.9 parasites/ μ l, respectively, for our in-house D6 *P. falciparum* culture. These detection limits remain an order of magnitude lower than those of commercially available ELISA kits for both biomarkers. Further, to detect both biomarkers using commercially available kits, two aliquots of sample would need to be processed in parallel for a total of more than 2 hours before results are available. In contrast, the on-bead SCSD ELISA for *p*LDH and HRP2 measures both biomarkers from the same sample with incubation times totaling just 35 minutes.

Table 8. Performance of on-bead SCSD ELISA for *p*LDH and HRP2

Parameter	<i>p</i> LDH	HRP2
Linear range	7 – 500 pM	1.5 – 80 pM
LOD	2.6 ± 1.5 pM	1.6 ± 1.0 pM
Intra-assay variability	3.9%	6.2%
Inter-assay variability	6.4%	12.6%
Inter-user variability	7.5%	20%

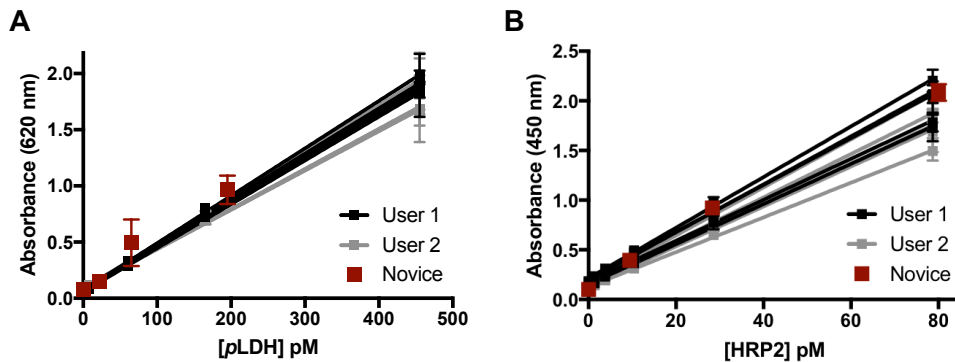


Figure 26. Two-user validation curves for SCSD on-bead ELISA for (A) *p*LDH and (B) HRP2. Novice measurements are highlighted in red.

The broad applicability of the on-bead SCSD ELISA was demonstrated by performing the assay on three additional *P. falciparum* strains. Standardized culture specimens (W2, Benin 1, and PH1 strains) designed for the development and evaluation of HRP2 diagnostics were obtained from the Foundation for Innovative New Diagnostics (FIND). These standards were received at a normalized concentration of 800 pg/ml HRP2, corresponding to 14.4 pM and confirmed in our laboratory by the commercially available HRP2 CELISA kit. These samples were diluted 2-fold in human whole blood to a final concentration of 7.2 pM HRP2 before lysis, and an on-bead SCSD ELISA was performed in triplicate. The assay successfully detected both *p*LDH and HRP2 for all three strains tested, and the HRP2 concentrations obtained were not significantly different from the FIND reference values (Figure 27). Because the assay performed well for multiple *P. falciparum* strains, and the *p*LDH portion of the assay was optimized for detection of the biomarker from both *P. falciparum* and *P. vivax*, we expect the on-bead SCSD ELISA to perform reliably with clinical samples.

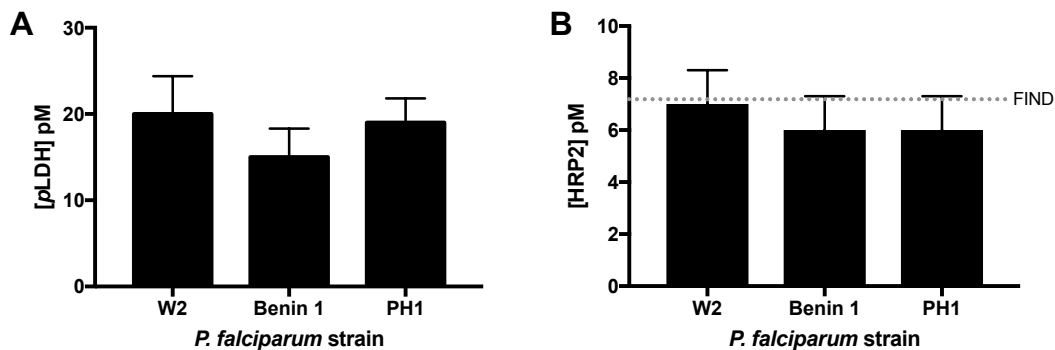


Figure 27. On-bead SCSD ELISA (A) *p*LDH and (B) HRP2 performance for W2, Benin 1, and PH1 strains as compared to reference values (for HRP2) obtained from FIND.

Magnetic particle-based immunoassays have been developed previously for *p*LDH and HRP2. For *p*LDH, magnetic microparticles were used to isolate *Plasmodium falciparum* lactate

dehydrogenase (*Pf*LDH) from lysed whole blood. The biomarker was then detected using the Malstat assay, an enzymatic turnover assay catalyzed by *Pf*LDH.¹³⁰ The detection limit for this method was 26 pM *Pf*LDH, an order of magnitude higher than the developed on-bead SCSD ELISA for *p*LDH and HRP2. Further, we have optimized the *p*LDH portion of the SCSD ELISA such that it can detect *p*LDH for both *P. falciparum* and *P. vivax*. For HRP2, Castilho et al. developed an immunomagnetic detection strategy in which a sandwich complex was formed on the surface of magnetic micro- or nanoparticles.¹³⁶ Electrochemical and optical detection strategies were used, and the limit of detection was found to be 12 pM, an order of magnitude higher than the dual on-bead SCSD developed herein.

The developed on-bead SCSD ELISA is a rapid, simple, and sensitive method to quantitatively measure two biomarkers. The simultaneous capture aspect of the developed assay allows two biomarkers to be measured from one sample, reducing the volume of sample required (100 μ l) to a single finger prick. The assay detection limits are lower than traditional well plate ELISAs, and the time-to-result is lower than currently available multiplexed immunoassays. Further, in contrast to commercially available multiplexed immunoassays, planar or suspension formats, the developed assay requires no laboratory equipment beyond what is required for conventional ELISAs. As such, it could be performed in settings where automated, hospital-grade diagnostic systems are impossible to implement due to lack of financial resources or infrastructure, efficiently providing accurate results with more clinical utility than traditional single-biomarker ELISAs. In the context of malaria elimination, the rapid and accurate detection of *p*LDH and HRP2 using our on-bead SCSD ELISA would be useful for several applications. For case management, the *p*LDH portion of the assay determines whether or not a patient has an active malaria infection, and the HRP2 portion distinguishes between *P. falciparum* and non-*falciparum* infections.

Additionally, the LODs of the developed assay are well within the asymptomatic regime, allowing for detection and treatment of asymptomatic infections that contribute to the malaria transmission reservoir and would have otherwise been missed by commercially available ELISA kits or rapid diagnostic tests.^{27,137} Finally, our assay would be advantageous in the context of surveillance and intervention management, allowing rapid and sensitive measurement of disease distribution and trends for both *P. falciparum* and non-*falciparum* malaria.

While this work focused on detection of malarial biomarkers, the format of the developed on-bead SCSD ELISA could be generalized to any disease for which the detection of two biomarkers is advantageous. As long as a validated pair of antibodies is available or can be found for each biomarker and cross-reactivity between the two biomarkers is at a minimum, an on-bead SCSD ELISA can be developed and optimized.

Conclusion

We have developed a magnetic bead-based ELISA for the detection of *p*LDH and HRP2 in which sandwich complexes form on the surface of the magnetic beads directly in lysed whole blood samples. The biomarkers are detected sequentially in the appropriate detection enzyme substrates, with detection limits of 2.6 ± 1.5 pM for *p*LDH and 1.6 ± 1.0 pM for HRP2, an order of magnitude better than commercially available ELISA kits for both biomarkers and within the asymptomatic regime for malaria. The low detection limits and high sensitivity of the assay can be attributed to active mixing of the beads within the sample to avoid mass transport limitations as well as careful assay optimization. The on-bead SCSD ELISA is repeatable and reproducible across multiple days and multiple users, and it is simple enough for novice users to produce accurate results. As such, it would be a valuable tool for case management and disease surveillance

in the context of malaria elimination. Further, the developed on-bead SCSD ELISA format could be applied to any disease in which the detection of two biomarkers is beneficial, provided that antibody pairs are available for both biomarkers of interest.

Acknowledgements

I would like to thank Dr. Keersten Ricks, Dr. Anna Bitting, and Dr. Lwiindi Mudenda for their contributions to this work. The material in this chapter was supported by the Bill and Melinda Gates Foundation Grand Challenges in Global Health Diagnostics (OPP 1028749), PATH: Diagnostics for malaria elimination toward eradication (1758-00-06-00), NIH/Fogarty International Center (D43 TW009348), Vanderbilt University through the Laboratories for Innovation in Global Health Technologies and the National Science Foundation Graduate Research Fellowship program under grants 1445197 (C.F.M and K.M.R.) and 0909667 (K.M.R.).

CHAPTER VI

CHARACTERIZATION OF *PLDH* AND *HRP2* CLEARANCE PATTERNS VIA RAPID ON-BEAD DETECTION FROM A SINGLE DRIED BLOOD SPOT^d

Introduction

In this Chapter, the SCSD ELISA developed in Chapter V is adapted for and applied to clinical samples from rural Zambia. All of the data presented in the previous chapter demonstrated that the SCSD ELISA could quantitatively measure *pLDH* and *HRP2* concentrations in mock patient samples. These mock samples, which consisted of venous whole blood spiked with parasitized red blood cells, were as close as possible to true clinical samples. However, the logistics and biohazard risk of venous whole blood sample collection, preservation, and transport in the field often make such samples impractical for large-scale clinical studies.

Many of these challenges are mitigated by the use of dried blood spot (DBS) cards for sample collection and preservation. In this sampling technique, which does not require specialized skills or equipment, microliter volumes of whole blood collected from a finger prick are spotted onto filter paper cards and allowed to dry at room temperature. These DBS samples are then easily stored or shipped, pose little biohazard risk, and result in improved biomarker stability compared to liquid samples.^{138,139} DBS cards are often cost-effective compared to venous whole blood sample tubes and require no instrumentation to carry out the minimally invasive collection procedure.¹⁴⁰

^d Portions of this chapter have been previously published in Markwalter, C.F. et al., *Am. J. Trop. Med. Hyg.* Accepted Feb 2018. © 2018 The American Society of Tropical Medicine and Hygiene.

Because of these advantages, DBS sample cards have been used extensively in surveillance and epidemiological studies of malaria. For example, extraction and detection/sequencing of nucleic acid material from DBS has not only allowed for malaria detection in symptomatic and asymptomatic patients,^{141–143} but also speciation,¹⁴⁴ determination of parasite diversity,¹⁶ identification of drug-resistant strains,^{145,146} and evaluation of rapid diagnostic tests on a population level.^{47,96,147} Dried blood spots also have been used for the detection of anti-malarial antibodies for serology-based epidemiological studies.¹⁴⁸

Quantitation of malarial protein biomarkers from DBS samples, while less common than nucleic acid detection, is also relevant in the context of malaria elimination. Recently, two studies have measured HRP2 in DBS patient samples. Rogier et al. used their DBS detection method to evaluate the accuracy of HRP2-based rapid diagnostic tests, and Gibson et al. demonstrated persistence of HRP2 in patient DBS samples after treatment compared to microscopy.^{41,149} While both of these studies demonstrated sensitive HRP2 quantitation from DBS, the species specificity, persistence, and increasing prevalence of *pfhrp2* gene deletions mean that measurement of HRP2 alone does not provide the full clinical picture.^{150,151}

The SCSD ELISA for detection of *p*LDH and HRP2 developed in Chapter V addresses these disadvantages.¹¹⁷ Not only does the SCSD assay distinguish between *falciparum* and non-*falciparum* infections, but it also differentiates between active and resolved *falciparum* infections. Additionally, the lower limit of detection of the SCSD assay, 2.0 parasites/ μ l for both *p*LDH and HRP2, was an order of magnitude improved over commercially available ELISA kits and would allow for detection of individuals with asymptomatic or submicroscopic malaria infections.¹¹⁷

In this Chapter, we adapt the previously developed SCSD assay for *p*LDH and HRP2 to detect these biomarkers from DBS and apply it to patient samples from rural Zambia. In particular,

the clearance patterns of both biomarkers relative to parasite clearance is investigated. The high sensitivity of this assay is ideal for DBS sample analysis, since these samples consist of just a few microliters of whole blood diluted into extraction buffer. Additionally, the total protocol requires only 45 minutes of total incubation time for quantitation of both biomarkers, increasing the throughput and information yield per sample.

Methods

Materials

Human Whole Blood (K3 EDTA) was purchased from Bioreclamation IVT (catalog no. HMWBEDTA3). Recombinant HRP2 protein (rcHRP2) was generously provided by PATH (Seattle, WA). Recombinant *P. falciparum* lactate dehydrogenase (rcPfLDH) was purchased from CTK Biotech (Cat #A3005). *P. falciparum* D6 strain was cultured in the lab (stock concentration 18,450 parasites/ μ l or 43,600 parasites/ μ l). Anti-HRP2 antibodies were purchased from Abcam (ab9203, ab9206, ab30384). Anti-pLDH antibodies were purchased from Vista Diagnostics (19g7, 1201). Vista 1201 was conjugated to alkaline phosphatase (1201:AP) using Abcam ab102850 and to horseradish peroxidase (1201:HRP \times) using Thermo #31489. BluePhos[®] Microwell Phosphatase substrate was purchased from KPL (#50-88-02), and TMB One was purchased from Promega (G7431). Dynabeads [®] MyOne[™] Streptavidin T1 beads were purchased from Life Technologies (#65601). Immulon 2HB ELISA plates (14-245-61) were purchased from Fisher Scientific. 903 Protein Saver Cards were purchased from GE Healthcare Life Sciences (10534612). 6 mm Biopunches were acquired from Ted Pella Inc. (catalog no. 15111-60). All other reagents were purchased from either Fisher Scientific or Sigma Aldrich. DBS extraction was performed with a Fisher Scientific Analog Vortex Mixer (02-215-365). Absorbance measurements

were collected on a Biotek Synergy H4 microplate reader (Vanderbilt University) or Biotek ELx808 microplate reader (Macha Research Trust).

Standardization of D6 P. falciparum culture

Two stocks of in-house D6 *P. falciparum* culture (18,450 parasites/ μ l and 43,600 parasites/ μ l) were used in this study. The *p*LDH and HRP2 concentrations in the 18,450 parasite/ μ l stock were previously reported as 1.3 and 1.7 pM per parasite/ μ l, respectively.^{41,117} Additionally, HRP2 in the 43,600 parasite/ μ l stock was previously determined to be 2.2 pM per parasite/ μ l.¹⁵² The *p*LDH concentration of in-house D6 *P. falciparum* culture (stock 43,600 parasites/ μ l) was determined to be 4.4 pM per parasite/ μ l using a standard well-plate ELISA, n = 6. Briefly, 100 μ l of 2 μ g/ml 19g7 in PBS was placed in a 96-well plate and incubated for 1 hour. The plate was washed three times with 250 μ l of 1x PBS with 0.1% Tween-20 (PBST). Next, 250 μ l of 15% non-fat dried milk in PBST was added to each well, and the plate was incubated for 2 hours. After washing three times with PBST, 100 μ l of standard *rcPf*LDH and in-house culture diluted in PBST with 0.1% non-fat dried milk were placed on the plate and incubated for 2 hours. The plate was then washed 5 times with PBST, and 100 μ l of 2 μ g/ml 1201:HRPx in PBST with 0.5% non-fat dried milk was added to each well, and the plate was incubated for 1 hour. After washing five times with PBST, 100 μ l of TMB One Solution was added to the wells, the plate was incubated for 15 minutes, and the reaction was quenched with 2M H₂SO₄. Absorbance was measured at 450 nm.

DBS preparation and extraction

DBS extraction was adapted from a previously reported method.⁴¹ DBS were prepared by depositing 10 µl of parasitized whole blood onto Whatman 903 Protein Saver cards. The spots were allowed to air dry for a minimum of 4 hours, removed using a 6-mm biopsy punch, and placed in 2 ml microcentrifuge tubes (one spot per tube). Next, 200 µl of PBST was added to each tube. The tubes were vortexed at 3200 rpm for 10 minutes and then placed in a mini-centrifuge for 30 – 60 seconds. The supernatant was removed and saved for analysis.

Bead preparation

Anti-*p*LDH and anti-HRP2 beads were prepared as reported previously in Chapter V.^{117,130} Stock solutions of antibody-functionalized beads were transported to Zambia in ambient conditions and stored at 4°C upon arrival.

SCSD ELISA with DBS extracts

The SCSD ELISA on DBS extracts was adapted from the previously reported method.¹¹⁷ To avoid bead aggregation, a low-resource filtering method was devised for removing small fibers and paper pieces from DBS extracts (Figure 29). Nylon fabric (Walmart, No Nonsense Knee Highs) was cut to the appropriate size and taped onto a Fisherbrand Flat-bottom PS 96-well plate (#12565501). A PCR plate with the bottoms of the wells cut off was then taped on top of the flat-bottom plate such that the nylon fabric was taut across the bottom of each well of the PCR plate, forming a nylon filter between the wells of the flat-bottom and PCR plates. Next, 100 µl of DBS extract was pipetted through the nylon fabric filter into the flat-bottom plate. The nylon fabric and PCR plate were removed, and 100 µl of 10% non-fat dried milk in PBST was added to each well.

Next, the SCSD ELISA was performed as described in Chapter V. Signal for *p*LDH detection was measured at 620 nm (Vanderbilt) or 630 nm (Macha), and HRP2 signal was measured at 450 nm.

Stability study

Dried blood spots were prepared and stored in Ziploc bags containing desiccant at room temperature (up to 8 days) and -20°C (up to 188 days). At varying time points, DBS were removed from storage and analyzed using the SCSD ELISA for *p*LDH and HRP2.

Study setting

Patient DBS samples were collected from the Nchelenge District of Zambia as part of a separate study on parasite clearance rates in children under 5 years of age presenting with uncomplicated malaria at a local clinic. These de-identified samples were made available to our team for assessment of *p*LDH and HRP2 clearance patterns relative to parasite clearance rates using the DBS SCSD ELISA.

Patient recruitment and ethics

Children at the clinic who tested positive for malaria (SD Bioline Pf) were recruited for this study only if a parent or guardian provided written informed consent. The samples were collected under IRB approval TDRC/C4/09/2014 and after approval was granted by the Zambian National Health Research Authority (MH/101/17/6).

Patient samples

Finger-prick blood samples were collected on Protein Saver 903 cards. At the time of collection, parasitemia was determined by thick smear microscopy; parasites were counted per 200 white blood cells (WBC) and parasite levels were determined using an estimate of 8000 WBC/ μ l. Samples were collected between December 2014 and August 2015, stored at -20°C, and analyzed by SCSD ELISA in July 2016. Patients were enrolled in the study and received treatment of artemether-lumefantrine (Coartem®) after malaria diagnosis by SD Bioline Pf RDT and confirmation of infection by thick smear. Samples (DBS and thick smears) were then collected at 15 time points after treatment: 0, 6, 12, 18, 24, 30, 36, 42, and 48 hours as well as 3, 7, 14, 21, 28 and 35 days. Samples for all time points for 15 patients were analyzed in this study.

Patient DBS sample SCSD ELISA

All patient samples were coded, and the assays were carried out blinded to microscopy results. Patient DBS samples were extracted and analyzed via the SCSD ELISA as described above with the following exceptions: (1) the standard curve (0 – 400 parasites/ μ l from 18,450 parasites/ μ l stock: 0 – 520 pM *p*LDH, 0 – 680 pM HRP2) consisted of 1:19 (v:v) parasitized whole blood diluted in PBST, mimicking the matrix of DBS extract, and (2) If the signal for either *p*LDH or HRP2 was above the linear range of the assay, the DBS extract was re-analyzed at the appropriate dilution.

Data analysis

Biomarker concentrations in DBS extracts were interpolated from best fits of linear standard curves. All error bars shown are the standard error of measurement. Limits of detection

were calculated as the biomarker concentration at $s_{blank} + 3SD_{blank}$. Intra-assay variation (%CV) was determined as the average relative standard deviation of triplicate measurements on a single plate. Inter-assay variation (%CV) was determined by finding the standard deviation of all measurements at a given concentration on different days and dividing by the average absorbance measurement at that concentration. For analysis of clearance rates across all patients, biomarker concentrations were normalized to their highest value across all time points for each patient.

Results and Discussion

DBS SCSD ELISA optimization

The protocol for the DBS sample SCSD ELISA was optimized systematically. Optimum conditions for HRP2 recovery from DBS were previously reported.⁴¹ In order to determine whether this method achieved sufficient elution of *p*LDH, the recoveries of both biomarkers were compared across multiple extraction times in PBST. The *p*LDH extraction efficiencies were not significantly different from those of HRP2 across all DBS extraction incubation times. In addition, increasing time did not result in significant differences in recoveries for either biomarker (Figure 28).

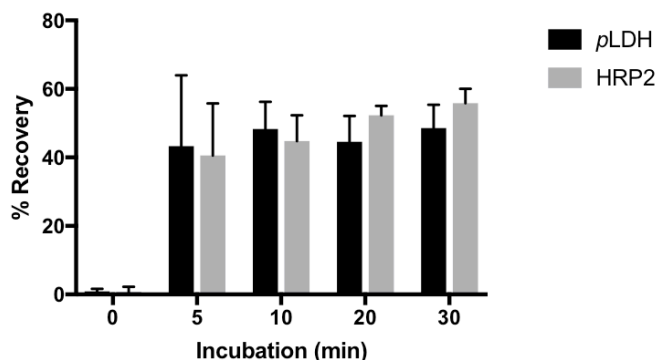


Figure 28. Recovery of *p*LDH and HRP2 as a function of DBS incubation time in PBST. No significant differences were found between extraction efficiencies of *p*LDH and HRP2, and 10 minutes was chosen as the optimum incubation time.

Once the DBS samples were extracted, the eluents were filtered in order to reduce nonspecific signal due to bead aggregation around small fibers and pieces of paper. To accomplish this, we developed an affordable, homemade filtering device that could be used in low-resource settings (Figure 29A). The filter consisted of a 96-well PCR plate with the tips of the tubes cut off. Cheap, commercially available nylon fabric covered the open bottoms of the PCR plate, which nested directly into a flat-bottomed 96-well plate. The nylon fabric was discarded after all samples and standards were filtered into the flat-bottomed plate, and the PCR plate was washed in 10% bleach, followed by three washes with DI water, and re-used with fresh nylon fabric for filtering. The total cost of the filtering device was \$0.10/sample, but recycling the PCR plate decreased filtering costs to as low as \$0.012/sample. As shown in Figure 29B, filtering DBS extracts through this device reduced nonspecific background signal by 4.0-fold for *p*LDH and 1.5 times for HRP2, increasing the signal-to-noise ratio from 1.6 to 3.2 and 3.3 to 4.5, respectively. Additionally, filtering the samples had the benefit of decreasing variation between repeated measurements for the *p*LDH portion of the assay (F test, $P = 0.02$).

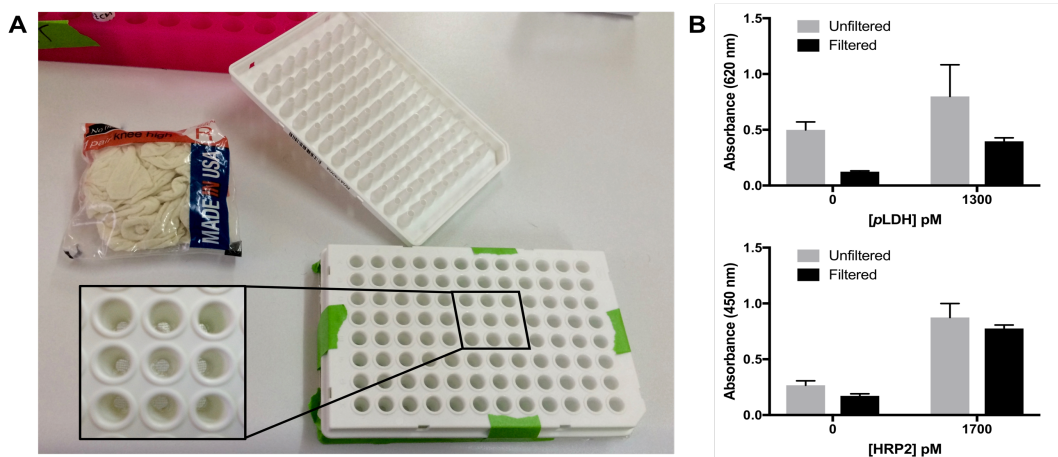


Figure 29. (A) Affordable 96-well plate filter for use in low-resource settings. (B) Filtering improves the performance of both the *p*LDH and HRP2 portions of the DBS SCSD ELISA.

After filtration, the SCSD ELISA was performed on DBS extracts. Because DBS extracts are more dilute than lysed whole blood, blocking conditions for the assay had to be re-optimized. It was found that adding an equal volume of 10% non-fat dried milk to DBS extracts resulted in the highest signal-to-noise ratio (Figure 30A). Magnetic bead volumes as well as detection antibody concentrations used in the SCSD ELISA for *p*LDH and HRP2 were screened in this new matrix, and it was found that the optimized conditions for these parameters were identical to those in the original protocol for both biomarkers (Figure 30B-C).

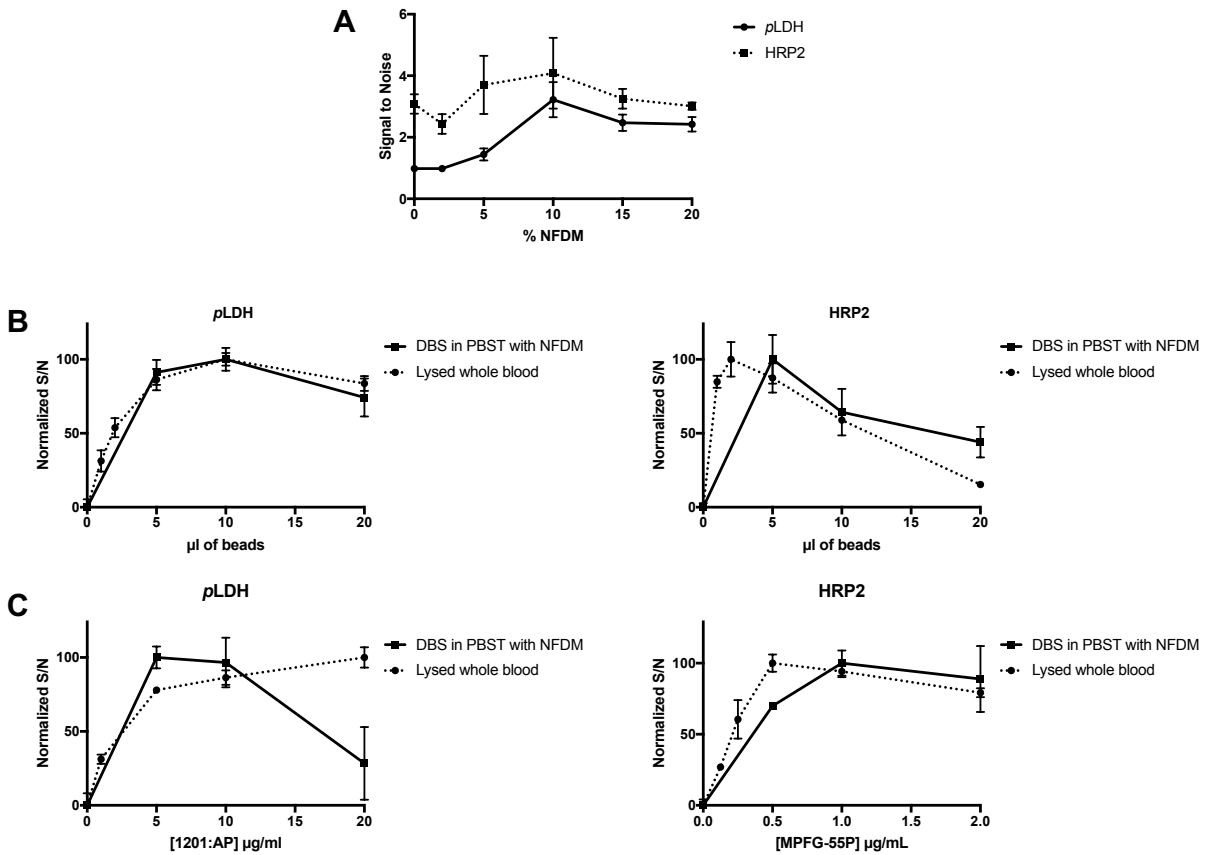


Figure 30. Optimization of (A) non-fat dried milk concentration in blocking solution, (B) antibody-functionalized magnetic bead volume for *p*LDH (left) and HRP2 (right), and (C) detection antibody concentration for *p*LDH (left) and HRP2 (right).

DBS SCSD ELISA performance

The performance of the DBS SCSD ELISA protocol was evaluated using DBS made from parasitized whole blood. The assay was performed in triplicate once per day for three days (Figure 31). The linear range of the assay was found to be 0.6 - 18 nM for *p*LDH and 0.15 – 9.5 nM for HRP2. The intra-assay variation was 10.5% for *p*LDH and 4.7% for HRP2. The inter-assay variation was 12.5% for *p*LDH and 16.9% for HRP2. All four %CV values demonstrate acceptable reproducibility. The limits of detection were 600 ± 500 pM *p*LDH and 69 ± 30 pM HRP2, corresponding to 150 and 24 parasites/ μ l in our in-house culture, respectively. It is important to note that these lower limits are reported as the biomarker concentrations in the original whole blood sample that was spotted onto the DBS card. Thus, the inherent dilution associated with DBS extraction as well as DBS extraction efficiency are taken into account. Although intended for laboratory use, the performance of the DBS SCSD ELISA was equal to or better than currently available malaria rapid diagnostic tests.

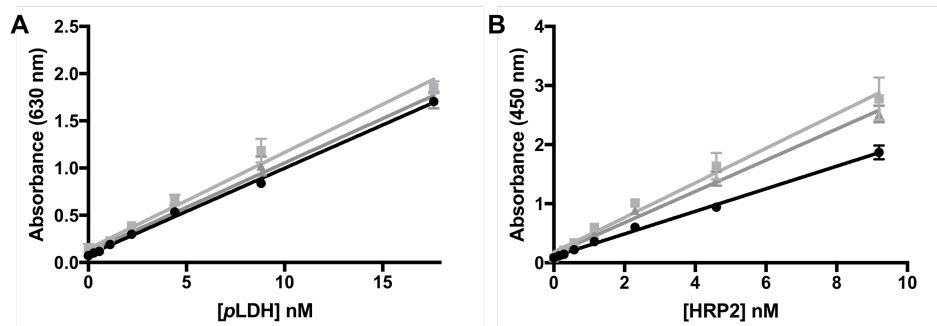


Figure 31. Standard curves for DBS on-bead SCSD ELISA for (A) *p*LDH and (B) HRP2.

Biomarker detectability over time

Dried blood spot cards are designed for long-term storage and preservation of biological samples. However, it has been shown that biomarker detectability from DBS changes over time.^{41,153} Thus, we measured *p*LDH and HRP2 signal from negative and positive (0 and 1000

parasites/ μ l) DBS stored at both -20°C and room temperature over time. As shown in Figure 32, neither *p*LDH nor HRP2 signal significantly changed after 6 months of storage at -20°C . However, for both biomarkers, recovery dramatically dropped over time when stored at room temperature. The *p*LDH signal at day 8 was reduced to 35% of the signal on day 0, and HRP2 signal was reduced to 31% in the same time period. This signal loss could be due to protein break-down and loss of structure over time or to reduced extraction efficiency off the dried blood spot card.

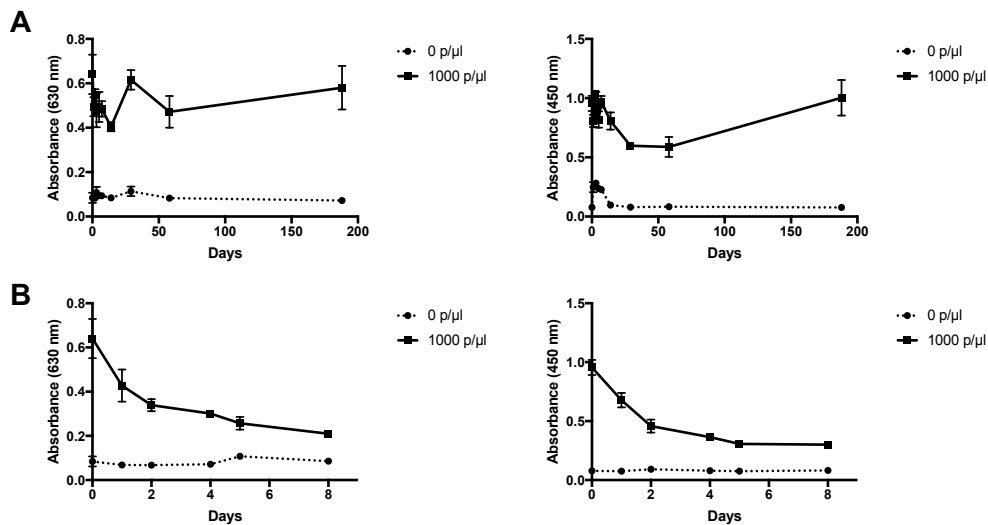


Figure 32. DBS Storage time at (A) -20°C and (B) room temperature vs. DBS SCSD ELISA signal for *p*LDH (left) and HRP2 (right).

Patient DBS samples from rural Zambia

Dried blood spot samples were collected over 15 time points after treatment for 15 patients; in total, 225 dried blood spots were analyzed for this study. Parasitemias at each time point were determined by microscopy at the time of collection. Because DBS patient samples were 1 to 2 years old when analyzed, it was not assumed that the extraction efficiency of these patient samples would be the same as freshly prepared DBS standards. Thus, rather than comparing patient DBS to a standard curve of freshly prepared DBS to determine biomarker concentrations in the original

whole blood sample that was spotted onto the card, biomarker concentrations in extracts were determined. This was performed at Macha Research Trust using standard curves in parasitized whole blood diluted 1:19, approximating the DBS extract matrix. Several assays were performed each day over the course of two weeks (n = 14). The intra-assay variation was 9.2% for *p*LDH and 6.1% for HRP2, and the inter-assay variation was 19.2% and 24.5% for *p*LDH and HRP2, respectively. Linear ranges for the assay were 10 – 520 pM *p*LDH and 10 – 680 pM HRP2. The limit of detection for the *p*LDH portion of the assay was 9 ± 6 pM, corresponding to 6 parasites/ μ l in our in-house culture. The detection limit for HRP2 was 7 ± 6 pM, which corresponds to 4 parasites/ μ l. These detection limits were used as cut-off values for determination of positive patient samples.

The relationships between biomarker concentrations and parasite levels for both *p*LDH and HRP2 based on all DBS patient samples analyzed in this study are shown in Figure 33. Similar to previous reports, HRP2 concentrations were several orders of magnitude higher than *p*LDH concentrations.⁵² Weak-to-moderate, but significant ($P < 0.001$), positive correlations with parasitemia were observed for both biomarkers. The Spearman correlation coefficient was 0.36 (0.23 – 0.47) for *p*LDH and parasitemia and 0.46 (0.36 – 0.57) for HRP2 and parasitemia, demonstrating the utility of these biomarkers for malaria diagnosis. The nonparametric Spearman correlation coefficient was chosen because the parasite densities and concentrations measured do not follow normal distributions (D'Agostino and Pearson normality test, $P < 0.001$). For *p*LDH, direct correlations with parasitemia have been demonstrated in the literature for both *P. falciparum* and *P. vivax* malaria.^{52,154,155} The strength of the correlation found in this study is lower than some reports, possibly due to lack of controlled DBS storage conditions upon sample collection. Previous reports have shown that uncontrolled DBS storage can lead to reduced *p*LDH recovery

in mock patient samples.¹⁵³ Similarly, we found DBS storage at room temperature resulted in a drastic reduction of *p*LDH detectability, potentially explaining why DBS from seven patients with high initial parasitemia had initial *p*LDH levels near or below the detection limit of the DBS SCSD ELISA. However, biological factors, such as parasite life cycle stage, also affect *p*LDH expression, potentially influencing the strength of the observed correlation.¹⁵⁶

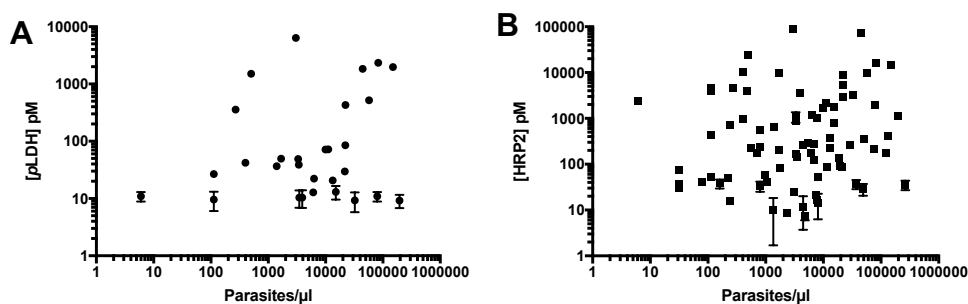


Figure 33. Correlations between (A) *p*LDH and parasitemia and (B) HRP2 and parasitemia in patient samples from rural Zambia. Weak correlations between biomarker concentrations and parasite burdens were observed. Note: for many data points, error bars are smaller than the size of the symbol representing the mean value.

Many studies have shown correlation between HRP2 and parasitemia, though some have found no correlation.^{41,52,157} While uncontrolled storage conditions have a similar detrimental impact on HRP2 detectability as for *p*LDH, initial HRP2 concentrations were detectable for all patients in this study. However, HRP2 expression has been shown to vary with parasite stage and strain.^{36,40} Additionally, the duration of infection and persistence of HRP2 in circulation, addressed in detail in the next section, likely influenced the strength of the correlation between biomarker concentration and parasite density.

Biomarker clearance

Unique parasite and biomarker clearance patterns were observed for each patient. Figure 34 shows clearance rates for 3 representative patients, and Figure 36 [Appendix C] shows

clearance rates for the remaining 12 patients. Overall, for the 15 patients in this study, the median parasite clearance time by microscopy after treatment with artemether-lumefantrine was 30 hours (Interquartile range: 24 – 36 hrs). Clearance times for the biomarkers were determined as the first time point in which the biomarker was undetectable for that time point and all subsequent time point measurements. The median *p*LDH clearance time was 36 hours (Interquartile range: 6 – 72 hrs) after treatment, following closely with parasite clearance time. In contrast, 13 of the 15 patients (87%) had measurable HRP2 levels at the final time point of this study (35 – 52 days after treatment). It should be noted that 5 of the 13 patients (38%) who were HRP2-positive at the last time point had undetectable HRP2 levels at least once in a previous time point. It is possible that uncontrolled storage conditions may have contributed to the undetectable HRP2 levels in the earlier time points. However, for one patient, *p*LDH levels also increased at the final time point, indicating possible reinfection or recrudescence (Table 12 [Appendix C], Patient 30).

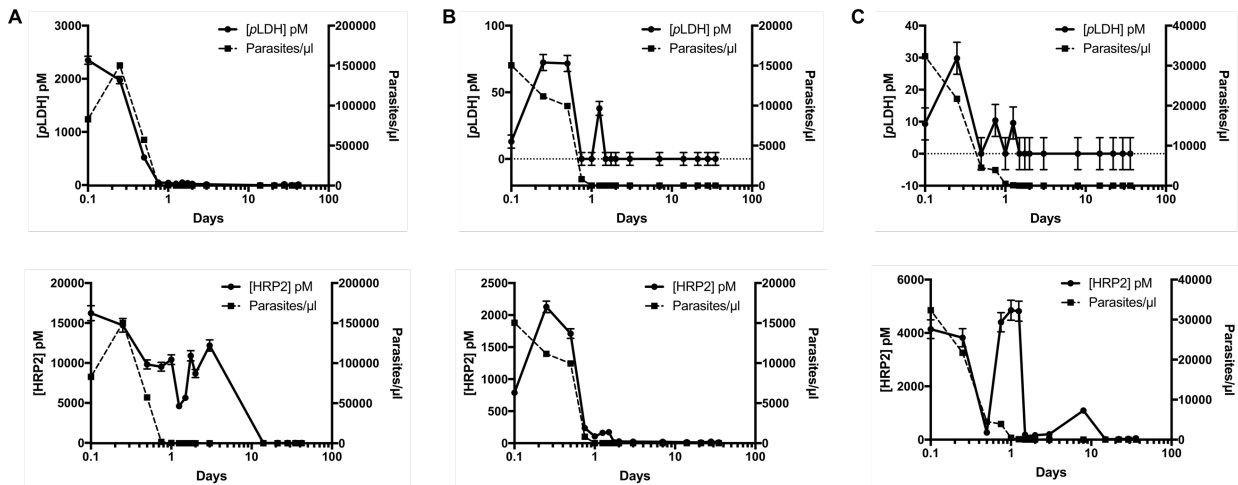


Figure 34. Biomarker clearance trends for three representative patients collected over 35 days. [*p*LDH] (top, solid) and [HRP2] (bottom, solid) in DBS extract and parasitemia (dashed) are plotted against time for (A) Patient 29, (B) Patient 55, and (C) Patient 58.

The relationship between intensity of infection and biomarker persistence was also investigated. Patient infection levels were classified based on initial parasitemias: low (0 – 14,999 parasites/ μ l, n = 7), medium (15,000 – 74,999 parasites/ μ l, n = 5), and high (\geq 75,000 parasites/ μ l, n = 3). Using a one-way ANOVA (df = 12), there were no significant differences in parasite clearance time (P = 0.4221), *p*LDH clearance time (P = 0.5543), or HRP2 clearance time (P = 0.3206) across all three groups.

The overall clearance patterns for all patients are represented in Figure 35. For each patient, parasite and biomarker levels were normalized to the highest concentration measured. The average across all patients at each time point was calculated and plotted, allowing for a clear visualization of the overall parasite, *p*LDH, and HRP2 clearance patterns in this study. In general, *p*LDH became undetectable before infections became submicroscopic. In contrast, HRP2 remained in circulation for the duration of the study, decreasing in concentration slowly over time. The persistence and accumulation of HRP2 in circulation over the duration of an infection likely explains why HRP2 concentrations were significantly higher than *p*LDH concentrations for all patients in this study.

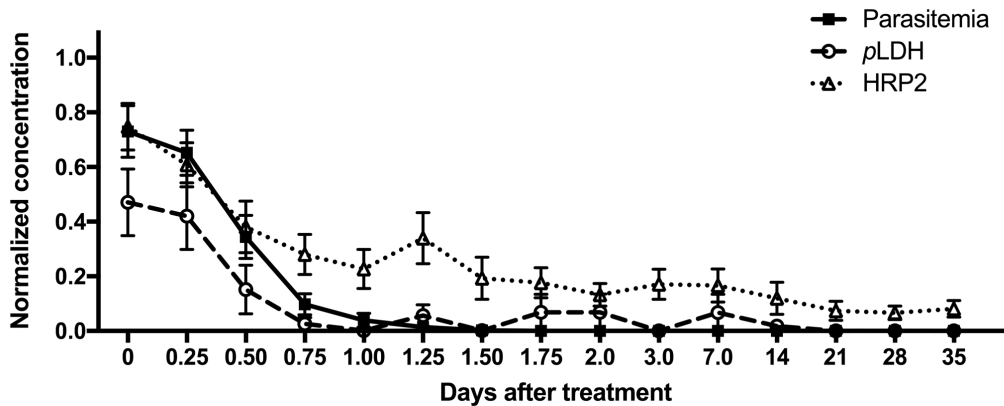


Figure 35. Normalized parasite, *p*LDH, and HRP2 clearance patterns plotted over time.

In the context of malaria elimination, an ideal evaluation tool would be positive when a patient has an active infection and negative in the absence of parasites. Distinguishing between

falciparum and non-*falciparum* infections would also be clinically useful and inform treatment and provide useful epidemiological data. A sensitive dual *p*LDH and HRP2 detection method could fulfill these ideals; however, this work highlights the challenges of developing a dual assay. While *p*LDH detection could overcome the lack of specificity of HRP2 that results from persistence in host circulation after parasite clearance, the relatively low levels of circulating *p*LDH mean that active infections could be missed in the dual format. Such a result would undermine malaria elimination efforts, allowing active infections to persist and contribute to transmission. In contrast, an HRP2-only diagnostic could result in over-diagnosis and treatment, potentially resulting in unnecessary costs and failure to treat other serious illnesses. Thus, there is a pressing need to develop more sensitive molecular recognition elements and detection methods for *p*LDH.

The previously developed SCSD ELISA fills the need for a sensitive dual *p*LDH and HRP2 assay and is an order of magnitude more sensitive than commercially available ELISA kits for both biomarkers.¹¹⁷ Here, the assay was adapted for detection of both biomarkers from a single dried blood spot. Uncontrolled DBS storage conditions and the inherent dilution when DBS are extracted into buffer contributed to reduced analytical sensitivity of the assay, though detection limits of the DBS SCSD ELISA remain comparable to commercially available ELISA kits for *p*LDH and HRP2 applied to whole blood samples. In contrast to commercially available ELISA kits, which are singleplex and take 3 – 6 hours to complete, we have demonstrated that the SCSD ELISA is capable of detecting two biomarkers from a single DBS in less than 1 hour. Additionally, the ease with which the antibody-functionalized beads were transported to Zambia and the possibility of lyophilizing the beads for stable ambient storage could allow the developed assay to be applied in laboratories in low-resource settings. Thus, the DBS SCSD ELISA has the potential

to increase the throughput and information yield of large epidemiological or surveillance studies based on DBS samples. To this end, we have demonstrated the utility of this assay for evaluation of biomarker clearance in a patient population from rural Zambia. In the future, the DBS SCSD ELISA will be useful for characterization of clearance patterns in other populations and could also serve as a rapid, preliminary screening tool for parasites with *pfhrp2* deletions.

Conclusion

In this Chapter, the on-bead simultaneous capture and sequential detection ELISA for *pLDH* and HRP2 was adapted for use with dried blood spot samples. For mock DBS samples, the assay was highly reproducible and could detect *pLDH* as low as 600 ± 500 pM and HRP2 as low as 69 ± 30 pM, corresponding to 150 and 24 parasites/ μ l in our in-house culture, respectively. Using the DBS SCSD ELISA, we demonstrated the need for controlled DBS storage; the detectability of both *pLDH* and HRP2 from DBS decreased nearly 70% after 8 days of storage at room temperature. Next, we applied the DBS SCSD ELISA to patient DBS samples from rural Zambia to measure *pLDH* and HRP2. In these samples, weak-to-moderate correlations between biomarker concentration and parasite density were found for both biomarkers, and the overall concentrations of HRP2 were several orders of magnitude higher than those of *pLDH* concentrations. Finally, biomarker clearance patterns relative to parasite clearance were studied. It was found that *pLDH* clearance followed closely with parasite clearance, while 87% of patients had detectable levels of HRP2 for 35 – 52 days after treatment. This work demonstrated the utility of the SCSD ELISA for quantifying *pLDH* and HRP2 from DBS samples and its potential for future application in epidemiological studies.

Acknowledgments

First, I would like to thank the children and guardians who participated in this study. I am also grateful to Macha Research Trust for collecting and providing the dried blood spot patient samples and for use of their on-site laboratories. Thank you to Dr. Lauren Gibson, Dr. Lwiindi Mudenda, Dr. Danielle Kimmel, Saidon Mbambara, and Dr. Phil Thuma for contributing to this work. We thank Dr. Kim League for culturing D6 *Plasmodium falciparum*. The assay development and sample analysis portions of this work were supported by the National Institute of Health/Fogarty International Center [D43 TW009348] and Vanderbilt University through Laboratories for Innovation in Global Health Technologies. The clinical portion of the study was supported by the National Institutes of Health as part of the International Centers of Excellence for Malaria Research [U19 AI089680]. Additional support was provided by the National Science Foundation Graduate Research Fellowship [1445197].

CHAPTER VII

CONCLUSION

Summary and Future Directions

In this work, each component of the conventional diagnostic format was examined and optimized with the goal of improving diagnosis of malaria and schistosomiasis in endemic settings. Specifically, Chapter II demonstrated that endogenous α -HRP2 antibodies present in the whole blood sample matrix form immune complexes with HRP2 in the symptomatic patient population of a low-transmission area in rural Southern Zambia. In Chapter III we developed a novel, equipment-free sample preparation method that relied on PAMAM dendrimer-coated magnetic particles to capture, purify, and concentrate CAA biomarker from its variable urine sample matrix before application to the ultrasensitive UCP lateral flow assay. Chapter IV evaluated the relationship between the kinetic parameters of molecular recognition elements and their respective performance in an immunoassay format for malarial biomarkers HRP2 and *p*LDH. In Chapter V, lessons learned about each diagnostic component in the previous chapters were synthesized to develop a highly sensitive magnetic bead-based assay for both *p*LDH and HRP2. Careful optimization of each component, including matrix interference reduction, sample preparation, and signal generation, resulted in a rapid multiplexed assay in which *p*LDH and HRP2 detection took 35 minutes and had detection limits an order of magnitude better than commercially available ELISA kits in venous blood. Finally, in Chapter VI, the developed assay was adapted for DBS sample extracts and used to characterize *p*LDH and HRP2 clearance patterns in patients living in a highly endemic region of Zambia.

Several major themes emerged over the course of this work. Perhaps most pervasive was the drastic impact that variation in biological sample matrices can have on diagnostic assays. The natural progression of assay development and optimization typically begins with initial experiments in simple buffered solutions at the relevant physiological pH and, upon successful demonstration of biomarker detection, advances through increasingly complex matrices (e.g. human serum albumin solution, serum, plasma, whole blood). The most complex mock samples typically consist of pooled control samples (e.g. whole blood) spiked with the native biomarker of interest and enable assay optimization based on an “average” patient from the geographic area where the control sample was collected. These samples are ideal for proof-of-concept demonstrations, and many novel diagnostic strategies are published in mock samples; however, patient-to-patient variation within and between geographic regions can lead to unexpected results and must be considered during initial assay design and optimization studies. In this work, the most obvious example of patient-to-patient variation within a single geographic area was highlighted in Chapter II, which demonstrated that some (but not all) patients in the Southern Province of Zambia with active or recent malaria infections had circulating α -HRP2 antibodies that formed complexes with the biomarker. Further, the extent to which these immune complexes affected HRP2 detectability varied among the patients who produced them. In Chapter III, we saw significant regional differences between spiked North American and/or European control urine and Egyptian patient urine samples in our ability to capture and concentrate *Schistosoma* biomarker CAA from large sample volumes. Egyptian patient samples needed to be diluted 10-fold in order to achieve similar performance to the N. American/European mock samples, and we hypothesized that this was due to differences in urine salt concentration, which could result from differences in diet,

hydration, and health status (i.e. patients infected with schistosomiasis may be more dehydrated than healthy European individuals).

These observations highlight the importance of anticipating and studying matrix variability and of validating novel diagnostic tools in endemic clinical samples. Mitigating variations in sample matrices often requires additional sample preparation steps such as sample dilution and acid/heat treatment. For laboratory-based detection methods (i.e. Level 3), these extra steps are frequently inconsequential. In the SCSD ELISA developed in Chapter V, for example, interference from human α -mouse antibodies (HAMA) and rheumatoid factor (RF) was anticipated and reduced simply by adding a blocking reagent containing mouse IgG. However, in low-resource settings, additional sample preparation steps must be fully integrated with a diagnostic test to minimize the total number of user steps (“U” in ASSURED). Our lab has demonstrated success in devising and producing integrated sample preparation devices for malaria RDT enhancement.^{106,112} I am confident that the group will continue to develop innovative solutions for immune complex dissociation (Chapter II) and enhancement of the UCP-LF CAA schistosomiasis test (Chapter III) that fit the ASSURED criteria and can be used at the point of care.

The second concept that permeates this work is the importance of the strength of molecular recognition element/target interactions to the performance of an assay or diagnostic test. It is safe to say that this notion is not groundbreaking or surprising; frankly, the idea that fast and/or high-affinity interactions lead to better diagnostics is basic intuition. However, this dissertation serves as a case-study of the real-world implications of differences in antibody/antigen affinities – a tale of two biomarkers, so to speak. First, there is HRP2, which I like to call the “best worst biomarker” for malaria. Its apparent lack of tertiary structure and unique primary amino acid sequence, which consists of a series of histidine-rich tandem repeat motifs, results in up to 19 repeated linear

epitopes per target, depending on the strain (and thus geographic region) of *P. falciparum* and the antibody in question.^{36,134} These repeated epitopes increase the avidity, or the cumulative strength, of antibody/antigen interactions, since the locally high epitope concentration enables multivalent interactions and quick re-binding after dissociation. Indeed, in Chapter IV, most affinity constants for commercially available and novel monoclonal α -HRP2 antibodies were below the 1 pM detection limit of the Octet BLI instrument due to off-rates so slow they could not be measured. These strong interactions result in highly sensitive HRP2-based laboratory assays and diagnostics, as evidenced by the remarkably sensitive magnetic bead-based HRP2 ELISA presented in Chapter V, which had a detection limit of 0.2 parasites/ μ l—well below the average asymptomatic parasitemia of 5 parasites/ μ l found by Imwong et al. using their ultrasensitive molecular detection techniques.^{31,32} The inherent advantages that the structure of HRP2 affords in terms of molecular recognition, along with its relatively high concentration in peripheral circulation of infected individuals, makes it the “best” biomarker for malaria and likely drove its adoption as the primary malarial biomarker used in RDTs. However, the numerous disadvantages of HRP2—the fact that it is only expressed by one *Plasmodium* species, its persistence in circulation after successful parasite clearance, and the rising incidence of *pfhrp2* gene deletions—may threaten elimination campaigns and surveillance strategies that rely on HRP2 detection alone.

In theory, *p*LDH is an ideal alternative to HRP2 as a malarial biomarker; it is expressed by all species of malarial parasites, clears from host circulation shortly after successful treatment, and is essential to parasite survival, decreasing the likelihood of *pldh* gene deletions. However, *p*LDH lacks repeated epitopes and has defined tertiary structure. As a result, we observed that antibody/antigen interactions for *p*LDH were on-average several orders of magnitude weaker than those for HRP2 (Chapter IV). The consequences of this are easily observed in Chapters V and VI.

In these sections, we developed and applied one of the most sensitive *p*LDH detection strategies compared to commercial kits and those published in the literature to date. However, for every developed and commercial assay for *p*LDH evaluated, the limits of detection and analytical sensitivities were significantly worse than those of HRP2. These observations are not limited to the work in this dissertation; the World Health Organization has reported on numerous occasions that *p*LDH-based RDTs severely and consistently underperform compared to HRP2-based RDTs at low parasite densities (200 parasites/ μ l).^{53,158} Thus, in settings with large subpatent infectious reservoirs, it is likely that these tests would be insufficient for effective case management and elimination campaigns.

It is clear that in many regions, malaria elimination will require more sensitive diagnostics that detect biomarkers other than HRP2. Thus far, *p*LDH is the best known alternative biomarker. So what strategies can be employed to develop more sensitive *p*LDH-based tests? This question is best approached by considering each component part of a diagnostic. Sample preparation techniques that enrich biomarkers from large-volume samples are advantageous for improving diagnostics that target biomarkers like *p*LDH, which are present in low concentrations in clinical samples. Our group has already developed one magnetic bead-based sample preparation approach in which *p*LDH is enriched before deposition onto an RDT.¹⁵⁹ In this strategy, similar in principle to the work performed in Chapter III, *p*LDH is removed from its variable whole blood mixture and concentrated from a large-volume sample, resulting in a greater number of target molecules delivered to the test. Like the CAA work, a simple-to-use paper device that fully integrates this sample preparation method with biomarker detection will enable implementation at the point of care. This work is ongoing in the Wright group and has demonstrated promise.

Another approach to improving *p*LDH-based tests would be to develop higher-affinity molecular recognition elements. An advantage to this strategy is that improved affinity reagents could be easily integrated into the standard lateral flow assay format—the diagnostic format that most fits the ASSURED criteria. There are a multitude of techniques that can be applied to developing and quantifying the affinities of novel molecular recognition elements, and the field remains fairly open for exploration for *p*LDH. Much of the initial work generating monoclonal antibodies against *p*LDH, both pan-specific and species-specific, was performed by the Makler group (1999 - 2011).^{50,128,132,155} The antibodies produced by the group represent a majority of the commercially available α -*p*LDH clones and are thus likely the most prevalent clones in commercial RDTs. Only a couple groups have since developed *p*LDH-targeting antibodies and used them in immunoassays, although no significant improvements over the status quo were achieved.^{160,161} Additionally, aptamers—short, single-stranded oligonucleotides that bind to a target—have been pursued as molecular recognition elements for *p*LDH. The thermal stability as well as the synthetic ease and reproducibility of aptamers make them attractive molecular recognition elements. Several distinct *p*LDH-specific aptamers have been developed, characterized, and employed in numerous assays in a variety of formats; however, their affinities were found to be on the order of 10^{-9} - 10^{-6} M, and overall assay performance has not proven to be better than their antibody-based counterparts.^{162–173}

One strategy that remains to be pursued for *p*LDH is the development of bispecific molecular recognition elements that target distinct or adjacent epitopes on the protein. *p*LDH is natively a tetramer and current antibodies are known to target at least three distinct epitopes on the protein (see Appendix D and Bauer et al.).¹⁵⁹ Based on our work with HRP2, it is clear that when a molecular recognition element has multiple opportunities (epitopes) to interact with the target,

the increased avidity results in stronger interactions. So why not engineer a molecular recognition element to do the same for *p*LDH? Most often utilized in therapeutic applications, bispecific antibodies have been developed and employed in diagnostics, although typically only to cross-link the target with a detection enzyme.¹⁷⁴ Dimerized aptamer pairs have been shown to have affinity constants an order of magnitude better than each of the monomers from which they were derived.¹⁷⁵ Multi-dentate macrocyclic peptides have also leveraged cooperative binding and have demonstrated impressive affinities for their targets.¹⁷⁶ Whether these strategies would result in improved molecular recognition elements for *p*LDH is unknown. However, it is clear that if malaria elimination campaigns must rely on *p*LDH-based RDTs for case management and surveillance, the molecular recognition elements in the tests must be improved.

Signal amplification is another approach for improving the sensitivity of a diagnostic. For the on-bead ELISA format discussed in Chapters V and VI, enzymes are used to generate colored signal. Further improvements on the signal-to-noise ratios of these assays could be achieved if a kinetic ELISA (measuring the rate of signal generation over time) were performed rather than endpoint measurements. For paper-based diagnostic tests, several techniques for enhancing signal have been proposed, including nanoparticle dissolution, reductive nanoparticle enlargement/silver enhancement, and nanoparticle enzyme mimics. These strategies increase the complexity of the tests and require creative device design to incorporate additional chemistry without increasing the number of user steps. The Yager and Fu groups have pioneered the development of 2-dimensional paper networks (2DPNs), which allow for precisely timed delivery of reagents to a test region and have demonstrated promise for enabling signal amplification (particularly silver enhancement) on paper-based tests.^{177–183} Appendix E is a short discussion of partially realized strategies I pursued to enable complex chemistry on paper diagnostics using a photopolymerizing valving system.

Finally, we must consider the possibility that the most ideal malarial biomarker has yet to be discovered. Recently Mu et al. screened proteomic data from 10 different studies in order to find a biomarker that combined the desirable characteristics of both HRP2 and *pLDH*, including tandem repeats (HRP2), necessity for parasite survival (*pLDH*), and conservation across all parasite species (*pLDH*). A previously unexplored biomarker (a *Plasmodium* homolog of insulin-degrading enzyme, *pIDE_h*) emerged, and the group developed an ELISA and immuno-PCR assay. Although the sensitivity of the *pIDE_h* assay was similar to that of *pLDH*, the work demonstrated that further proteomic research may lead to a more ideal malarial biomarker.

In the context of malaria elimination, it is worth noting that in certain geographic regions, the tools that we currently have are sufficient for achieving elimination. Between 2011 and 2016, 10 previously malaria-endemic countries reported zero indigenous malaria cases for 3 years or more, a measure of elimination established by the World Health Organization.⁸ However, in regions with high malaria burdens, accurate and detailed surveillance are critical for determining the diagnostic tools and interventions needed for elimination. Careful tracking of *pfhrp2* deletions, antimalarial resistance, and insecticide resistance informs elimination strategies by defining the constraints and challenges within a given region. For example, in an area with a large subpatent infectious reservoir in which there is no evidence of *pfhrp2* deletions, the ultrasensitive HRP2 RDT discussed in Chapter I would likely be the best diagnostic tool to use for case management and surveillance. However, in populations where *pfhrp2* deletions are on the rise, alternative rapid tests are needed. The strategies and potential alternatives discussed above could fill this need.

Outlook and Perspective

The scientific outcomes of this dissertation and the future work that will follow have and will continue to require meticulous lab work and rigorous data analysis. However, the motivations behind this work and its potential impact are perhaps best understood by looking beyond the laboratory at the broader human context. It does not take many morning newspapers or evening news reports to understand that there is extreme inequity in access to healthcare in our own country and around the world. That there are entire categories of diseases labeled “diseases of poverty” and “neglected tropical diseases” claiming millions of lives every year is telling in and of itself. As human beings, we should find it unacceptable that a person’s birthplace, income, education, race, ethnicity, zip code, gender, or gender identity defines the standard of care they receive. Poor and vulnerable populations die from diseases and conditions that are easily treatable and preventable in resource-rich facilities (like Vanderbilt). In the local, national, and global communities, these are our neighbors.

So what can be done? It is clear that health equity will not be achieved by a single person, organization, government, or field of work. Progress will require effort from every field to overcome the social, political, medical, and scientific challenges of bringing equitable health solutions to communities in poverty. In the increasingly nationalistic—and often discriminatory—global political climate, we have to be activists for policy and funding to support local, national, and global efforts toward health equity.

Politics aside, the global health field has never been in a better position to eliminate diseases of poverty. Tools and knowledge accumulated over the last several decades of work have contributed to improvements in drugs, vaccines, diagnostics, and insecticides. Increased connectivity and data processing capacity allows us to look at trends in real time on a population

level. Many challenges remain, including those discussed in this dissertation, and they should be addressed in a way that empowers those who have the most at stake. Innovative solutions will require investment in health and education systems that can support them. Over the last five years, I have found purpose in this mission and plan to commit my skills (analytical and others) toward health equity for the remainder of my career.

APPENDIX A

SUPPORTING INFORMATION: CHAPTER II

Table 9. HRP2 concentrations measured in the heat dissociation and pull-down assays for all 126 patient samples analyzed in this study. Grey cells represent samples for which the immune complex assay was not performed.

Sample Collection Strategy	Sample ID	Symptoms?	Parasites/ µl	Heat Dissociation ELISA				Immune Complex Pull-Down Assay		Total HRP2		% Immune-Complexed HRP2	
				Untreated [HRP2] (pM)	Error	Heated [HRP2] (pM)	Error	Complexed [HRP2] (pM)	Error	pM	Error	%	Error
Passive case detection	VZH060	Y	0	0	0	0	0						
	VZH061	Y	0	0	0	0	0						
	VZH062	Y	0	0	0	0	0						
	VZH064	Y	0	0	0	0	0	0	0	0	0	-	-
	VZH065	Y	448	655	35	618	9	3.6	0.7	658.3	35.4	0.55	0.11
	VZH066	Y	171	60	4	14	1	0	0	60.2	3.8	0	0
	VZH067	Y	0	0	0	0	0	0	0	0	0	-	-
	VZH070	Y	0	0	0	0	0	0	0	0	0	-	-
	VZH071	Y	0	0	0	0	0						
	VZH072	Y	0	0	0	0	0	0	0	0	0	-	-
	VZH073	Y	0	0	0	0	0	0	0	0	0	-	-
	VZH074	Y	0	0	0	0	0	0	0	0	0	-	-
	VZH075	Y	0	0	0	0	0	0	0	0	0	-	-
	VZH076	Y	0	0	0	0	0	0	0	0	0	-	-
	VZH077	Y	0	0	0	0	0	0	0	0	0	-	-
	VZH078	Y	0	0	0	0	0	0	0	0	0	-	-
	VZH079	Y	85853	912	40	665	65						
	VZH080	Y	0	0	0	0	0	0	0	0	0	-	-
	VZH082	Y	0	0	0	0	0	0	0	0	0	-	-
	VZH083	Y	0	0	0	0	0	0	0	0	0	-	-
	VZH084	Y	0	0	0	0	0	0	0	0	0	-	-
	VZH085	Y	0	0	0	0	0	0	0	0	0	-	-
	VZH086	Y	0	0	0	0	0	0	0	0	0	-	-
	VZH087	Y	0	0	0	0	0						
	VZH088	Y	0	0	0	0	0	0	0	0	0	-	-
	VZH089	Y	0	0	0	0	0						
	VZH090	Y	0	0	0	0	0	0	0	0	0	-	-
	VZH092	Y	149	1990	87	1787	11	33	12	2024	88	1.6	0.6
	VZH095	Y	0	0	0	0	0	0	0	0	0	-	-
	VZH098	Y	0	0	0	0	0						
VZH099	Y	0	0	0	0	0	0	0	0	0	-	-	
VZH100	Y	0	0	0	0	0	0	0	0	0	-	-	
VZH104	Y	153377	538	25	462	14							
VZH105	Y	89236	1556	45	2646	178	2.6	0.4	1559	45	0.17	0.02	
VZH106	Y	34648	1042	11	1099	58							
VZH107	Y	0	0	0	0	0							
VZH108	Y	0	0	0	0	0	0	0	0	0	-	-	
VZH109	Y	0	0	0	0	0	0	0	0	0	-	-	
VZH110	Y	0	0	0	0	0	0	0	0	0	-	-	
VZH111	Y	48903	332	11	402	32	5.5	0.7	338	11	1.6	0.2	
VZH112	Y	19139	308	24	303	12	3.3	0.3	311	24	1.08	0.12	
VZH113	Y	3978	456	55	436	14	4.9	0.7	461	55	1.1	0.2	

	VZH114	Y	161764	3475	242	4479	155	29	2.6	3504	242	0.83	0.09	
	VZH115	Y	0	0	0	0	0	0	0	0	0	-	-	
	VZH116	Y	0	0	0	0	0	0	0	0	0	-	-	
	VZH118	Y	0	0	0	0	0							
	VZH119	Y	0	0	0	0	0							
	VZH120	Y	0	0	0	0	0							
	VZH121	Y	0	0	0	0	0	0	0	0	0	-	-	
	VZH122	Y	3068	64	2	65	4							
	VZH124	Y	0	5	0	5	1	0	0	5.0	0.4	0	0	
	VZH125	Y	59	20	1	13	0	5.0	0.6	25.0	1.4	20	3	
	VZH126	Y	0	0	0	0	0	0	0	0	0	-	-	
	VZH127	Y	0	0	0	0	0	0	0	0	0	-	-	
	VZH128	Y	121	6	0	7	1	2.9	0.2	9.3	0.4	31	2	
	VZH129	Y	0	0	0	0	0	0	0	0	0	-	-	
	VZH130	Y	0	0	0	0	0	1.6	0.2	1.6	0.2	100	16	
	VZH131	Y	0	0	0	0	0	0	0	0	0	-	-	
	VZH132	Y	8165	657	54	718	31	34.0	1.3	691	54	4.9	0.4	
	VZH133	Y	0	0	0	0	0	1.7	0.4	1.7	0.4	100	33	
	VZH134	Y	0	0	0	0	0	0	0	0	0	-	-	
	VZH135	Y	0	0	0	0	0	0	0	0	0	-	-	
	VZH136	Y	0	0	0	0	0	0	0	0	0	-	-	
	VZH138	Y	0	0	0	0	0	0	0	0	0	-	-	
	VZH139	Y	0	0	0	0	0	0	0	0	0	-	-	
	VZH142	Y	0	0	0	0	0	0	0	0	0	-	-	
	VZH143	Y	0	362	22	369	17	3.4	0.2	365	22	0.94	0.08	
	VZH144	Y	0	273	51	301	7	4.9	1.1	278	51	1.8	0.5	
	VZH145	Y	0	128	4	52	5	0	0	128	4	0	0	
	VZH146	Y	1840	1912	115	2211	155	0	0	1912	115	-	-	
Active Case Detection	VZA301	N	0	0	0	0.10	0.02	0	0	0	0	-	-	
	VZA302	Y	0	0.25	0.02	0.44	0.02	0	0	0.3	0.2	0	0	
	VZA303	Y	0	18.1	1.4	24	3	0	0	18.1	1.4	0	0	
	VZA304	N	0	0	0	0	0	0	0	0	0	-	-	
	VZA305	N	0	0	0	0	0	0	0	0	0	-	-	
	VZA306	N	0	0	0	0	0	0	0	0	0	-	-	
	VZA307	N	0	0	0	0	0	0	0	0	0	-	-	
	VZA308	N	0	0	0	0.12	0.02	0	0	0	0	0	-	-
	VZA309	Y	0	0	0	0	0	0	0	0	0	0	-	-
	VZA310	N	0	0	0	0	0	0	0	0	0	0	-	-
	VZA311	N	0	0	0	0	0	0	0	0	0	0	-	-
	VZA312	N	0	0	0	0.14	0.07	0	0	0	0	0	-	-
	VZA313	N	0	196	9	196	12	13.6	1.3	209	9	6.5	0.7	
	VZA314	Y	84	615	30	697	66	7.7	0.2	623	30	1.23	0.07	
	VZA315	N	0	0	0	0.10	0.03	0	0	0	0	0	-	-
	VZA316	N	0	0	0	0.08	0.04	0	0	0	0	0	-	-
	VZA317	N	0	0	0	0	0	0	0	0	0	0	-	-
	VZA318	N	0	0	0	0	0	0	0	0	0	0	-	-
	VZA319	Y	0	0	0	0.10	0.03	0	0	0	0	0	-	-
	VZA320	N	0	19.5	0.6	19.8	1.3	1.2	0.3	20.8	0.6	6.0	1.3	
	VZA321	N	0	0	0	0	0	0	0	0	0	0	-	-
	VZA322	N	0	0	0	0.08	0.03	0	0	0	0	0	-	-
	VZA323	Y	0	0	0	0	0	0	0	0	0	0	-	-
	VZA324	N	0	0	0	0.09	0.02	0	0	0	0	0	-	-
	VZA325	N	0	0	0	0	0	0	0	0	0	0	-	-
	VZA326	Y	0	0.23	0.03	0.31	0.04	0	0	0.23	0.12	0	0	
	VZA327	Y	0	0.0	0.0	0	0	0	0	0	0	0	-	-
	VZA328	Y	0	14.2	0.9	17	2	6.4	0.4	20.7	1.0	31	2	
	VZA329	N	0	0	0	0	0	0	0	0	0	0	-	-
	VZA330	Y	0	0	0	0	0	0	0	0	0	0	-	-
	VZA331	Y	0	0	0	0	0	0	0	0	0	0	-	-
	VZA332	N	0	0	0	0	0	0	0	0	0	0	-	-
	VZA333	Y	0	0	0	0	0	0	0	0	0	0	-	-

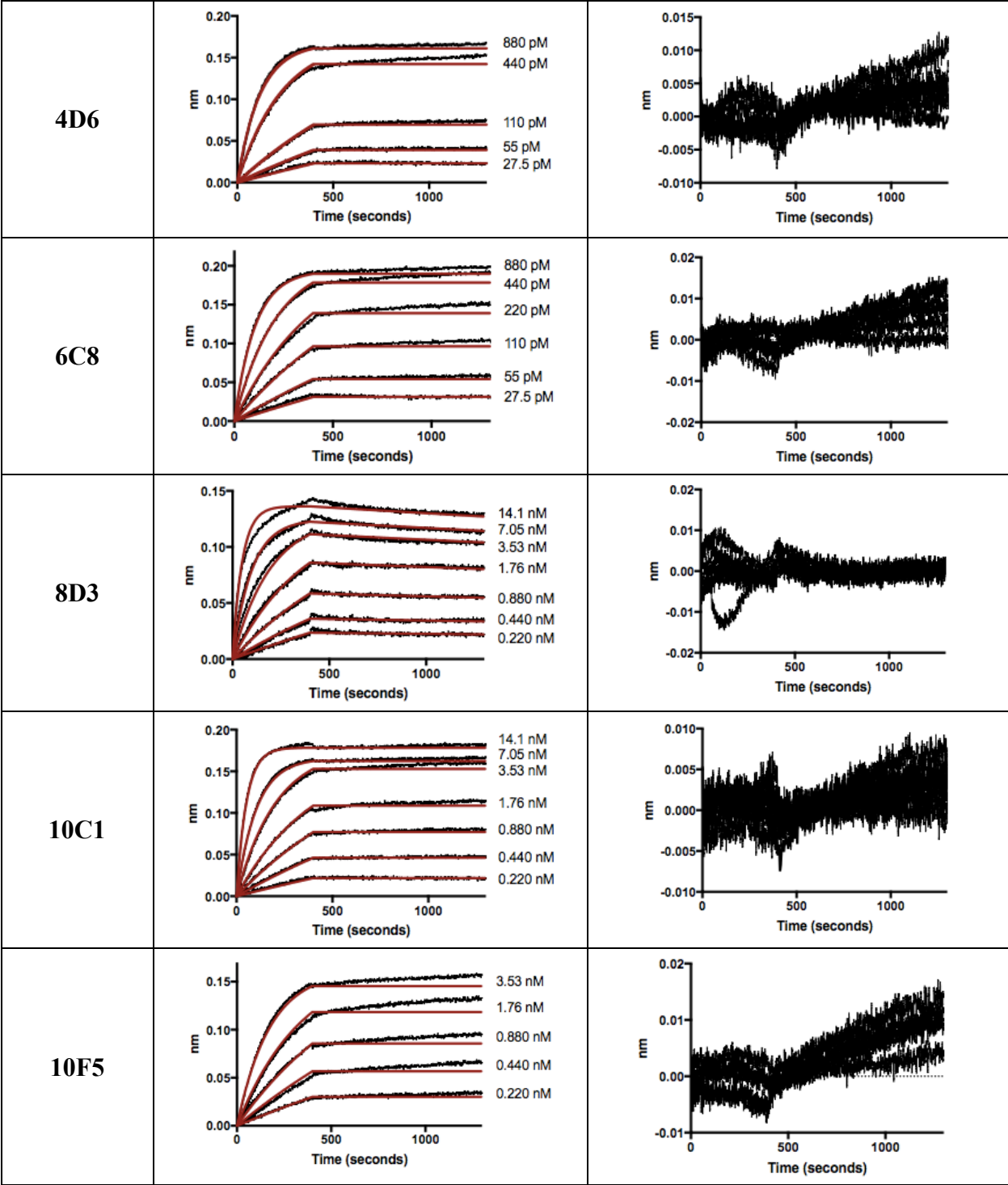
VZA334	Y	0	0	0	0	0	0	0	0	0	0	-	-
VZA335	Y	0	0	0	0	0	0	0	0	0	0	-	-
VZA336	N	0	0	0	0	0	0	0	0	0	0	-	-
VZA338	Y	0	0	0	0	0	0	0	0	0	0	-	-
VZA339	Y	0	0	0	0	0	0	0	0	0	0	-	-
VZA340	Y	0	0	0	0	0	0	0	0	0	0	-	-
VZA341	Y	0	0	0	0.10	0.04	0	0	0	0	0	-	-
VZA342	N	0	0	0	0	0	0	0	0	0	0	-	-
VZA343	Y	0	0	0	0	0	0	0	0	0	0	-	-
VZA344	N	0	0	0	0	0	0	0	0	0	0	-	-
VZA345	N	0	537	31	336	10	1.7	0.3	539	31	0.32	0.05	
VZA346	N	0	0	0	0.09	0.02	0	0	0	0	0	-	-
VZA347	N	0	0	0	0.11	0.03	0	0	0	0	0	-	-
VZA348	N	426	28	2	30	2	1.1	0.2	29	2	3.8	0.7	
VZA349	N	0	0	0	0	0	0	0	0	0	0	-	-
VZA350	N	0	0	0	0	0	0	0	0	0	0	-	-
VZA351	Y	0	0.15	0.14	0.11	0.03	0	0	0.1	0.2	0	0	
VZA352	Y	0	0	0	0	0	0	0	0	0	0	-	-
VZA353	N	0	0	0	0	0	0	0	0	0	0	-	-
VZA354	N	0	0	0	0	0	0	0	0	0	0	-	-
VZA355	N	0	0	0	0	0	0	0	0	0	0	-	-
VZA356	N	0	0	0	0	0	0	0	0	0	0	-	-
VZA357	N	0	0	0	0.10	0.02	0	0	0	0	0	-	-

APPENDIX B

SUPPORTING INFORMATION: CHAPTER IV

Table 10. Binding profiles and fit residuals for α -HRP2 IgG. Data is shown in black, calculated fits are red.

IgG Clone	Binding profile	Residual plot
MPFG-55A		
C1-13		
0445		
2g6		



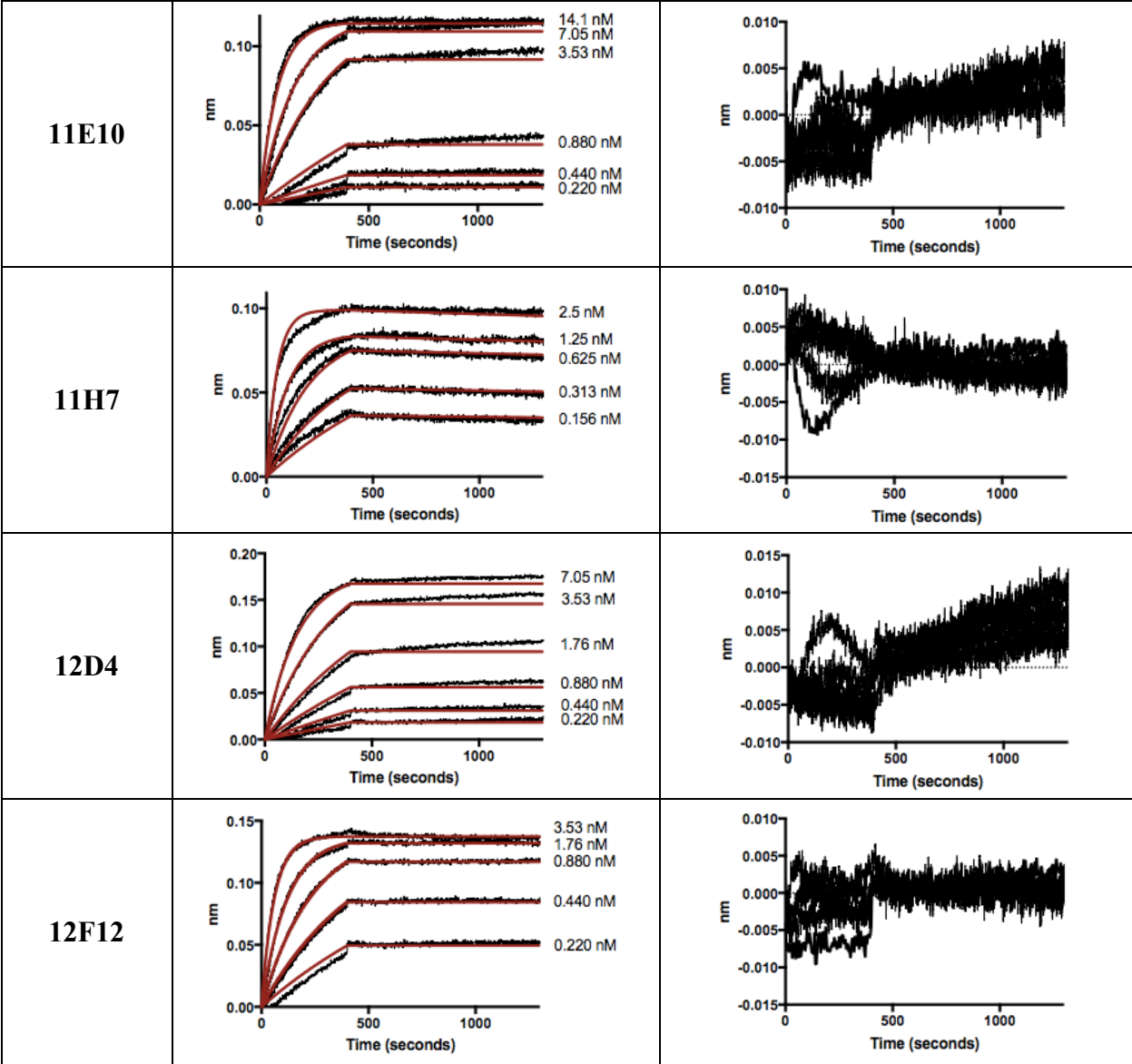


Table 11. Binding profiles and fit residuals for α -HRP2 IgM. Data is shown in black, calculated fits are red.

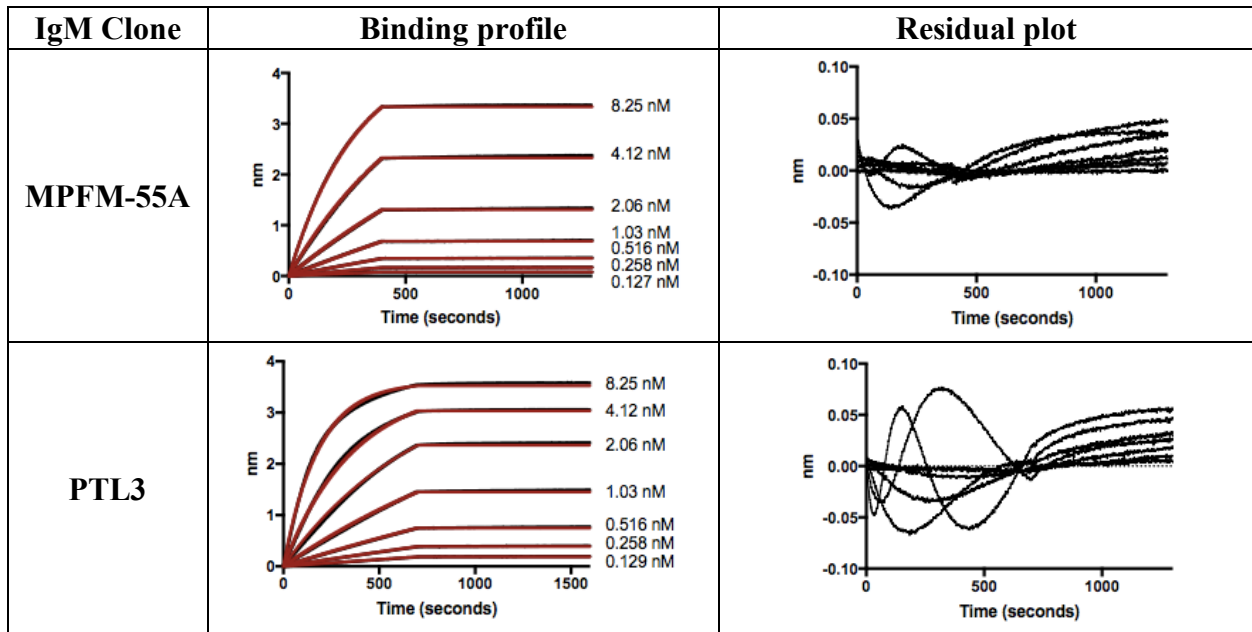
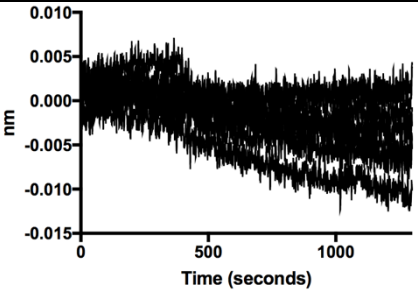
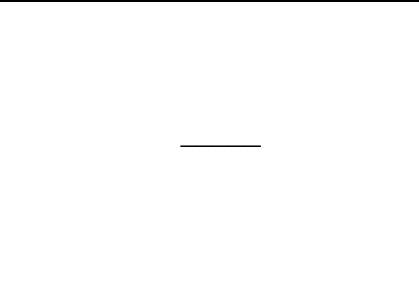
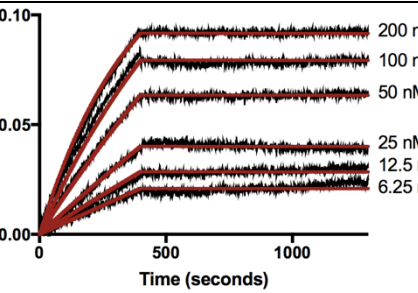
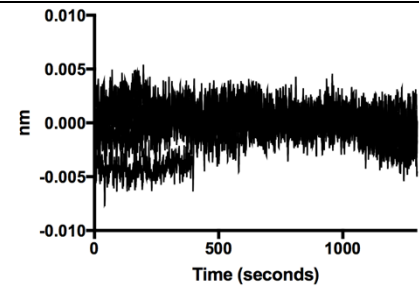
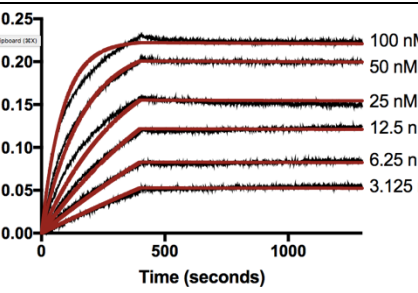
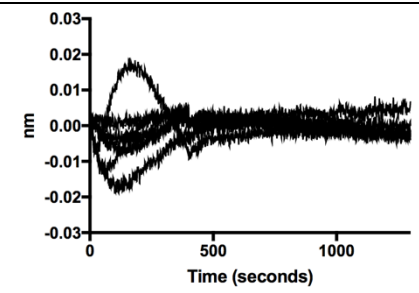
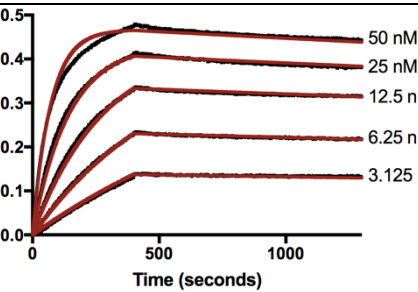
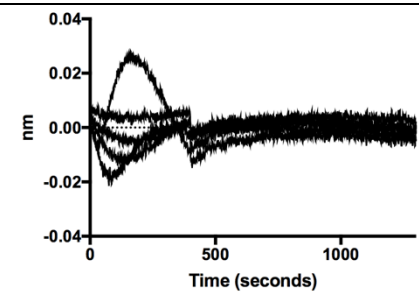
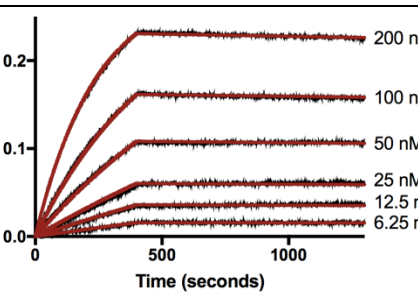
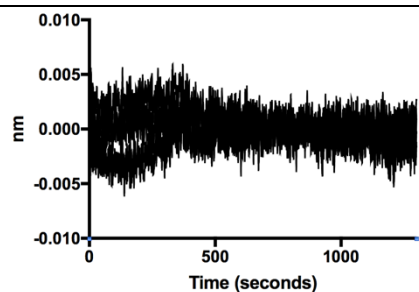
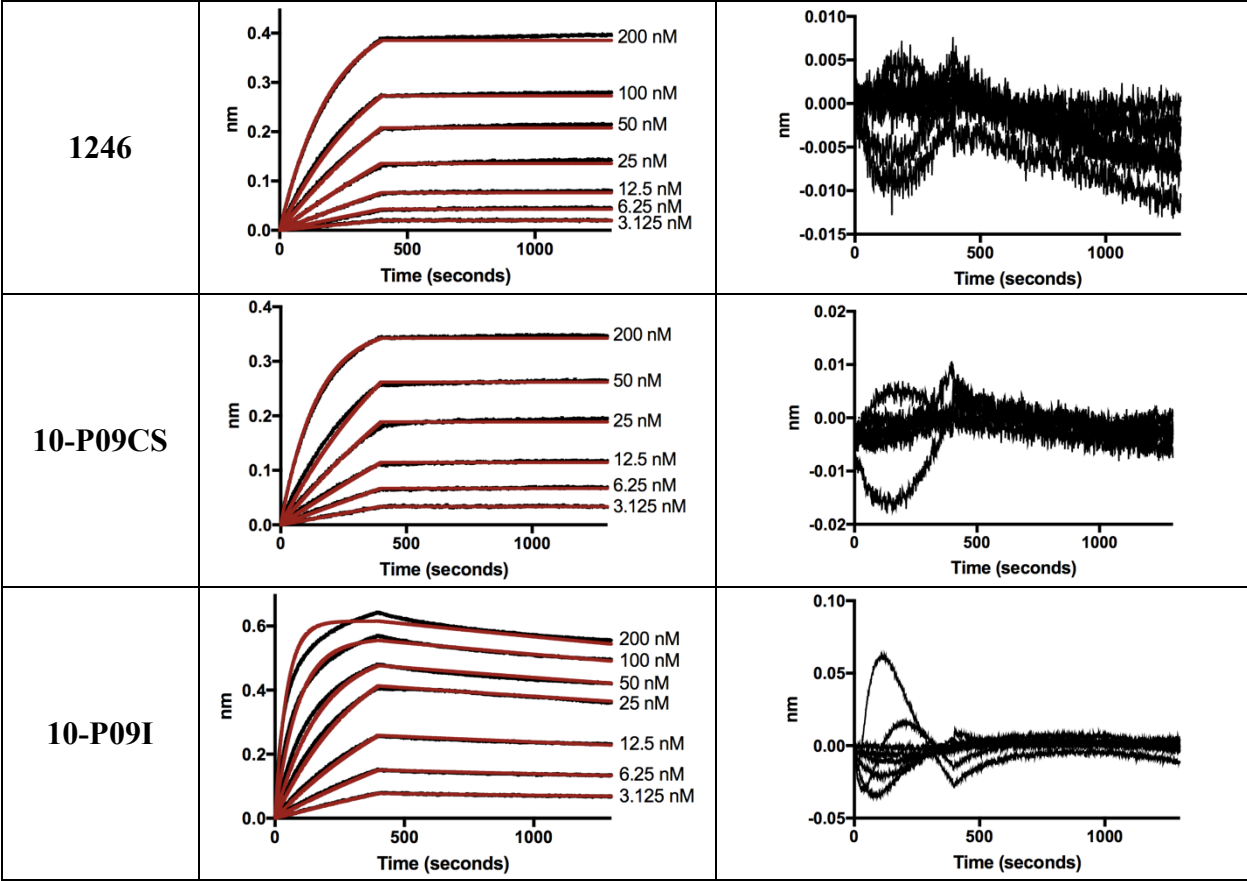


Table 12. Binding profiles and fit residuals for α -pLDH IgG against recombinant *P. vivax* LDH. Data is shown in black, while calculated fits are shown in red.

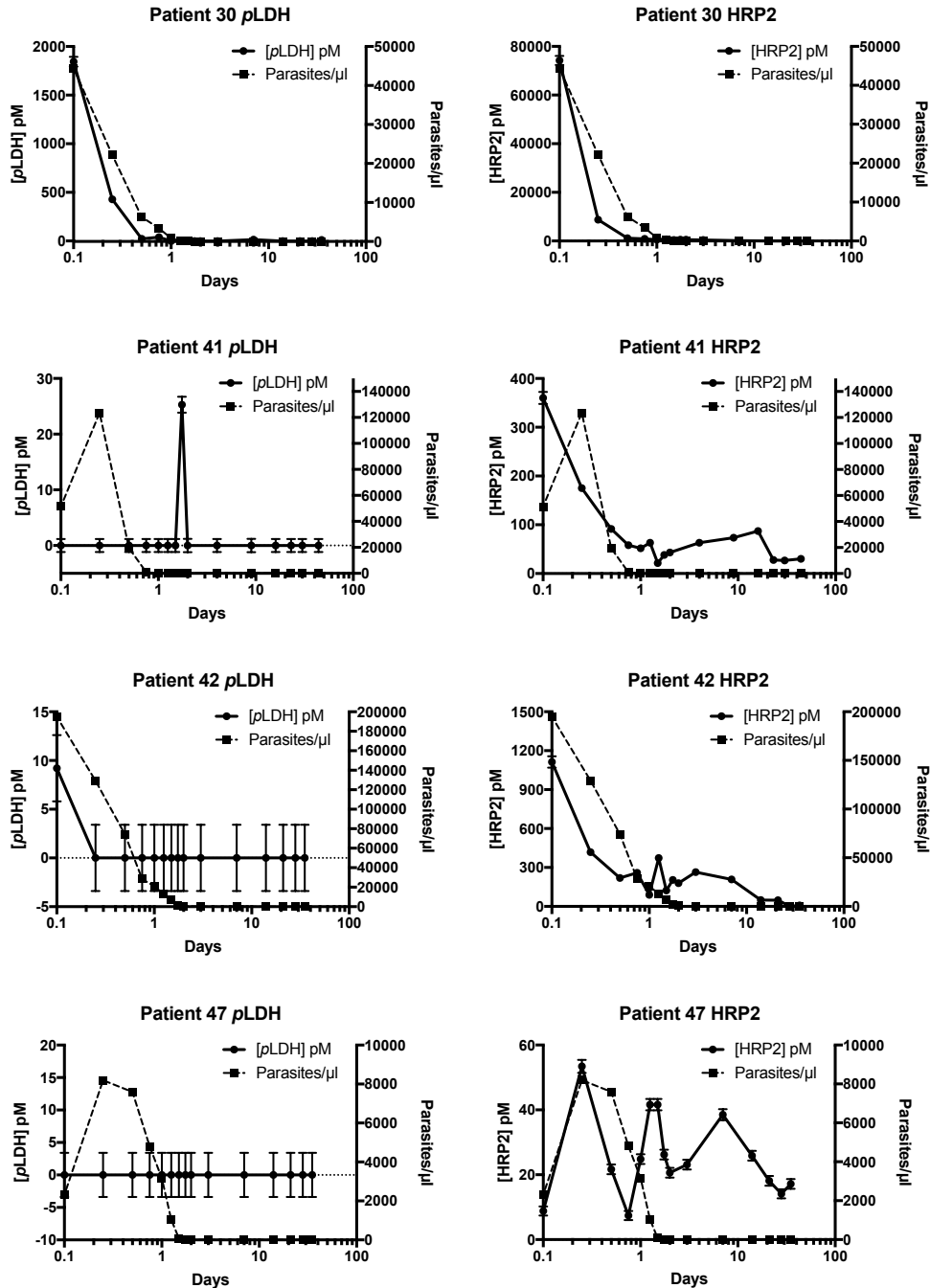
IgG Clone	Binding profile	Residual plot
14c2		
6c9		
12g1		
19g7		
1201		

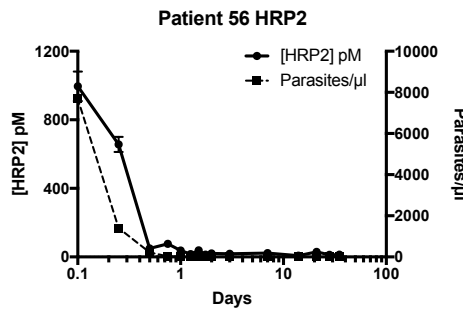
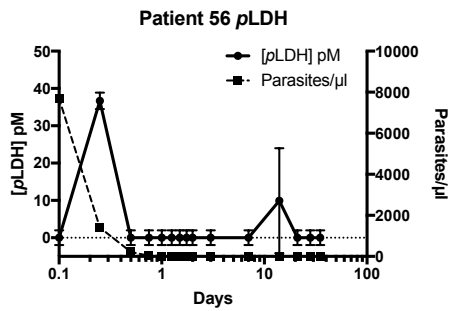
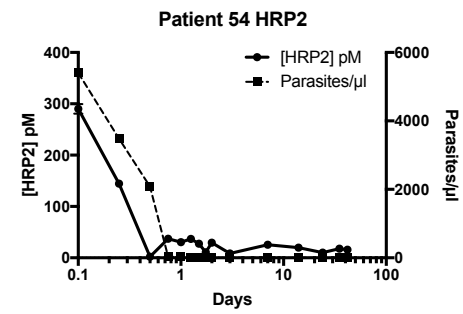
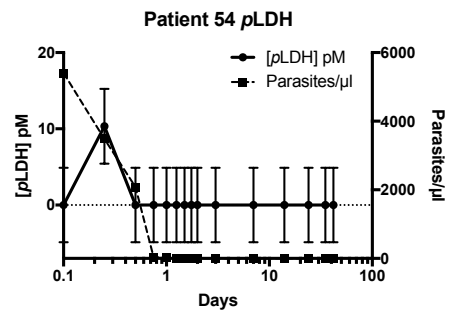
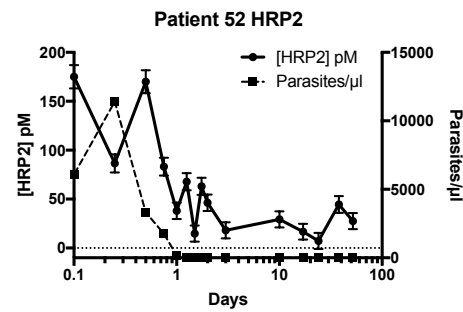
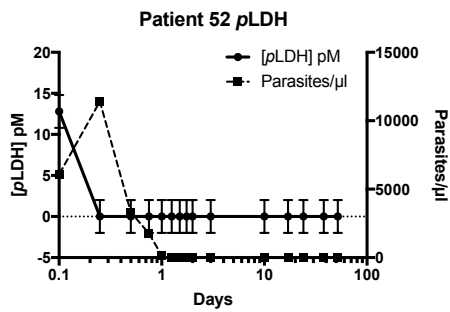
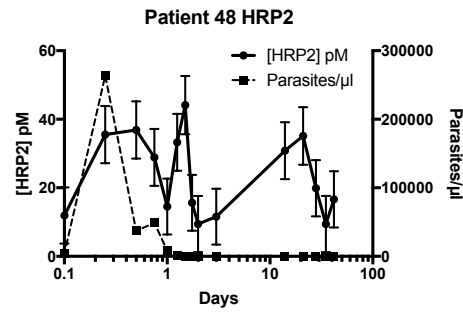
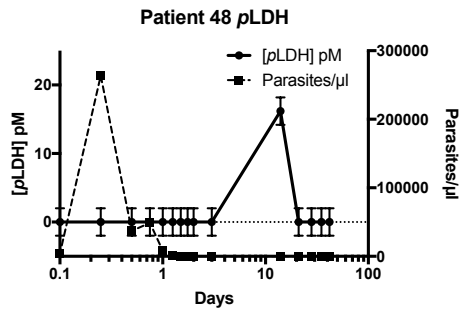


APPENDIX C

SUPPORTING INFORMATION: CHAPTER VI

Figure 36. Biomarker clearance patterns for individual patients from rural Zambia measured by DBS SCSD ELISA.





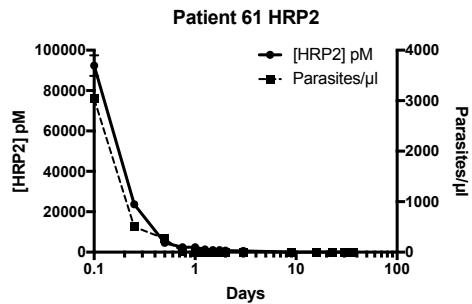
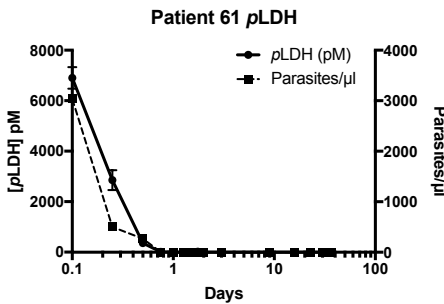
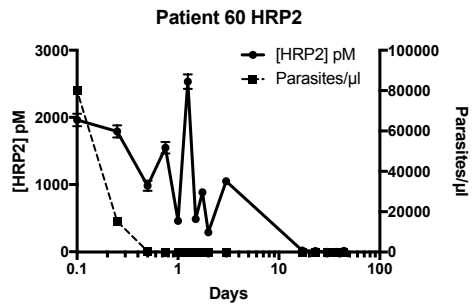
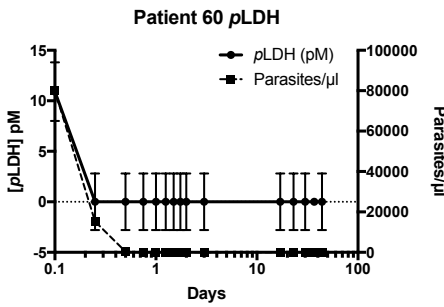
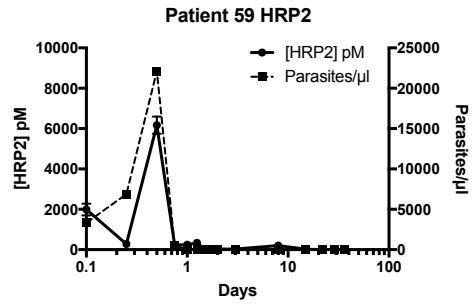
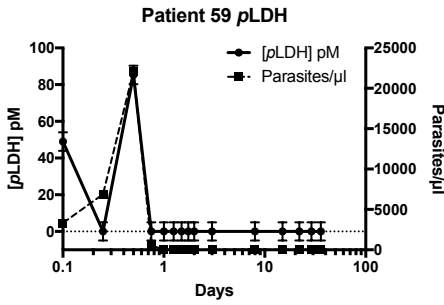
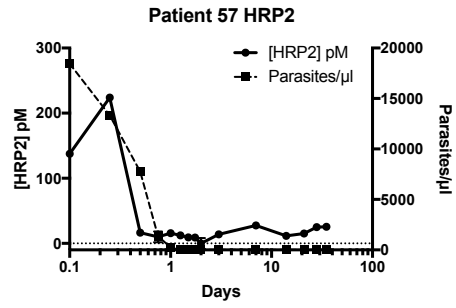
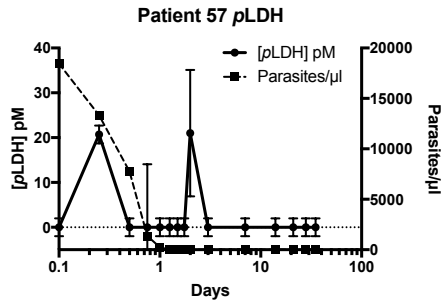


Table 13. Patient biomarker concentrations over time measured by DBS SCSD ELISA

Patient ID	Time (days)	Parasites/ μ l	[pLDH] pM		[HRP2] pM	
			Average	Error	Average	Error
Patient 29	0	82880	2350	70	16200	900
	0.25	150189	1980	70	14700	900
	0.5	57258	520	13	9800	600
	0.75	1680	49.6	2.0	9500	600
	1	400	42.0	1.9	10400	600
	1.25	112	26.8	1.7	4600	300
	1.5	0	50.0	2.0	5600	300
	1.75	0	35.9	1.8	10900	600
	2	0	22.8	1.6	8688.4	500
	3	0	13	1.6	12200	709.4
	14	0	0	1.5	0	8
	21	0	0	1.5	0	8
	28	0	16.3	1.6	0	8
	35	0	0	1.5	0	8
42	0	0	11.6	1.6	0	8
Patient 30	0	44400	1840	50	74000	2000
	0.25	22194	428	14	8800	200
	0.5	6280	22.3	1.4	1180	40
	0.75	3400	38.8	1.8	890	30
	1	800	0	1.2	564	19
	1.25	240	0	1.2	700	20
	1.5	112	0	1.2	446	15
	1.75	0	0	1.2	562	19
	2	0	0	1.2	534	18
	3	0	0	1.2	442	15
	7	0	14.7	1.3	134	5
	14	0	0	1.2	14.9	2.0
	21	0	0	1.2	0	2.3
	28	0	0	1.2	0	2.3
35	0	0	10.1	1.2	22.9	2.4
Patient 41	0	51480	0	1.2	360	12
	0.25	123579	0	1.2	175	6
	0.5	19440	0	1.2	92	4
	0.75	960	0	1.2	58	3
	1	112	0	1.2	52	3
	1.25	0	0	1.2	63	3
	1.5	0	0	1.2	21.6	2.4
	1.75	0	25.3	1.4	38	3
	2	0	0	1.2	43	3
	4	0	0	1.2	63	3
	9	0	0	1.2	73	3
	16	0	0	1.2	87	4
	23	0	0	1.2	27	3
	30	0	0	0	1.2	26

	44	0	0	1.2	30	3
Patient 42	0	194840	9	3	1110	40
	0.25	129298	0	3	417	11
	0.5	74267	0	3	220	6
	0.75	28480	0	3	260	7
	1	20840	0	3	89	3
	1.25	12960	0	3	373	10
	1.5	6800	0	3	123	4
	1.75	1720	0	3	204	6
	2	720	0	3	180	5
	3	0	0	3	264	7
	7	0	0	3	209	6
	14	0	0	3	49.2	1.9
	21	0	0	3	47.8	1.9
	28	0	0	3	0	1.4
	35	0	0	3	7.7	1.4
Patient 47	0	2320	0	3	8.8	1.4
	0.25	8200	0	3	53.4	2.0
	0.5	7600	0	3	21.7	1.5
	0.75	4800	0	3	7.4	1.4
	1	3160	0	3	24.8	1.5
	1.25	1040	0	3	41.6	1.8
	1.5	80	0	3	41.6	1.8
	1.75	0	0	3	26.2	1.5
	2	0	0	3	20.6	1.5
	3	0	0	3	23.1	1.5
	7	0	0	3	38.5	1.7
	14	0	0	3	25.9	1.5
	21	0	0	3	18.1	1.5
	28	0	0	3	14.1	1.4
	35	0	0	3	17.2	1.5
Patient 48	0	4480	0	2.0	12	8
	0.25	263530	0	2.0	36	8
	0.5	37212	0	2.0	37	8
	0.75	48989	0	2.0	29	8
	1	8080	0	2.0	15	8
	1.25	800	0	2.0	33	8
	1.5	0	0	2.0	44	8
	1.75	0	0	2.0	16	8
	2	0	0	2.0	9	8
	3	0	0	2.0	12	8
	14	0	16.2	2.0	31	8
	21	0	0	2.0	35	8
	28	0	0	2.0	20	8
	35	0	0	2.0	9	8
	42	0	0	2.0	17	8
Patient 52	0	6080	12.8	2.0	175	12
	0.25	11400	0	2.0	87	9

	0.5	3320	0	2.0	170	13
	0.75	1760	0	2.0	83	9
	1	160	0	2.0	38	8
	1.25	0	0	2.0	68	8
	1.5	0	0	2.0	15	8
	1.75	0	0	2.0	63	8
	2	0	0	2.0	46	8
	3	0	0	2.0	18	8
	10	0	0	2.0	29	8
	17	0	0	2.0	17	8
	24	0	0	2.0	7	8
	38	0	0	2.0	45	8
	52	0	0	2.0	28	8
Patient 54	0	5400	0	5	290	9
	0.25	3480	10	5	145	5
	0.5	2080	0	5	0	0.9
	0.75	32	0	5	37.3	1.5
	1	32	0	5	30.6	1.3
	1.25	0	0	5	36.9	1.5
	1.5	0	0	5	27.5	1.3
	1.75	0	0	5	10.8	1.0
	2	0	0	5	29.5	1.3
	3	0	0	5	8.4	0.9
	7	0	0	5	25.7	1.2
	14	0	0	5	19.7	1.1
	24	0	0	5	10.2	1.0
35	0	0	5	17.9	1.1	
42	0	0	5	15.9	1.0	
Patient 55	0	15040	13	5	790	40
	0.25	11160	72	6	2130	90
	0.5	9960	72	6	1710	80
	0.75	800	0	5	237	7
	1	0	0	5	107	4
	1.25	0	38	5	162	5
	1.5	0	0	5	171	5
	1.75	0	0	5	12.8	1.0
	2	0	0	5	28.2	1.3
	3	0	0	5	24.0	1.2
	7	0	0	5	20.9	1.1
	14	0	0	5	15.7	1.0
	21	0	0	5	11.9	1.0
28	0	0	5	23.7	1.2	
35	0	0	5	11.0	1.0	
Patient 56	0	7680	0	2.0	1000	90
	0.25	1400	36.7	2.2	660	40
	0.5	224	0	2.0	49.0	1.3
	0.75	32	0	2.0	76.5	2.0
	1	0	0	2.0	37.9	1.0
1.25	0	0	2.0	16.6	0.5	

	1.5	0	0	2.0	38.1	1.0
	1.75	0	0	2.0	13.7	0.4
	2	0	0	2.0	20.6	0.6
	3	0	0	2.0	18.8	0.5
	7	0	0	2.0	22.6	0.6
	14	0	10	14	8	8
	21	0	0	2.0	29.5	0.8
	28	0	0	2.0	12.5	0.4
	35	0	0	2.0	13.5	0.4
Patient 57	0	18440	0	2.0	138	4
	0.25	13320	20.7	2.0	224	6
	0.5	7760	0	2.0	16.6	0.5
	0.75	1360	0	14	10	8
	1	240	0	2.0	15.7	0.4
	1.25	0	0	2.0	12.3	0.4
	1.5	0	0	2.0	9.2	0.3
	1.75	0	0	2.0	9	0.3
	2	0	21	14	0	8
	3	0	0	2.0	13.9	0.4
	7	0	0	2.0	27.7	0.8
	14	0	0	2.0	11.7	0.3
	21	0	0	2.0	15.1	0.4
	28	0	0	2.0	24.9	0.7
35	0	0	2.0	25.5	0.7	
Patient 58	0	32360	9	5	3200	300
	0.25	21720	30	5	2900	300
	0.5	4520	0	5	266	4
	0.75	3920	10	5	3500	300
	1	480	0	5	3900	300
	1.25	112	10	5	3900	300
	1.5	0	0	5	182	3
	1.75	0	0	5	77	3
	2	0	0	5	166	3
	3	0	0	5	201	3
	8	0	0	5	910	70
	15	0	0	5	18	3
	22	0	0	5	23	2.0
	29	0	0	5	33	2.0
36	0	0	5	54	2.0	
Patient 59	0	3320	49	5	1100	300
	0.25	6880	0	5	283	4
	0.5	22120	85	5	5300	400
	0.75	560	0	5	230	4
	1	0	0	5	250	4
	1.25	0	0	5	339	4
	1.5	0	0	5	16	3
	1.75	0	0	5	25	3
	2	0	0	5	31	3
3	0	0	5	27	3	

	8	0	0	5	177	3
	15	0	0	5	22	3
	22	0	0	5	0	3
	29	0	0	5	14	3
	36	0	0	5	16	3
Patient 60	0	79840	11	3	1960	90
	0.25	15320	0	3	1790	90
	0.5	400	0	3	980	80
	0.75	0	0	3	1550	90
	1	0	0	3	460	40
	1.25	0	0	3	2530	110
	1.5	0	0	3	490	40
	1.75	0	0	3	880	50
	2	0	0	3	290	40
	3	0	0	3	1050	50
	17	0	0	3	19	7
	23	0	0	3	12	7
	30	0	0	3	0	7
	37	0	0	3	0	7
44	0	0	3	15	7	
Patient 61	0	3035	6400	300	89000	5000
	0.25	503	1510	100	23700	1300
	0.5	269	360	60	4600	200
	0.75	6	11	3	2400	100
	1	0	0	3	2420	90
	1.25	0	0	3	1390	60
	1.5	0	0	3	1010	50
	1.75	0	0	3	1050	50
	2	0	0	3	750	40
	3	0	0	3	590	40
	9	0	0	3	18	7
	16	0	0	3	0	7
	23	0	0	3	0	7
	30	0	0	3	0	7
37	0	0	3	0	7	

APPENDIX D

IMMUNOMAGNETIC CAPTURE AND COLORIMETRIC DETECTION OF MALARIAL BIOMARKER *PLASMODIUM FALCIPARUM* LACTATE DEHYDROGENASE[°]

Introduction

Before developing the *p*LDH on-bead ELISA and the SCSD ELISA presented in Chapter V and evaluated in clinical samples in Chapter VI, I developed an alternative magnetic-bead based detection strategy for *p*LDH. The method leverages the fact that the target itself is an enzyme, using *p*LDH activity to generate colorimetric signal rather than employing an enzyme-conjugated detection antibody. As mentioned in Chapter I, *p*LDH is the terminal enzyme in the glycolytic pathway, converting pyruvate to lactate using cofactor NADH.¹⁸⁴ Slight structural changes in the active site of *p*LDH result in substrate and cofactor specificity distinguishable from host human lactate dehydrogenase (*h*LDH).¹⁸⁵ Specifically, the replacement of Ser 163 in *h*LDH with Leu 163 in *p*LDH confers activity with 3-acetylpyridine adenine dinucleotide (APAD⁺), an analog of NAD⁺.¹⁸⁵ The parasite enzyme is 300 times more active with APAD⁺ than is *h*LDH.¹⁸⁶ Taking advantage of this kinetic difference, Makler and Hinrichs developed the Malstat assay for the specific detection of *p*LDH.¹⁸⁷ In this assay (Figure 37), *p*LDH in an infected lysed blood sample oxidizes lactate to pyruvate while reducing cofactor APAD⁺ to APADH. The APADH then reduces a yellow tetrazolium dye, nitroblue tetrazolium (NBT), to a blue diformazan compound with the assistance of phenazine ethosulfate (PES). Reaction progress is followed at 650 nm. This assay is

[°] Portions of this chapter were previously published in Markwalter C.F. et al. *Analytical Biochemistry*, 2016. 493: 30 - 34. © 2015 The Authors. Published by Elsevier Inc.

frequently used to assess parasite viability in drug susceptibility assays, as *p*LDH activity has been shown to follow closely with parasitemia.¹⁸⁸

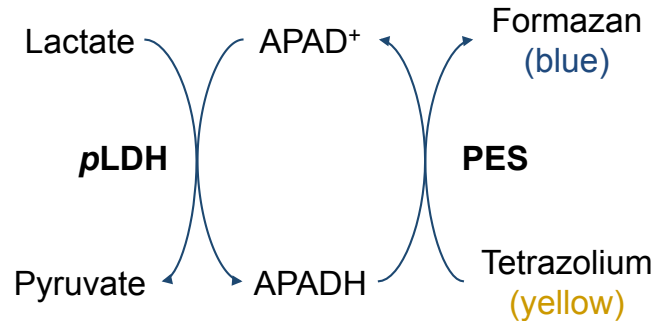


Figure 37. The Malstat assay for the detection of *Plasmodium* lactate dehydrogenase.

Measuring *p*LDH activity using the Malstat assay is attractive as a diagnostic tool due to its simplicity and short assay time; however studies have shown that samples with low parasite densities cannot be measured due to nonspecific reductases in blood.¹⁸⁹ To address this, Piper et al. developed an immunocapture Malstat assay in which immobilized monoclonal α -*p*LDH antibodies in the wells of a 96-well plate captured *P. falciparum* lactate dehydrogenase (*Pf*LDH) from lysed parasitized blood. The wells were washed and incubated with Malstat reagents, and the resulting signal was measured at 650 nm. Although this process eliminated nonspecific reductases from blood, the assay only proved to have a sensitivity of 62% for samples with parasite densities between 50 and 500 parasites per microliter, likely due to un-optimized signal detection conditions.¹⁵⁵

This work sought to increase the analytical sensitivity and decrease the detection limit of the Malstat assay into diagnostically relevant parasitemias using antibody-functionalized magnetic microparticles to separate and purify *Pf*LDH from parasitized lysed whole blood. Immunomagnetic biomarker capture is advantageous because nonspecific reductases and other interfering species are eliminated from the detection step. Further, high surface area for antigen

binding as well as active mixing allow for increased analytical sensitivity and decreased time-to-result respectively compared to 96-well plate-based immunoassays.

Experimental

Reagents and materials

Sodium L-lactate, 3-Acetylpyridine adenine dinucleotide (APAD), and phenazine ethosulfate (PES) were purchased from Sigma Aldrich (Cat # L7022, A5251, P4544, respectively). Nitroblue tetrazolium chloride (NBT) was purchased from Life Technologies (Cat # N-6495). Recombinant *P. falciparum* lactate dehydrogenase (rcPfLDH) was purchased from CTK Biotech (Cat #A3005). *P. falciparum* D6 strain was cultured in the lab. Anti-*P. falciparum* LDH antibodies were purchased from mybiosource (MBS832018). Dynabeads® MyOne™ Streptavidin T1 beads were purchased from Life Technologies (Cat #65601).

Magnetic bead preparation

Anti-*P. falciparum* LDH (α -PfLDH) antibodies were biotinylated with EZ-Link NHS-PEG4-Biotin, No-Weigh Format (Thermo Pierce #21329) in PBS with a 50x excess of NHS-PEG4 Biotin. Excess NHS-PEG4 biotin was removed using Zebra Spin Desalting Columns with a 7K molecular weight cut-off (Thermo Pierce #89882). Next, 3 mg of Dynabeads® MyOne™ Streptavidin T1 were washed three times with PBS containing 0.01% Tween-20 (PBST) before 30 min incubation with 600 μ L of 0.33 mg/mL of biotinylated α -PfLDH antibody in PBS. The beads were then washed three times with PBST and blocked with excess D-biotin in PBS for 30 minutes. Finally, the beads were washed three times and resuspended in 300 μ L of PBST.

PfLDH activity assay optimization

Optimizing the *PfLDH* activity assay involved maximizing reaction rates and minimizing background signal. In the first kinetics experiment, [APAD] was held constant and [L-lactate] was varied. A 2.86 M solution of sodium L-lactate 0.22 M TRIS buffer pH 9 (TB) was prepared (3.2g in 10 mL) and serially diluted by a factor of two. 62.5 μL of each sodium L-lactate dilution, 62.5 μL of 1.33 mM APAD in TB, and 50 μL of 7 nM rc*PfLDH* in TB were placed in wells in triplicate of a Costar $\text{\textcircled{R}}$ UV Transparent 96-well plate (#3635) such that the final well concentrations were: 0.474 mM APAD; 2 nM rc*PfLDH*; and 0.00, 15.9, 31.9, 63.8, 128, 255, 510, and 1020 mM sodium L-lactate. The plate was immediately placed in a BioTek Synergy H4 Hybrid Multi-Mode Microplate Reader, and APADH generation was measured by absorbance (362 nm, $\epsilon = 9.1 \times 10^3 \text{ M}^{-1}\text{cm}^{-1}$)¹⁹⁰ in intervals of 25 seconds for 30 minutes. The rate of reaction in each well was measured as the slope of the steepest increase in absorbance, namely the interval 0s – 205s. Based on these rates, a well concentration of 510 mM sodium L-lactate was chosen for further optimization experiments.

For the second kinetics experiment, [L-lactate] was held constant and [APAD] was varied. A 21.3 mM solution of APAD in TB was prepared (70.4 mg in 5 mL) and serially diluted by a factor of two. 62.5 μL of each APAD dilution, 62.5 μL of 510 mM sodium L-lactate in TB, and 50 μL of 7 nM rc*PfLDH* in TB were placed in wells in triplicate of a UV transparent 96-well plate such that the final well concentrations were: 510 mM APAD; 2 nM rc*PfLDH*; and 0.00, 0.119, 0.237, 0.474, 0.949, 1.9, 3.8, and 7.6 mM APAD. The plate was immediately placed in a microplate reader, and absorbance was measured (362 nm) in intervals of 25 seconds for 30 minutes. The rate of reaction in each well was measured as the slope of the steepest increase in absorbance, namely the interval 0s – 205s.

Finally, the signal-to-noise ratio of the *Pf*LDH activity assay was maximized. First, 25 μ L of blank (0 nM) or positive control (14 nM) rc*Pf*LDH in TB were placed in separate wells of a 96 well plate. Next, 25 μ L of NBT/PES solution (See *Pf*LDH Activity Assay Reagents), 25 μ L of 3.57 M lactate, and 100 μ L of 0.58 mM, 1.16 mM, or 3.32 mM APAD were added to each well. The plate was covered with foil and incubated for 30 minutes on an orbital plate shaker before measuring absorbance (650 nm) on a plate reader. The assay was performed in triplicate.

*Pf*LDH activity assay reagents

The *Pf*LDH activity assay required two solutions. First, sodium L-Lactate (4.00 g), Tris(hydroxymethyl)aminomethane (TRIS) (1.32 g), and APAD (0.022 g) were dissolved in 40 mL of DI water, the pH was adjusted to 9, and the solution was diluted to 50 mL. This Malstat solution was stored at 4°C. Second, nitroblue tetrazolium chloride (NBT) (0.080 g) and phenazine ethosulfate (PES) (0.004 g) were dissolved in 50 mL of DI water. The NBT/PES solution was wrapped in foil and stored at 4°C.

*On-bead Pf*LDH activity assay

Solutions (100 μ L) of parasitized lysed whole blood or rc*Pf*LDH-spiked lysed whole blood were placed in a Fisherbrand Flat-bottom PS 96-well plate (#12565501). Five μ L of α -*Pf*LDH magnetic beads (myone Streptavidin T1) were added to each well and incubated on an orbital shaker for 15 minutes. Using a MagWell™ Magnetic Separator (EdgeBio #57624), the beads were separated from the supernatant and washed three times with 1x TRIS buffered saline with 0.05% Tween-20 (TBST). On the final wash, the beads were moved to new wells. Next, 25 μ L of TBST, 25 μ L of NBT/PES solution and 125 μ L of the prepared Malstat solution were added to

each well containing beads. The final concentrations of the *Pf*LDH substrates in each well were: 510 mM Lactate, 0.474 mM APAD. The plate was immediately covered with Parafilm and foil and incubated on an orbital shaker for 30 minutes. *Pf*LDH activity was assessed by measuring absorbance (580 nm) on a plate reader. All assays were performed in triplicate. The limit of detection (LOD) was calculated as the concentration at the minimum detectable signal ($3SD_{\text{blank}} + S_{\text{blank}}$). See Figure 38 for a summary of the assay workflow.

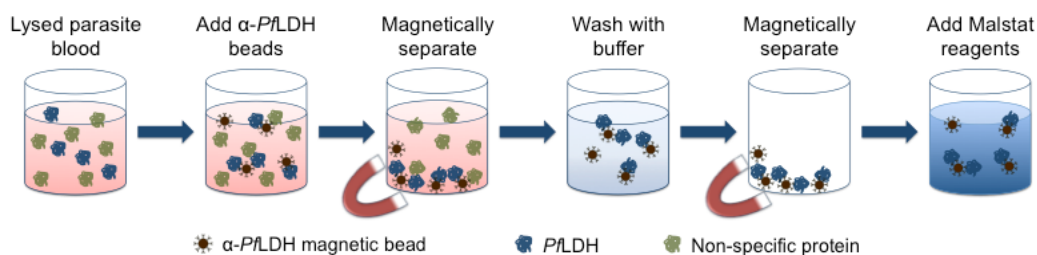


Figure 38. Summary of workflow for on-bead *Pf*LDH activity assay.

Results and Discussion

*Pf*LDH activity assay optimization

The Malstat assay for *Pf*LDH activity was optimized through kinetic analysis and minimization of background signal. For optimal determination of enzyme concentration, substrate concentrations should be saturated to maximize the rate of reaction. Two-substrate enzyme-catalyzed reactions, such as *Pf*LDH oxidizing lactate to pyruvate using APAD⁺, obey simple Michaelis-Menten kinetics when one substrate is held constant and the other is varied.¹⁹¹ As such, initial kinetics experiments were conducted in which [APAD⁺] was held constant (0.474 mM) and [Lactate] was varied (0 – 1.02 M) while rc*Pf*LDH was held constant (2 nM). Production of APADH was followed at 362 nm. The corresponding curve (Figure 39A) demonstrated that 0.51 M lactate yielded a saturating reaction rate and was selected for further optimization experiments.

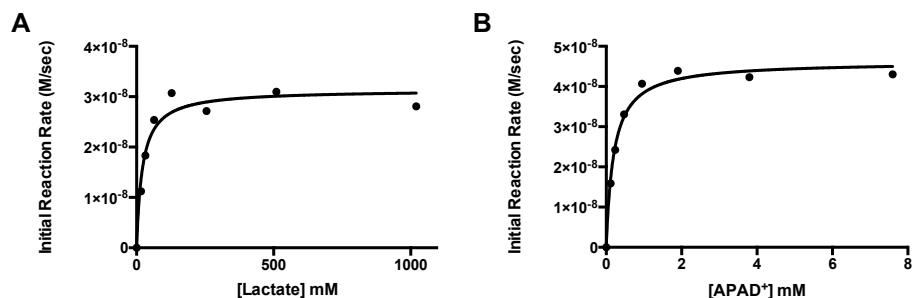


Figure 39. Michaelis-Menten curves for (A) constant [APAD⁺], varied [Lactate] and (B) constant [Lactate], varied [APAD⁺].

Next, [Lactate] was held constant (0.51 M) and [APAD⁺] was varied (0 – 7.6 mM) at a constant rc*Pf*LDH concentration (2 nM). The resulting Michaelis-Menten curve revealed that saturating conditions began at 1.9 mM APAD⁺ (Figure 39B). However, when several APAD⁺ concentrations were tested in the *Pf*LDH activity assay, it was found that saturating conditions resulted in high background signal, and 0.474 mM APAD⁺ yielded the highest signal-to-noise ratio (Figure 40A). For this reason, 0.474 mM was selected as the optimal concentration for the *Pf*LDH activity assay.

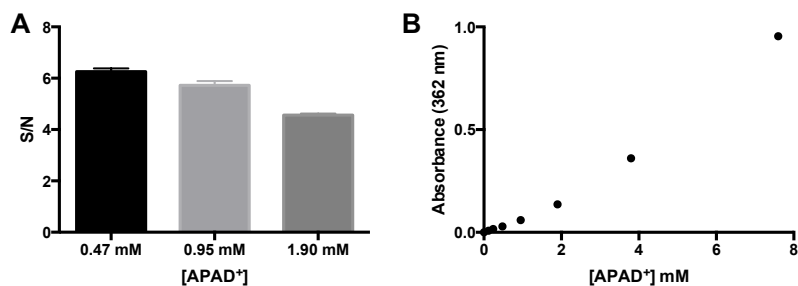


Figure 40. (A) Decreasing signal-to-noise ratios with increasing [APAD⁺]. (B) Increasing absorbance at 362 nm suggests increasing [APADH] contaminant.

We postulate that the increase in background signal in the *Pf*LDH activity assay with increasing [APAD⁺] could be due to a small amount of APADH contaminant. To support this hypothesis, a standard curve of APAD⁺ in TB was placed in a UV-transparent 96-well plate. As

shown in Figure 40B, absorbance at 362 nm, a maximum for APADH, increased with increasing [APAD⁺], indicating that APADH could account for $(1.8 \pm 0.5)\%$ reagent contamination.

Detection of *Pf*LDH was further optimized when it was discovered that, although previous literature^{155,187} measures progress of the Malstat reaction at 650 nm, the wavelength of maximum absorbance for the products of the *Pf*LDH activity assay reaction is 580 nm. Others likely follow the reaction at 650 nm because oxyhemoglobin in lysed whole blood has a peak in absorbance near 580 nm, which would interfere with Malstat signal (Figure 41A) when the assay is performed in the lysed blood sample.¹⁹² Measuring reaction progress at 580 nm results in a nearly two-fold enhancement of analytical sensitivity of the Malstat assay (Figure 41B). By using antibody-functionalized magnetic particles to isolate and purify *Pf*LDH from a blood sample and then performing the Malstat assay directly on the solid phase, our assay strategy eliminates the interfering species in blood from the detection step and takes advantage of the two-fold enhancement at 580 nm.

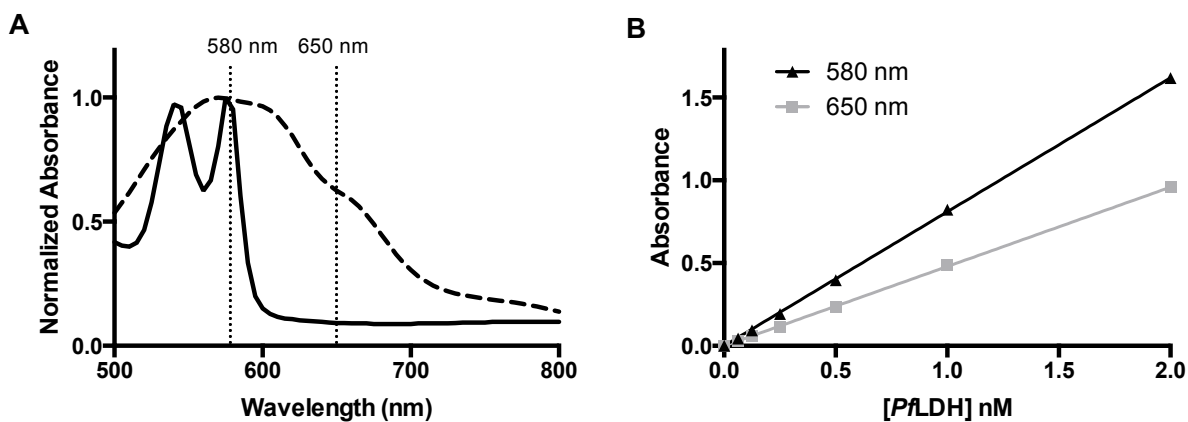


Figure 41. (A) Absorbance spectra for lysed whole blood (solid) and products of *Pf*LDH activity assay (dotted). (B) Analytical sensitivity of *Pf*LDH activity assay at 580 nm ($0.810 \pm 0.004 A_{580}/\text{nM}$) is nearly twice the sensitivity at 650 nm ($0.479 \pm 0.002 A_{650}/\text{nM}$).

Selecting antibodies for on-bead activity assay

To perform an on-bead activity assay based on immunomagnetic capture, it is imperative that the enzyme target maintains its activity when bound to the capture antibody. Three monoclonal antibodies were evaluated for use in the on-bead *p*LDH activity assay. Recombinant *Pf*LDH was incubated with equimolar concentrations of antibody before performing a solution-based Malstat reaction. As shown in Figure 42, two of the antibodies completely blocked *Pf*LDH activity in the Malstat reaction, indicating that they would not be suitable for the on-bead activity assay. However, when *Pf*LDH bound to 10-P09DS, activity was maintained. Thus, 10-P09DS was selected for use in the on-bead *Pf*LDH activity assay.

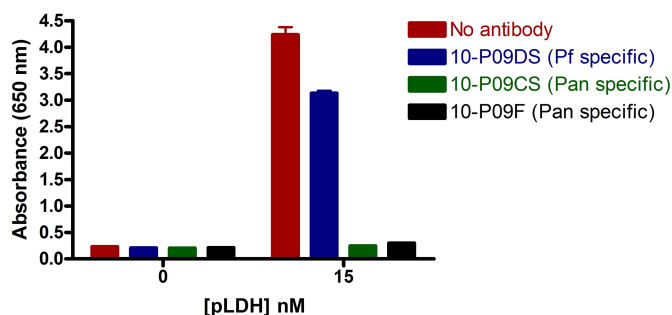


Figure 42. Malstat activity of recombinant *Pf*LDH with three α -*p*LDH monoclonal antibodies. Only 10-P09DS allowed for turnover of the Malstat reaction.

This experiment demonstrated the utility of the Malstat assay as a tool for “binning” monoclonal antibodies into two categories: (1) those that block *p*LDH activity and (2) those that do not block enzyme activity. This simple categorization could be extremely useful for selecting antibody pairs for the enzyme target, since the two groups are exclusive of one another; in other words, an antibody that blocks *p*LDH activity would not bind the same epitope as an antibody that does not block *p*LDH activity. Thus, it is possible that for enzyme targets, if a panel of antibodies are first screened by the Malstat assay for initial binning, BLI could be employed to select the best

performing antibody pair (based on k_{on} and k_{off} — similar to the analysis for HRP2 in Chapter IV) as long as the capture and detection antibodies come from distinct Malstat “bins.”

On-bead PfLDH activity assay

Capitalizing on the optimized assay conditions and enhanced analytical sensitivity at 580 nm, we developed a strategy for magnetic capture and purification of *Pf*LDH that eliminated lysed whole blood from the assay detection step. Magnetic capture beads were synthesized by coupling biotinylated anti-*Pf*LDH antibody to commercially available streptavidin-coated magnetic particles. These beads were incubated in a 96-well plate with lysed whole blood spiked with *rcPf*LDH or lysed parasite culture to capture *Pf*LDH, washed, and incubated with *Pf*LDH activity assay reagents protected from light at the optimized conditions for 30 minutes. The resulting signal was measured at 580 nm.

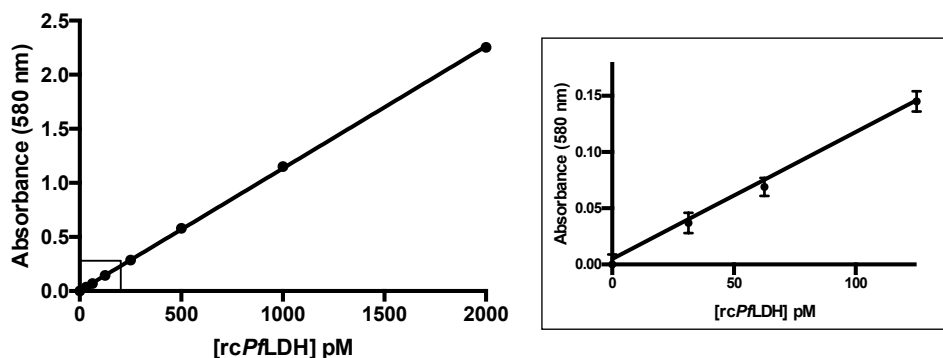


Figure 43. *rcPf*LDH standard curve for immunomagnetic *Pf*LDH activity assay.

A standard curve for this immunomagnetic *Pf*LDH activity assay was first developed in lysed whole blood spiked with *rcPf*LDH (Figure 43). The limit of detection of the assay was 25.7 ± 1.1 pM *rcPf*LDH, on the same order of magnitude of commercially available *p*LDH ELISA kits. However, the developed immunomagnetic *Pf*LDH activity assay is 3 – 5 hours shorter than a

typical ELISA assay. Figure 44 shows the results of the on-bead *Pf*LDH assay for a titration of parasitized whole blood. The limit of detection was found to be 21.1 ± 0.4 parasites/ μ L. This detection limit is two orders of magnitude lower than literature LODs for the Malstat assay performed in blood samples due to the removal of blood from the detection step as well as the thoroughly optimized substrate conditions and detection wavelength.¹⁹³ Further, our detection limit is less than half of that found by Piper et al. for their 96-well plate-based immunocapture *p*LDH activity assay, and the time-to-result for our immunomagnetic assay (45 minutes) is lower than 1 – 2 hours as reported by Piper et al.¹⁵⁵

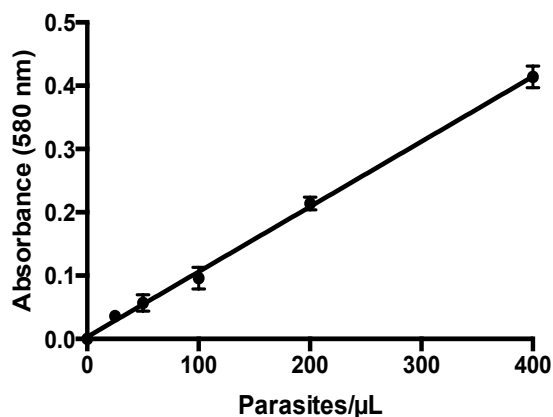


Figure 44. Parasite culture titration for immunomagnetic *Pf*LDH activity assay.

While, in principle, the developed immunomagnetic assay for *Pf*LDH is similar to the 96-well plate immunocapture Malstat strategy developed by Piper et al., the activity assay reported here affords several advantages. The optimized assay reagent concentrations and detection wavelength are responsible, in part, for our improved limit of detection. The use of magnetic microparticles for immunocapture and purification also contributes to the improved detection limits for this assay; compared to a typical 96-well plate, the microparticles used in this assay offer 40% more surface area for antibody functionalization and antigen binding (1.3 cm^2 vs. 0.9 cm^2).

Another advantage of capture and detection *Pf*LDH on magnetic particles is the reduced time-to-result. Active mixing of the magnetic beads with the sample also allows for a faster *Pf*LDH association time from a blood sample of 15 minutes compared to 30 – 60 minutes reported by Piper *et al.*¹⁵⁵ The decreased time-to-result and low detection limit of the developed *Pf*LDH assay makes it an attractive *p*LDH detection strategy in clinics and hospitals in malaria-endemic areas.

Future directions include generalizing the developed assay to detect *p*LDH from all species of malaria by functionalizing magnetic particles with a pan-specific capture antibody or a series of species-specific antibodies. Further, aptamers, short single-stranded oligonucleotide sequences capable of sensitive and specific recognition of target molecules, are promising molecular recognition elements for diagnostic applications due to their thermal stability. In fact, Dirkzwager *et al.* successfully used aptamers in a plate-based assay as capture agents for *Pf*LDH, which was then detected with a similar colorimetric *p*LDH activity assay (LOD 600 parasites/ μ L).¹⁶⁹ Conjugating an aptamer to magnetic particles for *p*LDH isolation and purification and using the optimized activity assay we developed would lead to a highly sensitive and thermally stable diagnostic strategy for malaria.

Conclusion

We have developed a magnetic bead-based colorimetric assay for *Pf*LDH in which the biomarker is extracted from parasitized whole blood and purified based on antigen binding to antibody-functionalized magnetic particles. *Pf*LDH activity was measured on-bead using an optimized colorimetric enzyme turnover reaction (LOD = 21.1 ± 0.4 parasites/ μ L). The low detection limits and high analytical sensitivity of this assay can be attributed to our optimized assay conditions as well as removal of blood from the detection step that would otherwise interfere with

colorimetric detection at the maximum wavelength for the diformazan assay products. The developed assay represents a simple, effective, and efficient diagnostic strategy for *P. falciparum* malaria that could be utilized in clinics or hospitals in place of time consuming ELISAs for *pLDH*. Future directions include generalizing this method for the detection of all species of malaria by functionalizing magnetic particles with a pan-specific *pLDH* antibody or a series of species-specific *pLDH* antibodies.

Acknowledgements

I would like to thank Keersten Ricks for her contributions to this work. Support for this work was provided by the Bill and Melinda Gates Foundation Grand Challenges in Global Health: Develop Technologies that Allow Assessment of Multiple Conditions and Pathogens at Point-of-Care. This material is based upon work supported by the National Science Foundation Graduate Research Fellowship Program under Grant No. 1445197.

APPENDIX E

TOWARD DYNAMIC PAPER-BASED DIAGNOSTICS

Introduction

Paper microfluidic devices, which rely on capillary forces to move microliter quantities of fluid through porous materials, are currently the best platform for field-applicable diagnostics in low-resource settings.¹⁰ These devices require no electricity or expertise, and are generally low-cost and disposable. The LFA is the most widely deployed paper diagnostic.¹⁰ While the LFA format works well for sandwich immunoassays, the simple design does not allow for more complex, multistep processes such as sample preparation and signal amplification.

The introduction of novel paper-based devices such as μ PADs (microfluidic paper-based analytical devices) and 2DPNs has increased the complexity of assays that can be performed in paper diagnostics. μ PADS consist of hydrophilic cellulose channels bound by hydrophobic barriers, such as wax or photoresist, and they allow for the distribution of fluid from a common source to multiple detection zones.¹¹ However, these devices are not suitable for complex matrices like whole blood, which may interfere with visual detection of colorimetric signal, and require preprocessing steps such as plasma separation.¹⁰ 2DPNs allow for sequential introduction of multiple fluids to one detection zone, allowing for multistep processes such as paper-based ELISAs.¹² However, more tools are needed to develop completely automated paper diagnostics capable of multistep processes such as sample preparation, target purification, colorimetric chemical detection, and signal amplification.

Dynamic and switchable valves that direct or control fluid flow would greatly enhance the capabilities of paper diagnostics. Toley et al. has shown that sponge-based actuators are capable of connecting and disconnecting channels in paper microfluidics, thereby allowing and disallowing fluid flow to or from particular channels.¹³ However, these actuators require several reagents and processing steps outside of the assay chemistry to achieve actuation. We attempted to employ an alternative strategy in which barriers to fluid flow were polymerized directly on the paper substrate after the sample has been introduced in order to (i) redirect fluid flow or (ii) capture colorimetric signal in a localized chamber.

Results and Discussion

An ideal valve for paper microfluidic devices would redirect fluid flow at a precise location and at an exact time. Further, for biomarker detection, valve chemistry should involve innocuous precursors and gentle reaction conditions. In order to provide maximum spatial and temporal flexibility, we first developed valves on a paper substrate via eosin-mediated polymerization of polyethylene glycol diacrylate (PEGDA) and 1-vinyl-2-pyrrolidone (VP) using triethanolamine (TEA) as a co-initiator. This polymerization reaction, which is initiated with visible light, has previously been used for surface-initiated polymerization from silica nanoparticles,¹⁵ cell encapsulation,¹⁶ and as an amplification detection strategy on glass microarrays and paper.¹⁷

To perform this polymerization on paper, eosin isothiocyanate (EITC) was conjugated to BSA, and two lines of the resulting macrophotoinitiator were printed onto a nitrocellulose membrane. After the membrane was dried, a polymer precursor mixture of PEGDA, TEA, VP, and Eosin Y (to overcome oxygen inhibition) were wicked up the membrane, which was subsequently illuminated with green light (522 nm) to initiate polymerization. Next, a small

volume of green food dye was added to the membrane in the area between the printed macrophotoinitiator lines (Figure 45A). A similar system using Irgacure® 2959-decorated polyacrylic acid (printed macrophotoinitiator), PEGDA, and ascorbic acid with illumination at 365 nm was also employed, although only one line of initiator was printed, and the ability to stop fluid flow of a red dye was measured. In both cases, autopolymerization proved to be a major challenge, regardless of the inhibitor concentration. Protecting LFAs from light as the polymer precursor mixture wicked up the membrane solved this problem, and as shown in Figure 45B-C we were able to demonstrate that, in principle, hydrogel barriers that were polymerized in situ could retain fluid on a lateral flow assay.

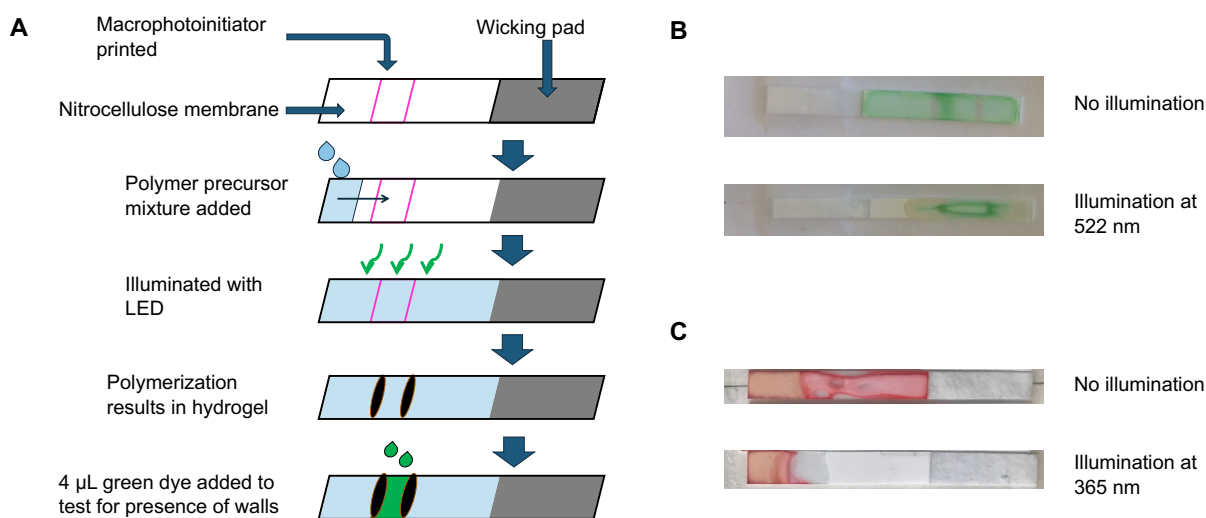


Figure 45. (A) Workflow for EITC-initiated dynamic walls proof-of-concept lateral flow assay. (B) Performance of EITC-initiated dynamic walls. (C) Performance of I2959-initiated dynamic walls.

Conclusion

The dynamic walls system requires a significant amount of optimization before it can be used to enable complex chemistries on lateral flow membrane. Additionally, a system that cannot tolerate exposure to ambient light would not be practical in a diagnostic setting, particularly in a

low-resource setting. Nonetheless, we have demonstrated in a proof-of-concept format, that barriers to fluid flow can be dynamically produced at precise times and locations on a lateral flow assay.

Acknowledgements

Kristina Pieteron and Sarah Hahn performed most of the experimental work on this project, which was funded by CTSA award No. UL1 TR002243 from the National Center for Advancing Translational Sciences through an internal pilot grant VICTR voucher VR18735.

APPENDIX F

MY PH.D. EXPERIENCE

My experience in graduate school has been more than I ever could have imagined.

Figure 46. My Ph.D. experience in postcards



REFERENCES

1. Institute for Health Metrics and Evaluation (IHME). *GBD Compare Data Visualization*. (IHME, University of Washington, 2016). at <<http://vizhub.healthdata.org/gbd-compare>>
2. Hensher, M., Price, M. & Adomakoh, S. in *Dis. Control Priorities Dev. Ctries.* (eds. Jamison, D. T., Breman, J. G., Measham, A. R., Alleyne, G., Claeson, M., Evans, D. B., Jha, P., Mills, A. & Musgrove, P.) (The International Bank for Reconstruction and Development / The World Bank, 2006). at <<http://www.ncbi.nlm.nih.gov/books/NBK11737/>>
3. Berendes, S., Heywood, P., Oliver, S. & Garner, P. Quality of Private and Public Ambulatory Health Care in Low and Middle Income Countries: Systematic Review of Comparative Studies. *PLOS Med.* **8**, e1000433 (2011).
4. Coulibaly, M., Meda, N., Yonaba, C., Ouedraogo, S., Congo, M., Barry, M., Thio, E., Siribié, I., Koueta, F., Ye, D., Kam, L., Blanche, S., Perre, P. V. D. & Leroy, V. Missed Opportunities for Early Access to Care of HIV-Infected Infants in Burkina Faso. *PLoS One* **9**, e111240 (2014).
5. Violari, A., Cotton, M. F., Gibb, D. M., Babiker, A. G., Steyn, J., Madhi, S. A., Jean-Philippe, P. & McIntyre, J. A. Early Antiretroviral Therapy and Mortality among HIV-Infected Infants. *N. Engl. J. Med.* **359**, 2233–2244 (2008).
6. Bourne, D. E., Thompson, M., Brody, L. L., Cotton, M., Draper, B., Laubscher, R., Abdullah, M. F. & Myers, J. E. Emergence of a peak in early infant mortality due to HIV/AIDS in South Africa. *AIDS* **23**, 101–106 (2009).
7. Drain, P. K., Hyle, E. P., Noubary, F., Freedberg, K. A., Wilson, D., Bishai, W., Rodriguez, W. & Bassett, I. V. Evaluating Diagnostic Point-of-Care Tests in Resource-Limited Settings. *Lancet Infect. Dis.* **14**, 239–249 (2014).
8. World Health Organization. *World Malaria Report 2017*. 196 (World Health Organization, 2017). at <<http://www.who.int/malaria/publications/world-malaria-report-2017/report/en/>>
9. World Health Organization. *World Malaria Report 2016*. 186 (World Health Organization, 2016). at <<http://www.who.int/malaria/publications/world-malaria-report-2016/report/en/>>
10. Onwujekwe, O., Uguru, N., Etiaba, E., Chikezie, I., Uzochukwu, B. & Adjagba, A. The Economic Burden of Malaria on Households and the Health System in Enugu State Southeast Nigeria. *PLOS ONE* **8**, e78362 (2013).
11. CDC-Centers for Disease Control and Prevention. CDC - Malaria - Malaria Worldwide - Impact of Malaria. (2017). at <https://www.cdc.gov/malaria/malaria_worldwide/impact.html>

12. World Health Organization. WHO | MDG 6: combat HIV/AIDS, malaria and other diseases. *WHO* at http://www.who.int/topics/millennium_development_goals/diseases/en/
13. Alonso, P. & Noor, A. M. The global fight against malaria is at crossroads. *The Lancet* **390**, 2532–2534 (2017).
14. World Health Organization. *Eliminating malaria*. 24 (World Health Organization, 2016). at <http://www.who.int/malaria/publications/atoz/eliminating-malaria/en/>
15. Grueninger, H. & Hamed, K. Transitioning from malaria control to elimination: the vital role of ACTs. *Trends Parasitol.* **29**, 60–64 (2013).
16. Searle, K. M., Katowa, B., Kobayashi, T., Siame, M. N. S., Mharakurwa, S., Carpi, G., Norris, D. E., Stevenson, J. C., Thuma, P. E. & Moss, W. J. Distinct parasite populations infect individuals identified through passive and active case detection in a region of declining malaria transmission in southern Zambia. *Malar. J.* **16**, 154 (2017).
17. Cowman, A. F., Healer, J., Marapana, D. & Marsh, K. Malaria: Biology and Disease. *Cell* **167**, 610–624 (2016).
18. Howes, R. E., Battle, K. E., Mendis, K. N., Smith, D. L., Cibulskis, R. E., Baird, J. K. & Hay, S. I. Global Epidemiology of Plasmodium vivax. *Am. J. Trop. Med. Hyg.* **95**, 15–34 (2016).
19. Collins, W. E. & Jeffery, G. M. Plasmodium ovale: Parasite and Disease. *Clin. Microbiol. Rev.* **18**, 570–581 (2005).
20. Collins, W. E. & Jeffery, G. M. Plasmodium malariae: Parasite and Disease. *Clin. Microbiol. Rev.* **20**, 579–592 (2007).
21. Barber, B. E., Grigg, M. J., William, T., Yeo, T. W. & Anstey, N. M. The Treatment of Plasmodium knowlesi Malaria. *Trends Parasitol.* **33**, 242–253 (2017).
22. Barber, B. E., Rajahram, G. S., Grigg, M. J., William, T. & Anstey, N. M. World Malaria Report: time to acknowledge Plasmodium knowlesi malaria. *Malar. J.* **16**, 135 (2017).
23. Klein, E. Y. Antimalarial drug resistance: a review of the biology and strategies to delay emergence and spread. *Int. J. Antimicrob. Agents* **41**, 311–317 (2013).
24. In *Merck Man. Diagn. Ther.* (eds. Porter, R. S. & Kaplan, J. L.) 1381–1390 (Merck Sharp & Dohme Corp, 2011).
25. Lindblade, K. A., Steinhardt, L., Samuels, A., Kachur, S. P. & Slutsker, L. The silent threat: asymptomatic parasitemia and malaria transmission. *Expert Rev. Anti Infect. Ther.* **11**, 623–639 (2013).

26. Babiker, H. A., Gadalla, A. A. H. & Ranford-Cartwright, L. C. The role of asymptomatic *P. falciparum* parasitaemia in the evolution of antimalarial drug resistance in areas of seasonal transmission. *Drug Resist. Updat.* **16**, 1–9 (2013).
27. Bousema, T., Okell, L., Felger, I. & Drakeley, C. Asymptomatic malaria infections: detectability, transmissibility and public health relevance. *Nat. Rev. Microbiol.* **12**, 833–840 (2014).
28. Slater, H. C., Ross, A., Ouédraogo, A. L., White, L. J., Nguon, C., Walker, P. G. T., Ngor, P., Aguas, R., Silal, S. P., Dondorp, A. M., La Barre, P., Burton, R., Sauerwein, R. W., Drakeley, C., Smith, T. A., Bousema, T. & Ghani, A. C. Assessing the impact of next-generation rapid diagnostic tests on *Plasmodium falciparum* malaria elimination strategies. *Nature* **528**, S94–S101 (2015).
29. Wu, L., van den Hoogen, L. L., Slater, H., Walker, P. G. T., Ghani, A. C., Drakeley, C. J. & Okell, L. C. Comparison of diagnostics for the detection of asymptomatic *Plasmodium falciparum* infections to inform control and elimination strategies. *Nature* **528**, S86-93 (2015).
30. Tadesse, F. G., Slater, H. C., Chali, W., Teelen, K., Lanke, K., Belachew, M., Menberu, T., Shumie, G., Shitaye, G., Okell, L. C., Graumans, W., van Gemert, G.-J., Kedir, S., Tesfaye, A., Belachew, F., Abebe, W., Mamo, H., Sauerwein, R., Balcha, T., Aseffa, A., Yewhalaw, D., Gadisa, E., Drakeley, C. & Bousema, T. The relative contribution of symptomatic and asymptomatic *Plasmodium vivax* and *Plasmodium falciparum* infections to the infectious reservoir in a low-endemic setting in Ethiopia. *Clin. Infect. Dis.* (2018).
doi:10.1093/cid/cix1123
31. Imwong, M., Stepniewska, K., Tripura, R., Peto, T. J., Lwin, K. M., Vihokhern, B., Wongsan, K., von Seidlein, L., Dhorda, M., Snounou, G., Keereecharoen, L., Singhasivanon, P., Sirithiranont, P., Chalk, J., Nguon, C., Day, N. P. J., Nosten, F., Dondorp, A. & White, N. J. Numerical Distributions of Parasite Densities During Asymptomatic Malaria. *J. Infect. Dis.* **213**, 1322–1329 (2016).
32. Imwong, M., Hanchana, S., Malleret, B., Rénia, L., Day, N. P. J., Dondorp, A., Nosten, F., Snounou, G. & White, N. J. High-Throughput Ultrasensitive Molecular Techniques for Quantifying Low-Density Malaria Parasitemias. *J. Clin. Microbiol.* **52**, 3303–3309 (2014).
33. Lin, J. T., Saunders, D. L. & Meshnick, S. R. The role of submicroscopic parasitemia in malaria transmission: what is the evidence? *Trends Parasitol.* **30**, 183–190 (2014).
34. Zainabadi, K., Adams, M., Han, Z. Y., Lwin, H. W., Han, K. T., Ouattara, A., Thura, S., Plowe, C. V. & Nyunt, M. M. A novel method for extracting nucleic acids from dried blood spots for ultrasensitive detection of low-density *Plasmodium falciparum* and *Plasmodium vivax* infections. *Malar. J.* **16**, 377 (2017).
35. Das, S., Jang, I. K., Barney, B., Peck, R., Rek, J. C., Arinaitwe, E., Adrama, H., Murphy, M., Imwong, M., Ling, C. L., Proux, S., Haohankhunnatham, W., Rist, M., Seilie, A. M., Hanron, A., Daza, G., Chang, M., Nakamura, T., Kalnoky, M., Labarre, P., Murphy, S. C.,

- McCarthy, J. S., Nosten, F., Greenhouse, B., Allauzen, S. & Domingo, G. J. Performance of a High-Sensitivity Rapid Diagnostic Test for *Plasmodium falciparum* Malaria in Asymptomatic Individuals from Uganda and Myanmar and Naive Human Challenge Infections. *Am. J. Trop. Med. Hyg.* **97**, 1540–1550 (2017).
36. Baker, J., McCarthy, J., Gatton, M., Kyle, D. E., Belizario, V., Luchavez, J., Bell, D. & Cheng, Q. Genetic Diversity of *Plasmodium falciparum* Histidine-Rich Protein 2 (PfHRP2) and Its Effect on the Performance of PfHRP2-Based Rapid Diagnostic Tests. *J. Infect. Dis.* **192**, 870–877 (2005).
 37. Chang, H. H., Falick, A. M., Carlton, P. M., Sedat, J. W., DeRisi, J. L. & Marletta, M. A. N-terminal processing of proteins exported by malaria parasites. *Mol. Biochem. Parasitol.* **160**, 107–115 (2008).
 38. Howard, R. J., Uni, S., Aikawa, M., Aley, S. B., Leech, J. H., Lew, A. M., Wellems, T. E., Rener, J. & Taylor, D. W. Secretion of a malarial histidine-rich protein (Pf HRP II) from *Plasmodium falciparum*-infected erythrocytes. *J. Cell Biol.* **103**, 1269–1277 (1986).
 39. Baker, J., Gatton, M. L., Peters, J., Ho, M.-F., McCarthy, J. S. & Cheng, Q. Transcription and Expression of *Plasmodium falciparum* Histidine-Rich Proteins in Different Stages and Strains: Implications for Rapid Diagnostic Tests. *PLOS ONE* **6**, e22593 (2011).
 40. Desakorn, V., Dondorp, A. M., Silamut, K., Pongtavornpinyo, W., Sahassananda, D., Chotivanich, K., Pitisuttithum, P., Smithyman, A. M., Day, N. P. J. & White, N. J. Stage-dependent production and release of histidine-rich protein 2 by *Plasmodium falciparum*. *Trans. R. Soc. Trop. Med. Hyg.* **99**, 517–524 (2005).
 41. Gibson, L. E., Markwalter, C. F., Kimmel, D. W., Mudenda, L., Mbambara, S., Thuma, P. E. & Wright, D. W. *Plasmodium falciparum* HRP2 ELISA for analysis of dried blood spot samples in rural Zambia. *Malar. J.* **16**, 350 (2017).
 42. Gamboa, D., Ho, M.-F., Bendezu, J., Torres, K., Chiodini, P. L., Barnwell, J. W., Incardona, S., Perkins, M., Bell, D., McCarthy, J. & Cheng, Q. A Large Proportion of *P. falciparum* Isolates in the Amazon Region of Peru Lack *pfhrp2* and *pfhrp3*: Implications for Malaria Rapid Diagnostic Tests. *PLOS ONE* **5**, e8091 (2010).
 43. Akinyi, S., Hayden, T., Gamboa, D., Torres, K., Bendezu, J., Abdallah, J. F., Griffing, S. M., Quezada, W. M., Arrospide, N., Oliveira, A. M. D., Lucas, C., Magill, A. J., Bacon, D. J., Barnwell, J. W. & Udhayakumar, V. Multiple genetic origins of histidine-rich protein 2 gene deletion in *Plasmodium falciparum* parasites from Peru. *Sci. Rep.* **3**, 2797 (2013).
 44. Parr, J. B., Verity, R., Doctor, S. M., Janko, M., Carey-Ewend, K., Turman, B. J., Keeler, C., Slater, H. C., Whitesell, A. N., Mwandagilirwa, K., Ghani, A. C., Likwela, J. L., Tshefu, A. K., Emch, M., Juliano, J. J. & Meshnick, S. R. *Pfhrp2*-Deleted *Plasmodium falciparum* Parasites in the Democratic Republic of the Congo: A National Cross-sectional Survey. *J. Infect. Dis.* **216**, 36–44 (2017).

45. Amoah, L. E., Abankwa, J. & Oppong, A. Plasmodium falciparum histidine rich protein-2 diversity and the implications for PfHRP 2: based malaria rapid diagnostic tests in Ghana. *Malar. J.* **15**, 101 (2016).
46. Beshir, K. B., Sepúlveda, N., Bharmal, J., Robinson, A., Mwanguzi, J., Busula, A. O., Boer, J. G., Sutherland, C., Cunningham, J. & Hopkins, H. Plasmodium falciparum parasites with histidine-rich protein 2 (pfhrp2) and pfhrp3 gene deletions in two endemic regions of Kenya. *Sci. Rep.* **7**, 14718 (2017).
47. Kozycki, C. T., Umulisa, N., Rulisa, S., Mwikarago, E. I., Musabyimana, J. P., Habimana, J. P., Karema, C. & Krogstad, D. J. False-negative malaria rapid diagnostic tests in Rwanda: impact of Plasmodium falciparum isolates lacking hrp2 and declining malaria transmission. *Malar. J.* **16**, 123 (2017).
48. Bharti, P. K., Chandel, H. S., Ahmad, A., Krishna, S., Udhayakumar, V. & Singh, N. Prevalence of pfhrp2 and/or pfhrp3 Gene Deletion in Plasmodium falciparum Population in Eight Highly Endemic States in India. *PLOS ONE* **11**, e0157949 (2016).
49. Watson, O. J., Slater, H. C., Verity, R., Parr, J. B., Mwandagalirwa, M. K., Tshefu, A., Meshnick, S. R. & Ghani, A. C. Modelling the drivers of the spread of Plasmodium falciparum hrp2 gene deletions in sub-Saharan Africa. *eLife* **6**, e25008 (2017).
50. Brown, W. M., Yowell, C. A., Hoard, A., Vander Jagt, T. A., Hunsaker, L. A., Deck, L. M., Royer, R. E., Piper, R. C., Dame, J. B., Makler, M. T. & Vander Jagt, D. L. Comparative Structural Analysis and Kinetic Properties of Lactate Dehydrogenases from the Four Species of Human Malarial Parasites. *Biochemistry (Mosc.)* **43**, 6219–6229 (2004).
51. Iqbal, J., Siddique, A., Jameel, M. & Hira, P. R. Persistent Histidine-Rich Protein 2, Parasite Lactate Dehydrogenase, and Panmalarial Antigen Reactivity after Clearance of Plasmodium falciparum Monoinfection. *J. Clin. Microbiol.* **42**, 4237–4241 (2004).
52. Martin, S. K., Rajasekariah, G.-H., Awinda, G., Waitumbi, J. & Kifude, C. Unified Parasite Lactate Dehydrogenase and Histidine-Rich Protein ELISA for Quantification of Plasmodium falciparum. *Am. J. Trop. Med. Hyg.* **80**, 516–522 (2009).
53. Cunningham, J. pfhrp2/3 Deletions: How Big is the Problem? (2017).
54. World Health Organization. Neglected tropical diseases. *WHO Neglected Trop. Dis.* at <http://www.who.int/neglected_diseases/en/>
55. World Health Organization. Schistosomiasis. *WHO Schistosomiasis* at <<http://www.who.int/schistosomiasis/en/>>
56. World Health Organization. Schistosomiasis (Bilharzia). *WHO Reg. Off. Afr.* at <<http://www.afro.who.int/health-topics/schistosomiasis-bilharzia>>
57. In *Merck Man. Diagn. Ther.* (eds. Porter, R. S. & Kaplan, J. L.) 1358–1361 (Merck Sharp & Dohme Corp, 2011).

58. Colley, D. G., Bustinduy, A. L., Secor, W. E. & King, C. H. Human schistosomiasis. *The Lancet* **383**, 2253–2264 (2014).
59. Ross, A. G. P., Bartley, P. B., Sleigh, A. C., Olds, G. R., Li, Y., Williams, G. M. & McManus, D. P. Schistosomiasis. *N. Engl. J. Med.* **346**, 1212–1220 (2002).
60. Gray, D. J., Ross, A. G., Li, Y.-S. & McManus, D. P. Diagnosis and management of schistosomiasis. *The BMJ* **342**, (2011).
61. World Health Organization. *Schistosomiasis: progress report 2001 - 2011, strategic plan 2012 - 2020*. 74 (World Health Organization, 2013). at <<http://www.who.int/iris/handle/10665/78074>>
62. Utzinger, J., Becker, S. L., Lieshout, L. van, Dam, G. J. van & Knopp, S. New diagnostic tools in schistosomiasis. *Clin. Microbiol. Infect.* **21**, 529–542 (2015).
63. Braunmunzinger, R. A. & Southgate, B. A. Repeatability and Reproducibility of Egg Counts of *Schistosoma haematobium* in Urine. *Trop. Med. Parasitol.* **43**, 149–154 (1992).
64. Dam, G. J. van, Wichers, J. H., Ferreira, T. M. F., Ghati, D., Amerongen, A. van & Deelder, A. M. Diagnosis of Schistosomiasis by Reagent Strip Test for Detection of Circulating Cathodic Antigen. *J. Clin. Microbiol.* **42**, 5458–5461 (2004).
65. Colley, D. G., Binder, S., Campbell, C., King, C. H., Tchuente, L.-A. T., N’Goran, E. K., Erko, B., Karanja, D. M. S., Kabatereine, N. B., Lieshout, L. van & Rathbun, S. A Five-Country Evaluation of a Point-of-Care Circulating Cathodic Antigen Urine Assay for the Prevalence of *Schistosoma mansoni*. *Am. J. Trop. Med. Hyg.* **88**, 426–432 (2013).
66. Adriko, M., Standley, C. J., Tinkitina, B., Tukahebwa, E. M., Fenwick, A., Fleming, F. M., Sousa-Figueiredo, J. C., Stothard, J. R. & Kabatereine, N. B. Evaluation of circulating cathodic antigen (CCA) urine-cassette assay as a survey tool for *Schistosoma mansoni* in different transmission settings within Bugiri District, Uganda. *Acta Trop.* **136**, 50–57 (2014).
67. Ochodo, E. A., Gopalakrishna, G., Spek, B., Reitsma, J. B., van Lieshout, L., Polman, K., Lambertson, P., Bossuyt, P. M. & Leeftang, M. M. Circulating antigen tests and urine reagent strips for diagnosis of active schistosomiasis in endemic areas. *Cochrane Database Syst. Rev.* (2015). doi:10.1002/14651858.CD009579.pub2
68. Silveira, A. M. S., Costa, E. G. D., Ray, D., Suzuki, B. M., Hsieh, M. H., Fraga, L. A. de O. & Caffrey, C. R. Evaluation of the CCA Immuno-Chromatographic Test to Diagnose *Schistosoma mansoni* in Minas Gerais State, Brazil. *PLoS Negl. Trop. Dis.* **10**, e0004357 (2016).
69. Greter, H., Krauth, S. J., Ngandolo, B. N. R., Alfaroukh, I. O., Zinsstag, J. & Utzinger, J. Validation of a Point-of-Care Circulating Cathodic Antigen Urine Cassette Test for *Schistosoma mansoni* Diagnosis in the Sahel, and Potential Cross-Reaction in Pregnancy. *Am. J. Trop. Med. Hyg.* **94**, 361–364 (2016).

70. Casacuberta, M., Kinunghi, S., Vennervald, B. J. & Olsen, A. Evaluation and optimization of the Circulating Cathodic Antigen (POC-CCA) cassette test for detecting *Schistosoma mansoni* infection by using image analysis in school children in Mwanza Region, Tanzania. *Parasite Epidemiol. Control* **1**, 105–115 (2016).
71. Vonghachack, Y., Sayasone, S., Khieu, V., Bergquist, R., van Dam, G. J., Hoekstra, P. T., Corstjens, P. L. A. M., Nickel, B., Marti, H., Utzinger, J., Muth, S. & Odermatt, P. Comparison of novel and standard diagnostic tools for the detection of *Schistosoma mekongi* infection in Lao People's Democratic Republic and Cambodia. *Infect. Dis. Poverty* **6**, 127 (2017).
72. Kittur, N., Castleman, J. D., Jr, C. H. C., King, C. H. & Colley, D. G. Comparison of *Schistosoma mansoni* Prevalence and Intensity of Infection, as Determined by the Circulating Cathodic Antigen Urine Assay or by the Kato-Katz Fecal Assay: A Systematic Review. *Am. J. Trop. Med. Hyg.* **94**, 605–610 (2016).
73. Stothard, J. R., Kabatereine, N. B., Tukahebwa, E. M., Kazibwe, F., Rollinson, D., Mathieson, W., Webster, J. P. & Fenwick, A. Use of circulating cathodic antigen (CCA) dipsticks for detection of intestinal and urinary schistosomiasis. *Acta Trop.* **97**, 219–228 (2006).
74. Corstjens, P. L. A. M., Lieshout, L. van, Zuiderwijk, M., Kornelis, D., Tanke, H. J., Deelder, A. M. & Dam, G. J. van. Up-Converting Phosphor Technology-Based Lateral Flow Assay for Detection of *Schistosoma* Circulating Anodic Antigen in Serum. *J. Clin. Microbiol.* **46**, 171–176 (2008).
75. Corstjens, P. L., Nyakundi, R. K., Dood, C. J. de, Kariuki, T. M., Ochola, E. A., Karanja, D. M., Mwinzi, P. N. & Dam, G. J. van. Improved sensitivity of the urine CAA lateral-flow assay for diagnosing active *Schistosoma* infections by using larger sample volumes. *Parasit. Vectors* **8**, 241 (2015).
76. van Dam, G. J., de Dood, C. J., Lewis, M., Deelder, A. M., van Lieshout, L., Tanke, H. J., van Rooyen, L. H. & Corstjens, P. L. A. M. A robust dry reagent lateral flow assay for diagnosis of active schistosomiasis by detection of *Schistosoma* circulating anodic antigen. *Exp. Parasitol.* **135**, 274–282 (2013).
77. Corstjens, P. L. A. M., de Dood, C. J., Kornelis, D., Fat, E. M. T. K., Wilson, R. A., Kariuki, T. M., Nyakundi, R. K., Loverde, P. T., Abrams, W. R., Tanke, H. J., van Lieshout, L., Deelder, A. M. & van Dam, G. J. Tools for diagnosis, monitoring and screening of *Schistosoma* infections utilizing lateral-flow based assays and upconverting phosphor labels. *Parasitology* **141**, 1841–1855 (2014).
78. Knopp, S., Corstjens, P. L. A. M., Koukounari, A., Cercamondi, C. I., Ame, S. M., Ali, S. M., Dood, C. J. de, Mohammed, K. A., Utzinger, J., Rollinson, D. & Dam, G. J. van. Sensitivity and Specificity of a Urine Circulating Anodic Antigen Test for the Diagnosis of *Schistosoma haematobium* in Low Endemic Settings. *PLoS Negl. Trop. Dis.* **9**, e0003752 (2015).

79. van Dam, G. J., Xu, J., Bergquist, R., de Dood, C. J., Utzinger, J., Qin, Z.-Q., Guan, W., Feng, T., Yu, X.-L., Zhou, J., Zheng, M., Zhou, X.-N. & Corstjens, P. L. A. M. An ultra-sensitive assay targeting the circulating anodic antigen for the diagnosis of *Schistosoma japonicum* in a low-endemic area, People's Republic of China. *Acta Trop.* **141**, 190–197 (2015).
80. van Dam, G. J., Odermatt, P., Acosta, L., Bergquist, R., de Dood, C. J., Cornelis, D., Muth, S., Utzinger, J. & Corstjens, P. L. A. M. Evaluation of banked urine samples for the detection of circulating anodic and cathodic antigens in *Schistosoma mekongi* and *S. japonicum* infections: A proof-of-concept study. *Acta Trop.* **141, Part B**, 198–203 (2015).
81. Corstjens, P. L. A. M., Hoekstra, P. T., de Dood, C. J. & van Dam, G. J. Utilizing the ultrasensitive *Schistosoma* up-converting phosphor lateral flow circulating anodic antigen (UCP-LF CAA) assay for sample pooling-strategies. *Infect. Dis. Poverty* **6**, 155 (2017).
82. Murray, C. K., Gasser, R. A., Magill, A. J. & Miller, R. S. Update on Rapid Diagnostic Testing for Malaria. *Clin. Microbiol. Rev.* **21**, 97–110 (2008).
83. Levinson, S. S. Antibody multispecificity in immunoassay interference. *Clin. Biochem.* **25**, 77–87 (1992).
84. Miles, S. A., Balden, E., Magpantay, L., Wei, L., Leiblein, A., Hofheinz, D., Toedter, G., Stiehm, E. R., Bryson, Y. & Consortium, the S. C. P. A. Rapid Serologic Testing with Immune-Complex-Dissociated HIV p24 Antigen for Early Detection of HIV Infection in Neonates. *N. Engl. J. Med.* **328**, 297–302 (1993).
85. Henrard, D. R., Wu, S., Phillips, J., Wiesner, D. & Phair, J. Detection of p24 antigen with and without immune complex dissociation for longitudinal monitoring of human immunodeficiency virus type 1 infection. *J. Clin. Microbiol.* **33**, 72–75 (1995).
86. Young, P. R., Hilditch, P. A., Bletchly, C. & Halloran, W. An Antigen Capture Enzyme-Linked Immunosorbent Assay Reveals High Levels of the Dengue Virus Protein NS1 in the Sera of Infected Patients. *J. Clin. Microbiol.* **38**, 1053–1057 (2000).
87. Libraty, D. H., Young, P. R., Pickering, D., Endy, T. P., Kalayanarooj, S., Green, S., Vaughn, D. W., Nisalak, A., Ennis, F. A. & Rothman, A. L. High Circulating Levels of the Dengue Virus Nonstructural Protein NS1 Early in Dengue Illness Correlate with the Development of Dengue Hemorrhagic Fever. *J. Infect. Dis.* **186**, 1165–1168 (2002).
88. Chan, E. D., Reves, R., Belisle, J. T., Brennan, P. J. & Hahn, W. E. Diagnosis of Tuberculosis by a Visually Detectable Immunoassay for Lipoarabinomannan. *Am. J. Respir. Crit. Care Med.* **161**, 1713–1719 (2000).
89. Minion, J., Leung, E., Talbot, E., Dheda, K., Pai, M. & Menzies, D. Diagnosing tuberculosis with urine lipoarabinomannan: systematic review and meta-analysis. *Eur. Respir. J.* **38**, 1398–1405 (2011).

90. Biswas, S., Tomar, D. & Rao, D. N. Investigation of the kinetics of histidine-rich protein 2 and of the antibody responses to this antigen, in a group of malaria patients from India. *Ann. Trop. Med. Parasitol.* **99**, 553–562 (2005).
91. Das, P., Grewal, J. S. & Chauhan, V. S. Antibody and cellular immune responses to *Plasmodium falciparum* histidine-rich protein II in malaria-exposed individuals in Orissa, India. *Trans. R. Soc. Trop. Med. Hyg.* **104**, 371–373 (2010).
92. Ho, M.-F., Baker, J., Lee, N., Luchavez, J., Arie, F., Nhem, S., Oyibo, W., Bell, D., González, I., Chiodini, P., Gatton, M. L., Cheng, Q. & McCarthy, J. S. Circulating antibodies against *Plasmodium falciparum* histidine-rich proteins 2 interfere with antigen detection by rapid diagnostic tests. *Malar. J.* **13**, 480 (2014).
93. Taylor, D. W., Bobbili, N., Khadka, V. S., Quakyi, I. A. & Leke, R. G. F. Individuals living in a malaria-endemic area of Cameroon do not have an acquired antibody response to *Plasmodium falciparum* histidine-rich protein 2. *Malar. J.* **16**, 58 (2017).
94. Davis, K. M., Swartz, J. D., Haselton, F. R. & Wright, D. W. Low-Resource Method for Extracting the Malarial Biomarker Histidine-Rich Protein II To Enhance Diagnostic Test Performance. *Anal. Chem.* **84**, 6136–6142 (2012).
95. Kent, R. J., Thuma, P. E., Mharakurwa, S. & Norris, D. E. Seasonality, Blood Feeding Behavior, and Transmission of *Plasmodium falciparum* by *Anopheles Arabiensis* after an Extended Drought in Southern Zambia. *Am. J. Trop. Med. Hyg.* **76**, 267–274 (2007).
96. Laban, N. M., Kobayashi, T., Hamapumbu, H., Sullivan, D., Mharakurwa, S., Thuma, P. E., Shiff, C. J. & Moss, W. J. Comparison of a PfHRP2-based rapid diagnostic test and PCR for malaria in a low prevalence setting in rural southern Zambia: implications for elimination. *Malar. J.* **14**, 25 (2015).
97. Searle, K. M., Hamapumbu, H., Lubinda, J., Shields, T. M., Pinchoff, J., Kobayashi, T., Stevenson, J. C., Bridges, D. J., Larsen, D. A., Thuma, P. E. & Moss, W. J. Evaluation of the operational challenges in implementing reactive screen-and-treat and implications of reactive case detection strategies for malaria elimination in a region of low transmission in southern Zambia. *Malar. J.* **15**, 412 (2016).
98. Plowe, C. V., Djimde, A., Bouare, M., Doumbo, O. & Wellems, T. E. Pyrimethamine and proguanil resistance-conferring mutations in *Plasmodium falciparum* dihydrofolate reductase: polymerase chain reaction methods for surveillance in Africa. *Am. J. Trop. Med. Hyg.* **52**, 565–568 (1995).
99. Shokoples, S. E., Ndao, M., Kowalewska-Grochowska, K. & Yanow, S. K. Multiplexed Real-Time PCR Assay for Discrimination of *Plasmodium* Species with Improved Sensitivity for Mixed Infections. *J. Clin. Microbiol.* **47**, 975–980 (2009).
100. Rougemont, M., Van Saanen, M., Sahli, R., Hinrikson, H. P., Bille, J. & Jaton, K. Detection of Four *Plasmodium* Species in Blood from Humans by 18S rRNA Gene Subunit-Based and Species-Specific Real-Time PCR Assays. *J. Clin. Microbiol.* **42**, 5636–5643 (2004).

101. Markwalter, C. F., Jang, I. K., Burton, R. A., Domingo, G. J. & Wright, D. W. Biolayer interferometry predicts ELISA performance of monoclonal antibody pairs for *Plasmodium falciparum* histidine-rich protein 2. *Anal. Biochem.* **534**, 10–13 (2017).
102. Leow, C. H., Jones, M., Cheng, Q., Mahler, S. & McCarthy, J. Production and characterization of specific monoclonal antibodies binding the *Plasmodium falciparum* diagnostic biomarker, histidine-rich protein 2. *Malar. J.* **13**, 277 (2014).
103. Vermeer, A. W. & Norde, W. The thermal stability of immunoglobulin: unfolding and aggregation of a multi-domain protein. *Biophys. J.* **78**, 394–404 (2000).
104. Eggleton, P., Javed, M., Pulavar, D. & Sheldon, G. in *eLS* (John Wiley & Sons, Ltd, 2001). doi:10.1002/9780470015902.a0001118.pub2
105. Scherr, T. F., Gupta, S., Wright, D. W. & Haselton, F. R. Mobile phone imaging and cloud-based analysis for standardized malaria detection and reporting. *Sci. Rep.* **6**, 28645 (2016).
106. Ricks, K. M., Adams, N. M., Scherr, T. F., Haselton, F. R. & Wright, D. W. Direct transfer of HRPII-magnetic bead complexes to malaria rapid diagnostic tests significantly improves test sensitivity. *Malar. J.* **15**, 399 (2016).
107. Deelder, A. M., Jonge, N. D., Boerman, O. C., Fillié, Y. E., Hilberath, G. W., Rotmans, J. P., Gerritse, M. J. & Schut, D. W. O. L. Sensitive Determination of Circulating Anodic Antigen in *Schistosoma mansoni* Infected Individuals by an Enzyme-Linked Immunosorbent Assay using Monoclonal Antibodies. *Am. J. Trop. Med. Hyg.* **40**, 268–272 (1989).
108. Lieshout, L. V., Jonge, N. D., Masry, N. A. E., Mansour, M. M., Krijger, F. W. & Deelder, A. M. Improved Diagnostic Performance of the Circulating Antigen Assay in Human Schistosomiasis by Parallel Testing for Circulating Anodic and Cathodic Antigens in Serum and Urine. *Am. J. Trop. Med. Hyg.* **47**, 463–469 (1992).
109. Niu, Y., Sun, L. & Crooks, R. M. Determination of the Intrinsic Proton Binding Constants for Poly(amidoamine) Dendrimers via Potentiometric pH Titration. *Macromolecules* **36**, 5725–5731 (2003).
110. Leech, S. & Penney, M. D. Correlation of specific gravity and osmolality of urine in neonates and adults. *Arch. Dis. Child.* **62**, 671–673 (1987).
111. Voinescu, G. C., Shoemaker, M., Moore, H., Khanna, R. & Nolph, K. D. The Relationship between Urine Osmolality and Specific Gravity. *Am. J. Med. Sci.* **323**, 39–42 (2002).
112. Bauer, W. S., Kimmel, D. W., Adams, N. M., Gibson, L. E., Scherr, T. F., Richardson, K. A., Conrad, J. A., Matakala, H. K., Haselton, F. R. & Wright, D. W. Magnetically-enabled biomarker extraction and delivery system: towards integrated ASSURED diagnostic tools. *Analyst* **142**, 1569–1580 (2017).

113. Sultana, A. & Lee, J. E. in *Curr. Protoc. Protein Sci.* (John Wiley & Sons, Inc., 2001). doi:10.1002/0471140864.ps1925s79
114. Concepcion, J., Witte, K., Wartchow, C., Choo, S., Yao, D., Persson, H., Wei, J., Li, P., Heidecker, B., Ma, W., Varma, R., Zhao, L.-S., Perillat, D., Carricato, G., Recknor, M., Du, K., Ho, H., Ellis, T., Gamez, J., Howes, M., Phi-Wilson, J., Lockard, S., Zuk, R. & Tan, H. Label-free detection of biomolecular interactions using BioLayer interferometry for kinetic characterization. *Comb. Chem. High Throughput Screen.* **12**, 791–800 (2009).
115. Noedl, H., Bronnert, J., Yingyuen, K., Attlmayr, B., Kollaritsch, H. & Fukuda, M. Simple Histidine-Rich Protein 2 Double-Site Sandwich Enzyme-Linked Immunosorbent Assay for Use in Malaria Drug Sensitivity Testing. *Antimicrob. Agents Chemother.* **49**, 3575–3577 (2005).
116. Delves, P. J., Martin, S. J., Burton, D. R. & Roitt, I. M. *Roitt's Essential Immunology*. (John Wiley & Sons, 2017).
117. Markwalter, C. F., Ricks, K. M., Bitting, A. L., Mudenda, L. & Wright, D. W. Simultaneous capture and sequential detection of two malarial biomarkers on magnetic microparticles. *Talanta* **161**, 443–449 (2016).
118. Bergwerff, A. A., Dam, G. J. van, Rotmans, J. P., Deelder, A. M., Kamerling, J. P. & Vliegthart, J. F. The immunologically reactive part of immunopurified circulating anodic antigen from *Schistosoma mansoni* is a threonine-linked polysaccharide consisting of --> 6)-(beta-D-GlcA-(1 --> 3))-beta-D-GalpNAc-(1 --> repeating units. *J. Biol. Chem.* **269**, 31510–31517 (1994).
119. Van Dam, G. J., Bergwerff, A. A., Thomas-Oates, J. E., Rotmans, J. P., Kamerling, J. P., Vliegthart, J. F. G. & Deelder, A. M. The Immunologically Reactive O-Linked Polysaccharide Chains Derived from Circulating Cathodic Antigen Isolated from the Human Blood Fluke *Schistosoma Mansoni* have Lewis x as Repeating Unit. *Eur. J. Biochem.* **225**, 467–482 (1994).
120. Tighe, P. J., Ryder, R. R., Todd, I. & Fairclough, L. C. ELISA in the multiplex era: potentials and pitfalls. *Proteomics Clin. Apl.* **9**, 406–22 (2015).
121. Ellington, A. A., Kullo, I. J., Bailey, K. R. & Klee, G. G. Antibody-based protein multiplex platforms: technical and operational challenges. *Clin. Chem.* **56**, 186–93 (2010).
122. Ekins, R. P. Multi-analyte immunoassay. *J. Pharm. Biomed. Anal.* **7**, 155–68 (1989).
123. Parpia, Z. A. & Kelso, D. M. Empirically optimized flow cytometric immunoassay validates ambient analyte theory. *Anal. Biochem.* **401**, 1–6 (2010).
124. Chou, J., Wong, J., Christodoulides, N., Floriano, P. N., Sanchez, X. & McDevitt, J. Porous bead-based diagnostic platforms: bridging the gaps in healthcare. *Sensors* **12**, 15467–99 (2012).

125. Elshal, M. F. & McCoy, J. P. Multiplex bead array assays: performance evaluation and comparison of sensitivity to ELISA. *Methods* **38**, 317–23 (2006).
126. Q-Plex™ vs. Traditional ELISA | Quansys Biosciences. (2016). at <<http://www.quansysbio.com/comparetoelisa/>>
127. Luminex® Multiplex Assays. (2016). at <<http://www.thermofisher.com/us/en/home/life-science/protein-biology/protein-assays-analysis/luminex-assays.html>>
128. McCutchan, T. F., Piper, R. C. & Makler, M. T. Use of Malaria Rapid Diagnostic Test to Identify Plasmodium knowlesi Infection. *Emerg. Infect. Dis.* **14**, 1750–1752 (2008).
129. World Health Organization. *Guidelines for the treatment of malaria. Third edition.* 316 (2015). at <<http://www.who.int/malaria/publications/atoz/9789241549127/en/>>
130. Markwalter, C. F., Davis, K. M. & Wright, D. W. Immunomagnetic capture and colorimetric detection of malarial biomarker Plasmodium falciparum lactate dehydrogenase. *Anal. Biochem.* **493**, 30–34 (2016).
131. Davis, K. M. Development of Rapid Immunoassays for Improved Point-of-Care Malaria Diagnostics. (2015). at <<http://etd.library.vanderbilt.edu/available/etd-07142015-135553/>>
132. Piper, R. C., Buchanan, I., Choi, Y. H. & Makler, M. T. Opportunities for improving pLDH-based malaria diagnostic tests. *Malar. J.* **10**, 1 (2011).
133. O'Farrell, B. in *Immunoass. Handb. Fourth Ed.* (ed. Wild, D.) 89–107 (Elsevier, 2013). doi:10.1016/B978-0-08-097037-0.00007-5
134. Lee, N., Gatton, M. L., Pelecanos, A., Bubb, M., Gonzalez, I., Bell, D., Cheng, Q. & McCarthy, J. S. Identification of optimal epitopes for Plasmodium falciparum rapid diagnostic tests that target histidine-rich proteins 2 and 3. *J. Clin. Microbiol.* **50**, 1397–405 (2012).
135. Food and Drug Administration Center for Drug Evaluation and Research (CDER). *Guidance for Industry: Bioanalytical Method Validation.* (2001).
136. de Souza Castilho, M., Laube, T., Yamanaka, H., Alegret, S. & Pividori, M. I. Magneto Immunoassays for Plasmodium falciparum Histidine-Rich Protein 2 Related to Malaria based on Magnetic Nanoparticles. *Anal. Chem.* **83**, 5570–5577 (2011).
137. Davis, K. M., Gibson, L. E., Haselton, F. R. & Wright, D. W. Simple sample processing enhances malaria rapid diagnostic test performance. *Analyst* **139**, 3026–3031 (2014).
138. Demirev, P. A. Dried Blood Spots: Analysis and Applications. *Anal. Chem.* **85**, 779–789 (2013).
139. Sharma, A., Jaiswal, S., Shukla, M. & Lal, J. Dried blood spots: Concepts, present status, and future perspectives in bioanalysis. *Drug Test. Anal.* **6**, 399–414 (2014).

140. Parker, S. P. & Cubitt, W. D. The use of the dried blood spot sample in epidemiological studies. *J. Clin. Pathol.* **52**, 633–639 (1999).
141. Wang, B., Han, S.-S., Cho, C., Han, J.-H., Cheng, Y., Lee, S.-K., Galappaththy, G. N. L., Thimasarn, K., Soe, M. T., Oo, H. W., Kyaw, M. P. & Han, E.-T. Comparison of Microscopy, Nested-PCR, and Real-Time-PCR Assays Using High-Throughput Screening of Pooled Samples for Diagnosis of Malaria in Asymptomatic Carriers from Areas of Endemicity in Myanmar. *J. Clin. Microbiol.* **52**, 1838–1845 (2014).
142. Singh, B., Cox-Singh, J., Miller, A. O., Abdullah, M. S., Snounou, G. & Abdul Rahman, H. Detection of malaria in Malaysia by nested polymerase chain reaction amplification of dried blood spots on filter papers. *Trans. R. Soc. Trop. Med. Hyg.* **90**, 519–521 (1996).
143. Hsiang, M. S., Lin, M., Dokomajilar, C., Kemere, J., Pilcher, C. D., Dorsey, G. & Greenhouse, B. PCR-Based Pooling of Dried Blood Spots for Detection of Malaria Parasites: Optimization and Application to a Cohort of Ugandan Children. *J. Clin. Microbiol.* **48**, 3539–3543 (2010).
144. Taylor, S. M., Juliano, J. J., Trottman, P. A., Griffin, J. B., Landis, S. H., Kitsa, P., Tshetu, A. K. & Meshnick, S. R. High-Throughput Pooling and Real-Time PCR-Based Strategy for Malaria Detection. *J. Clin. Microbiol.* **48**, 512–519 (2010).
145. Gil, J. P., Nogueira, F., Strömberg-Nörklit, J., Lindberg, J., Carrolo, M., Casimiro, C., Lopes, D., Arez, A. P., Cravo, P. V. & Rosário, V. E. Detection of atovaquone and Malarone™ resistance conferring mutations in Plasmodium falciparum cytochrome b gene (cytb). *Mol. Cell. Probes* **17**, 85–89 (2003).
146. Pimentel, S., Nogueira, F., Benchimol, C., Quinhentos, V., Bom, J., Varandas, L., do Rosário, V. & Bernardino, L. Detection of atovaquone-proguanil resistance conferring mutations in Plasmodium falciparum cytochrome b gene in Luanda, Angola. *Malar. J.* **5**, 30 (2006).
147. Ndao, M., Bandyayera, E., Kokoskin, E., Gyorkos, T. W., MacLean, J. D. & Ward, B. J. Comparison of Blood Smear, Antigen Detection, and Nested-PCR Methods for Screening Refugees from Regions Where Malaria Is Endemic after a Malaria Outbreak in Quebec, Canada. *J. Clin. Microbiol.* **42**, 2694–2700 (2004).
148. Corran, P. H., Cook, J., Lynch, C., Leendertse, H., Manjurano, A., Griffin, J., Cox, J., Abeku, T., Bousema, T., Ghani, A. C., Drakeley, C. & Riley, E. Dried blood spots as a source of anti-malarial antibodies for epidemiological studies. *Malar. J.* **7**, 195 (2008).
149. Rogier, E., Plucinski, M., Lucchi, N., Mace, K., Chang, M., Lemoine, J. F., Candrinho, B., Colborn, J., Dimbu, R., Fortes, F., Udhayakumar, V. & Barnwell, J. Bead-based immunoassay allows sub-picogram detection of histidine-rich protein 2 from Plasmodium falciparum and estimates reliability of malaria rapid diagnostic tests. *PLOS ONE* **12**, e0172139 (2017).

150. Nyunt, M. H., Kyaw, M. P., Win, K. K., Myint, K. M. & Nyunt, K. M. Field evaluation of HRP2 and pan pLDH-based immunochromatographic assay in therapeutic monitoring of uncomplicated falciparum malaria in Myanmar. *Malar. J.* **12**, 123 (2013).
151. Cheng, Q., Gatton, M. L., Barnwell, J., Chiodini, P., McCarthy, J., Bell, D. & Cunningham, J. Plasmodium falciparum parasites lacking histidine-rich protein 2 and 3: a review and recommendations for accurate reporting. *Malar. J.* **13**, 283 (2014).
152. Bauer, W. S., Richardson, K. A., Adams, N. M., Ricks, K. M., Gasperino, D. J., Ghionea, S. J., Rosen, M., Nichols, K. P., Weigl, B. H., Haselton, F. R. & Wright, D. W. Rapid concentration and elution of malarial antigen histidine-rich protein II using solid phase Zn(II) resin in a simple flow-through pipette tip format. *Biomicrofluidics* **11**, 034115 (2017).
153. Versteeg, I. & Mens, P. F. Development of a stable positive control to be used for quality assurance of rapid diagnostic tests for malaria. *Diagn. Microbiol. Infect. Dis.* **64**, 256–260 (2009).
154. Jang, J. W., Cho, C. H., Han, E. T., An, S. S. A. & Lim, C. S. pLDH level of clinically isolated Plasmodium vivax and detection limit of pLDH based malaria rapid diagnostic test. *Malar. J.* **12**, 181 (2013).
155. Piper, R., Lebras, J., Wentworth, L., Hunt-Cooke, A., Houzé, S., Chiodini, P. & Makler, M. Immunocapture diagnostic assays for malaria using Plasmodium lactate dehydrogenase (pLDH). *Am. J. Trop. Med. Hyg.* **60**, 109–118 (1999).
156. Vivas, L., Easton, A., Kendrick, H., Cameron, A., Lavandera, J.-L., Barros, D., de las Heras, F. G., Brady, R. L. & Croft, S. L. Plasmodium falciparum: Stage specific effects of a selective inhibitor of lactate dehydrogenase. *Exp. Parasitol.* **111**, 105–114 (2005).
157. Rubach, M. P., Mukemba, J., Florence, S., John, B., Crookston, B., Lopansri, B. K., Yeo, T. W., Piera, K. A., Alder, S. C., Weinberg, J. B., Anstey, N. M., Granger, D. L. & Mwaikambo, E. D. Plasma Plasmodium falciparum Histidine-Rich Protein-2 Concentrations Are Associated with Malaria Severity and Mortality in Tanzanian Children. *PLOS ONE* **7**, e35985 (2012).
158. World Health Organization, FIND & CDC-Centers for Disease Control and Prevention. *WHO product testing round 7*. 160 (World Health Organization, 2017). at <http://www.who.int/malaria/areas/diagnosis/rapid-diagnostic-tests/product-testing-round7/en/>
159. Bauer, W. S., Gulka, C. P., Silva-Baucage, L., Adams, N. M., Haselton, F. R. & Wright, D. W. Metal Affinity-Enabled Capture and Release Antibody Reagents Generate a Multiplex Biomarker Enrichment System that Improves Detection Limits of Rapid Diagnostic Tests. *Anal. Chem.* **89**, 10216–10223 (2017).
160. Sousa, L. P., Mariuba, L. A. M., Holanda, R. J., Pimentel, J. P., Almeida, M. E. M., Chaves, Y. O., Borges, D., Lima, E., Crainey, J. L., Orlandi, P. P., Lacerda, M. V. & Nogueira, P.

- A. A novel polyclonal antibody-based sandwich ELISA for detection of *Plasmodium vivax* developed from two lactate dehydrogenase protein segments. *BMC Infect. Dis.* **14**, 49 (2014).
161. Kaushal, N. A. & Kaushal, D. C. Production and characterization of monoclonal antibodies against substrate specific loop region of *Plasmodium falciparum* lactate dehydrogenase. *Immunol. Invest.* **43**, 556–571 (2014).
162. Lee, S., Song, K.-M., Jeon, W., Jo, H., Shim, Y.-B. & Ban, C. A highly sensitive aptasensor towards *Plasmodium* lactate dehydrogenase for the diagnosis of malaria. *Biosens. Bioelectron.* **35**, 291–296 (2012).
163. Cheung, Y.-W., Kwok, J., Law, A. W. L., Watt, R. M., Kotaka, M. & Tanner, J. A. Structural basis for discriminatory recognition of *Plasmodium* lactate dehydrogenase by a DNA aptamer. *Proc. Natl. Acad. Sci.* **110**, 15967–15972 (2013).
164. Jeon, W., Lee, S., Dh, M. & Ban, C. A colorimetric aptasensor for the diagnosis of malaria based on cationic polymers and gold nanoparticles. *Anal. Biochem.* **439**, 11–16 (2013).
165. Lee, S., Manjunatha, D. H., Jeon, W. & Ban, C. Cationic Surfactant-Based Colorimetric Detection of *Plasmodium* Lactate Dehydrogenase, a Biomarker for Malaria, Using the Specific DNA Aptamer. *PLOS ONE* **9**, e100847 (2014).
166. Godonoga, M., Lin, T.-Y., Oshima, A., Sumitomo, K., Tang, M. S. L., Cheung, Y.-W., Kinghorn, A. B., Dirkwager, R. M., Zhou, C., Kuzuya, A., Tanner, J. A. & Heddle, J. G. A DNA aptamer recognising a malaria protein biomarker can function as part of a DNA origami assembly. *Sci. Rep.* **6**, 21266 (2016).
167. Jain, P., Chakma, B., Singh, N. K., Patra, S. & Goswami, P. Aromatic Surfactant as Aggregating Agent for Aptamer-Gold Nanoparticle-Based Detection of *Plasmodium* Lactate Dehydrogenase. *Mol. Biotechnol.* **58**, 497–508 (2016).
168. Choi, S.-J. & Ban, C. Crystal structure of a DNA aptamer bound to *Pv*LDH elucidates novel single-stranded DNA structural elements for folding and recognition. *Sci. Rep.* **6**, 34998 (2016).
169. Dirkwager, R. M., Liang, S. & Tanner, J. A. Development of Aptamer-Based Point-of-Care Diagnostic Devices for Malaria Using Three-Dimensional Printing Rapid Prototyping. *ACS Sens.* **1**, 420–426 (2016).
170. Kenry, Geldert, A., Zhang, X., Zhang, H. & Lim, C. T. Highly Sensitive and Selective Aptamer-Based Fluorescence Detection of a Malarial Biomarker Using Single-Layer MoS₂ Nanosheets. *ACS Sens.* **1**, 1315–1321 (2016).
171. Kim, C. & Searson, P. C. Detection of *Plasmodium* Lactate Dehydrogenase Antigen in Buffer Using Aptamer-Modified Magnetic Microparticles for Capture, Oligonucleotide-Modified Quantum Dots for Detection, and Oligonucleotide-Modified Gold Nanoparticles for Signal Amplification. *Bioconjug. Chem.* **28**, 2230–2234 (2017).

172. Cheung, Y.-W., Dirkzwager, R. M., Wong, W.-C., Cardoso, J., D'Arc Neves Costa, J. & Tanner, J. A. Aptamer-mediated Plasmodium-specific diagnosis of malaria. *Biochimie* **145**, 131–136 (2018).
173. Figueroa-Miranda, G., Feng, L., Shiu, S. C.-C., Dirkzwager, R. M., Cheung, Y.-W., Tanner, J. A., Schöning, M. J., Offenhäusser, A. & Mayer, D. Aptamer-based electrochemical biosensor for highly sensitive and selective malaria detection with adjustable dynamic response range and reusability. *Sens. Actuators B Chem.* **255**, 235–243 (2018).
174. Byrne, H., Conroy, P. J., Whisstock, J. C. & O'Kennedy, R. J. A tale of two specificities: bispecific antibodies for therapeutic and diagnostic applications. *Trends Biotechnol.* **31**, 621–632 (2013).
175. Hasegawa, H., Taira, K., Sode, K. & Ikebukuro, K. Improvement of Aptamer Affinity by Dimerization. *Sensors* **8**, 1090–1098 (2008).
176. Lai, B. T., Wilson, J. A., Malette Loredó, J., Pitram, S. M., LaBerge, N. A., Heath, J. R. & Agnew, H. D. Epitope-Targeted Macrocyclic Peptide Ligand with Picomolar Cooperative Binding to Interleukin-17F. *Chem. – Eur. J.* (2018). doi:10.1002/chem.201704752
177. Fu, E., Kauffman, P., Lutz, B. & Yager, P. Chemical signal amplification in two-dimensional paper networks. *Sens. Actuators B Chem.* **149**, 325–328 (2010).
178. Fu, E., Liang, T., Houghtaling, J., Ramachandran, S., Ramsey, S. A., Lutz, B. & Yager, P. Enhanced Sensitivity of Lateral Flow Tests Using a Two-Dimensional Paper Network Format. *Anal. Chem.* **83**, 7941–7946 (2011).
179. Fu, E., Liang, T., Spicar-Mihalic, P., Houghtaling, J., Ramachandran, S. & Yager, P. Two-Dimensional Paper Network Format That Enables Simple Multistep Assays for Use in Low-Resource Settings in the Context of Malaria Antigen Detection. *Anal. Chem.* **84**, 4574–4579 (2012).
180. Lutz, B., Liang, T., Fu, E., Ramachandran, S., Kauffman, P. & Yager, P. Dissolvable fluidic time delays for programming multi-step assays in instrument-free paper diagnostics. *Lab. Chip* **13**, 2840–2847 (2013).
181. Toley, B. J., McKenzie, B., Liang, T., Buser, J. R., Yager, P. & Fu, E. Tunable-Delay Shunts for Paper Microfluidic Devices. *Anal. Chem.* **85**, 11545–11552 (2013).
182. Fridley, G. E., Le, H. & Yager, P. Highly Sensitive Immunoassay Based on Controlled Rehydration of Patterned Reagents in a 2-Dimensional Paper Network. *Anal. Chem.* **86**, 6447–6453 (2014).
183. Toley, B. J., Wang, J. A., Gupta, M., Buser, J. R., Lafleur, L., Lutz, B. R., Fu, E. & Yager, P. A versatile valving toolkit for automating fluidic operations in paper microfluidic devices. *Lab. Chip* **15**, 1432–1444 (2015).

184. Basco, L., Marquet, F., Makler, M. & Lebras, J. Plasmodium-Falciparum and Plasmodium-Vivax - Lactate-Dehydrogenase Activity and Its Application for in-Vitro Drug Susceptibility Assay. *Exp. Parasitol.* **80**, 260–271 (1995).
185. Turgut-Balik, D., Shoemark, D. K., Moreton, K. M., Sessions, R. B. & Holbrook, J. J. Over-production of lactate dehydrogenase from Plasmodium falciparum opens a route to new antimalarials. *Biotechnol. Lett.* **23**, 917–921 (2001).
186. Gomez, M. S., Piper, R. C., Hunsaker, L. A., Royer, R. E., Deck, L. M., Makler, M. T. & Vander Jagt, D. L. Substrate and cofactor specificity and selective inhibition of lactate dehydrogenase from the malarial parasite P-falciparum. *Mol. Biochem. Parasitol.* **90**, 235–246 (1997).
187. Makler, M. & Hinrichs, D. Measurement of the Lactate-Dehydrogenase Activity of Plasmodium-Falciparum as an Assessment of Parasitemia. *Am. J. Trop. Med. Hyg.* **48**, 205–210 (1993).
188. Makler, M., Ries, J., Williams, J., Bancroft, J., Piper, R., Gibbins, B. & Hinrichs, D. Parasite Lactate-Dehydrogenase as an Assay for Plasmodium-Falciparum Drug-Sensitivity. *Am. J. Trop. Med. Hyg.* **48**, 739–741 (1993).
189. Oduola, A. M. J., Omitowoju, G. O., Sowunmi, A., Makler, M. T., Falade, C. O., Kyle, D. E., Fehintola, F. A., Ogundahunsi, O. a. T., Piper, R. C., Schuster, B. G. & Milhous, W. K. Plasmodium falciparum: Evaluation of lactate dehydrogenase in monitoring therapeutic responses to standard antimalarial drugs in Nigeria. *Exp. Parasitol.* **87**, 283–289 (1997).
190. Witt, I. in *Methods Enzym. Anal.* (ed. Bergmeyer, H.-Ui.) (Elsevier, 2012).
191. Marangoni, A. G. in *Enzyme Kinet.* (ed. Marangoni, A. G.) 90–101 (John Wiley & Sons, Inc., 2002). doi:10.1002/0471267295.ch7
192. Zijlstra, W. G., Buursma, A. & Meeuwssen-van der Roest, W. P. Absorption spectra of human fetal and adult oxyhemoglobin, de-oxyhemoglobin, carboxyhemoglobin, and methemoglobin. *Clin. Chem.* **37**, 1633–1638 (1991).
193. Jelinek, T., Kilian, A. H. D., Henk, M., Mughusu, E. B., Nothdurft, H. D., Loscher, T., Knobloch, J. & VonSonnenburg, F. Parasite-specific lactate dehydrogenase for the diagnosis of Plasmodium falciparum infection in an endemic area in West Uganda. *Trop. Med. Int. Health* **1**, 227–230 (1996).